Master's thesis

NTNU
Norwegian University of Science and Technology
Faculty of Information Technology and Electrical Engineering
Department of Electric Power Engineering

Emil Aune Jakobsen

Performance Efficiency and Reliability Analysis of Offshore Wind Power Plants:

Case Study of Utsira Nord

Master's thesis in Energy and Environmental Engineering
Supervisor: Vijay Venu Vadlamudi
June 2023

NTNU
Norwegian University of Science and Technology

ZEPHYR

Emil Aune Jakobsen

Performance Efficiency and Reliability Analysis of Offshore Wind Power Plants:

Case Study of Utsira Nord

Master's thesis in Energy and Environmental Engineering
Supervisor: Vijay Venu Vadlamudi
June 2023

Norwegian University of Science and Technology
Faculty of Information Technology and Electrical Engineering
Department of Electric Power Engineering

NTNU
Norwegian University of
Science and Technology

Abstract

This Master's thesis aims to address questions raised during a specialisation project on grid architectures for Offshore Wind, with a specific focus on the collection system and transmission to shore of an offshore wind power plant. The objective of this research is twofold.

Firstly, the performance efficiency of an offshore wind power plant will be analyzed using three identified relevant methodologies – a Newton Raphson-based power flow, a Backward/Forward Sweep methodology termed as Distribution System Analysis, and a combinatorial approach. This analysis includes evaluating different system configurations, such as the use of conventional AC-technology and LFAC-technology, while also investigating the impact of different collection system topologies. The analysis will also assess the reliability of these system configurations using the RELRAD methodology.

Secondly, this thesis aims to compare the usage and results obtained from these methodologies in order to establish a basis for methodology comparisons. Furthermore, it seeks to reflect on the approach taken in analyzing offshore wind power plants.

By realizing these objectives, through a pertinent case study of Utsira Nord, this research seeks to contribute to a better understanding of the performance efficiency and reliability aspects of offshore wind power plants, and provide helpful insights for future analyses in this field. Moreover, a key aspiration of this Master's Thesis is to provide foundational knowledge and theory that can serve as a basis for potential future research on performance efficiency and reliability evaluations of offshore wind power plants.

Sammendrag

Denne masteroppgaven har som mål å besvare spørsmål som ble stilt i løpet av et spesialiseringsprosjekt om nettarkitekturer for havvind-/offshore vindkraftverk, med et spesielt fokus på innsamlingssystemer og overføringen til land fra et offshore vindkraftverk. Målet med denne forskningen er todelt.

For det første vil ytelseseffektiviteten til et offshore vindkraftverk bli analysert ved hjelp av tre relevante metoder: Newton-Raphson effektflyt, en metode kalt "Distribution System Analysis" som benytter en "Backward/Forward Sweep"-algoritme og en kombinatorisk tilnærming. Analysen inkluderer en vurdering av ulike systemkonfigurasjoner, som bruk av konvensjonell AC-teknologi og LFAC-teknologi, samt undersøkelse av ulike innsamlingssystemtopologier. Påliteligheten til disse systemkonfigurasjonene vil også bli vurdert ved hjelp av RELRAD-metoden.

For det andre har oppgaven som mål å sammenligne bruken av og resultatene fra disse metodene for å etablere et grunnlag for sammenligninger. Oppgaven tilsikter til slutt å reflektere over tilnærmingen som er valgt for å analysere et offshore vindkrafverk.

Ved å gjennomføre disse målene, ved hjelp av en relevant case-studie av Utsira Nord, tilsikter denne oppgaven å bidra til en bedre forståelse av ytelseseffektiviteten og pålitelighetsaspektene ved et offshore vindkraftverk, samt gi verdifulle innsikter for fremtidige analyser på dette området. I tillegg er et sentralt mål med denne masteroppgaven å legge grunnlaget for fremtidig forskning på evaluering av effektivitet og pålitelighet ved offshore vindkraftverk ved å bidra med grunnleggende kunnskap og teori.

Acknowledgement

This work marks the conclusion of my Master of Science (MSc) degree in Energy and Environmental Engineering at the Department of Electric Energy (formerly, Department of Electric Power Engineering) at the Norwegian University of Science and Technology (NTNU).

The execution of this work would not have been possible without the exceptional guidance and support I received from my supervisor, Associate Professor Vijay Venu Vadlamudi, at the Department of Electric Energy, NTNU. I would like to express my gratitude to him for entrusting me with the freedom to explore my own ideas and for his remarkable ability to provide support in his own inimitable manner throughout this process. Additionally, I would like to extend my gratitude for the inspiring conversations we had during our supervision meetings.

I would also like to express my gratitude to Trym A. Christensen and Eivind Fuglum from Zephyr who provided me with valuable insights into the industry's expectations within this research field. Also, I want to thank my parents and girlfriend, Anna Hanset, for always being positive and supporting me throughout this journey.

Emil A. Jakobsen

Trondheim, June 2023

Contents

List of Figures

List of Tables

Abbreviations

ASAI	Average System Availability Index
B2B	Back-To-Back
BFS	Backward/Forward Sweep
CAPEX	Capital Expenditure
CS	Collection System
DFIG	Doubly Fed Induction Generator
DSA	Distribution System Analysis
ENS	Energy Not Supplied
HV	High Voltage
HVAC	High Voltage Alternating Current
HVDC	High Voltage Direct Current
LCI	Load Commutated Inverter
LV	Low Voltage
MMC	Modular Multi-Level Converter
MTTR	Mean Time To Repair
MV	Medium Voltage
NR	Newton Raphson
O&M	Operation And Maintenance
OCP	Onshore Connection Point
OES	Offshore Electrical System

OPEX	Operational Expenditure
OSS	Offshore Sub Station
OW	Offshore Wind
OWPP	Offshore Wind Power Plant
PCC	Point of Common Coupling
PMSG	Permanent Magnet Synchronous Generator
RELRAD	Reliability in Readial Systems
STATCOM	Static Synchronous Compensator
STC	System Operator-Transmission Owner Code
TSO	Transmission System Operator
VSC	Voltage Source Converter
WT	Wind Turbine

1 Introduction

1.1 Background and Motivation

The first Offshore Wind Power Plants (OWPPs) were generally less than 20 meters deep and within 10 kilometers of the shore [1]. New OWPPs have relocated to deeper and further-off regions as the availability of such sites has diminished and public opposition to wind energy has grown [2]. Developing larger OWPPs further offshore might, in general, allow for a greater rate of energy generation, and as a consequence better financial returns. Individual Wind Turbine (WT) electricity is gathered by WTs in a Collection System (CS) connecting the WTs to an offshore substation (OSS), or occasionally to more than one OSS. Through a subsea transmission system, which occasionally comprises of numerous lines to maximize the reliability, the power generated is transferred to the shore in either alternating current (AC) or direct current (DC) form [1]. In this report, Transmission To Shore (TTS) is defined as the power transmission from OWPP between the OSS and the onshore connection point (OCP) or point of common coupling (PCC), and these terms will be introduced further in the following section.

Future OWPP expansions will inevitably result in an increase in size and longer distances out from coast [1]. Floating WTs have been suggested and have made significant progress in development over the past several years in an effort to lessen reliance on shallow water locations and investigate strong wind potential in further offshore and deeper water regions. However, there are obstacles to overcome before Offshore Wind (OW), and particularly floating OW, becomes a firmly established and cost competitive technology. Operational stability, load stress, subsea cable technology and maintenance options are a few of them [1].

The OW sector has experienced noteworthy progress in recent years, indicating a continuous trend of advancement and development. However, there is still a lack of standardized models and tools in the industry for the development of state-of-the-art OWPPs, particularly regarding the design of their electrical systems, as observed from the previous work experience of the author of this thesis. Consequently, this knowledge gap serves as the motivation behind the present project.

1.2 Scope and Contributions

This Master's thesis was the result of a collaborative research effort between the Department of Electric Energy (formerly, Department of Electric Power Engineering) at NTNU and the Norwegian company Zephyr AS. The main focus of the thesis is to assess the performance efficiency and reliability of the electrical system in an OWPP using suitable methodologies; doing so enables a comparative analysis of these methodologies within the field, providing helpful insights into their usage. Furthermore, this Master's Thesis aims to add value through the exploration of new approaches within the field of OWPP analysis. The exploration of new ideas throughout the research process has shaped the methodology employed, leading to helpful insights into the performance efficiency and reliability of OWPPs.

- This research explores various system configurations in the analysis of OWPPs, specifically focusing on two different CS topologies: radial and single-sided ring.
- The impact of utilizing both AC and LFAC in both the CS and the TTS is examined.
- The analysis of different grid technologies, AC and LFAC, primarily relates to the performance efficiency analysis, while the investigation of CS topologies is centered around reliability analysis.

Note that in this report, the combination of conventional MVAC in the CS and HVAC in the TTS is referred to as an AC system. However, in previous work (Chapters 2 and 3), it was referred to as an HVAC system. This adjustment in terminology has been made for clarity purposes within the context of this thesis.

This research is based on a study of fundamentals and a literature review conducted, documented as a specialisation project report [3], prior to the time frame of the Master's project work.

- The purpose of these fundamentals and literature review has been to identify gaps in the existing literature and offer insights into various system configurations and possibilities. They serve as a foundational basis for the Master's project work, providing a framework for further exploration and analysis.

Specific contributions of the thesis are listed below:

1. Performance Efficiency Analysis: Three methods have been employed for the analysis of performance efficiency of OWPPs – a Newton Raphson (NR)-based power flow, a Backward/Forward Sweep (BFS) methodology termed as Distribution System Analysis (DSA), and a combinatorial approach. The combinatorial approach emerged from initial work conducted during the research process and enabled a straightforward evaluation of performance efficiency in the CS of an OWPP.

2. Reliability Analysis: The reliability analysis performed in this Master's project work builds upon the RELRAD (RELiability in RADial systems) methodology from the literature. As the application of this methodology within the field of OWPPs had not been previously documented, a different interpretation of the methodology was developed in this work.

Scripts were written in Python to conduct the above analyses. Python data files related to the DSA algorithm [4] that can be accessed through [5] have been employed; some additional scripts were developed indigenously.

To the best of the knowledge of the author of this thesis, both the application of DSA and the utilization of the RELRAD methodology in the context of offshore wind had not been previously undertaken; thus, the applicability of these methods in the specific context of OWPPs could be thought of as a unique contribution of the thesis.

The aforementioned methodologies were applied in a case study of an OWPP situated at Utsira Nord. Through the analysis of performance efficiency and reliability, the case site OWPP was examined, enabling a comparison of the different methodologies. The results of this analysis, along with discussions and reflections, were presented at the conclusion of the case study. Consequently, this process yielded conclusions and insights that can inform future work and advancements within the field.

1.3 Structure of Thesis

Chapter 1 - *Introduction*: The introduction chapter of this report serves to explain the background, motivation, and scope of the research. It also outlines the structure of the thesis, giving a clear overview of how the content is presented.

Chapter 2 - *Previous Work: Fundamentals on Grid Architectures for Offshore Wind*: This chapter is from the previous work of the author of this thesis [3], and is included to enhance the narrative clarity and provide foundational knowledge for the subsequent sections of the Master's work. It focuses primarily on the CS, OSS, and TTS of OWPPs. By delving into these aspects, the chapter establishes a solid framework for the further exploration and analysis in the following sections.

Chapter 3 - *Previous Work: State of the Art Literature Review on Offshore Wind Grid Architectures*: This chapter presents a literature review from the previous work of the author of this thesis [3], which explores the state-of-the-art research on two specific technologies: AC system and Low Frequency AC system. Within this review, dedicated subchapters evaluate each technology's CS, OSS, and TTS. Moreover, an analysis of reliability and performance efficiency is conducted for both technologies. By drawing from this prior research, a comprehensive understanding of the advancements and considerations within these technological domains is established.

Chapter 4 - *Supplemental Theory*: The inclusion of a supplementary theory chapter serves the purpose of providing additional foundational knowledge that was not covered in the initial fundamentals chapter from previous work. This chapter addresses certain gaps in the mentioned fundamentals, such as delving into the basics of the relevant CS topologies, explaining the mathematical theories employed in the relevant methodologies, and providing further observations on transmission cables. By addressing these additional theoretical aspects, the objectives of this chapter are twofold: to achieve a more comprehensive understanding of the subject matter, and to provide fundamental knowledge for others to comprehend the practical application of this theory within the context of OWPPs.

Chapter 5 - *Methodologies: Performance Efficiency and Reliability Analysis of Offshore*

Wind Power Plants: This chapter outlines the approach taken to implement the methodologies in the case study and provides a detailed explanation of these methodologies in general. Specifically, it focuses on the DSA, the NR-based power flow methodology, and the previously mentioned combinatorial methodology for performance efficiency analysis. Furthermore, the chapter provides a comprehensive explanation of the RELRAD methodology for reliability analysis.

Chapter 6 - *Case Study: Utsira Nord*: The case study utilizes the reviewed methodologies to analyze the performance efficiency and reliability of a specific OWPP located at Utsira Nord. The case site is based on a set of assumptions and data presented at the beginning of the chapter. The chapter concludes with the presentation of results and discussions.

Chapter 7 - *Conclusions and Further Work*: As mentioned earlier, a key aspect of this Master's work was to gain knowledge on the various approaches for analyzing OWPPs in terms of performance efficiency and reliability. This final chapter provides a conclusion on how the objectives of the work were achieved and highlights the contributions of the research. Additionally, it offers suggestions for potential future work that can build upon the questions raised throughout this process.

1.4 Preface

The objective of this Master's work can be viewed from a dual perspective. Firstly, it involves conducting a comprehensive analysis of a case study of OWPP using various methodologies. This analysis includes examining different CS configurations and grid technologies, such as AC and LFAC, with a focus on evaluating their performance efficiency and reliability. Secondly, the thesis aims to compare the application and outcomes derived from these methodologies to establish a foundation for methodology comparisons. This work pursues to contribute to the research field by providing insights into the approach undertaken in the analysis of OWPPs, reflecting on the strengths and limitations of the methodologies employed. By doing so, the aim is to discover new possibilities and enhance the understanding of analyzing the performance efficiency and reliability of OWPPs from a methodological perspective.

An extensive literature review was conducted during the specialisation project phase, which preceded the Master's thesis work, in Autumn 2022. The Master's project problem formulation has been a direct result of the investigations conducted during the specialisation project, and as such it has been deemed essential to replicate some portions of the specialisation project report [3] in this Master's thesis in order to make this thesis a self-contained document with narrative clarity. It must be clearly pointed out that chapters 2 and 3 in this thesis are taken from the specialisation project report [3]. A majority of the sub-section 1.1 from the specialisation project report is used in sub-section 1.1 of this thesis.

In the mentioned specialisation project report [3], the possibility of including DC CS technology as a system configuration was considered. However, for the Master's project work, the AC-system and the LFAC-system were chosen due to the minor adjustments required in the methodologies compared to the DC CS technology. This strategic decision enabled a more effective analysis of at least two different technologies within the allocated time frame. By focusing on these systems, the Master's project work achieved a balance between exploring multiple technologies and ensuring the required robustness of the research.

2 Fundamentals on Grid Architectures for Offshore Wind

This chapter is replicated almost in its entirety from the previously mentioned specialisation project report [3], written in Autumn 2022. The only modifications made include the removal of content not further relevant to this Master's project work, and the editing of some sentences, including the appropriate re-numbering of references, to indicate the relevant transition from the specialisation project report to this Master's thesis.

2.1 Grid Architecture

A definition of grid architecture may be found in [6], which states: *"Grid Architecture is the application of system architecture, network theory, and control theory to the electric power grid. A grid architecture is the highest level description of the complete grid, and is a key tool to help understand and define the many complex interactions that exist in present and future grids"*. Grid architecture is a discipline based on system architecture, network theory, control engineering, and software architecture, which we apply to the electric power grid. An architectural description is a structural depiction of a system that helps users understand about the general shape of the system, qualities, and how the elements interact. Grid architecture provides a variety of functions, such as [7]:

- addressing grid modernization complexities
- detecting and reducing structural barriers, as well as setting important grid behavior boundaries
- constructing new structures to provide new capabilities or to improve grid characteristics such as resilience
- discovering theoretical, technological, and organizational gaps
- establishing a foundation for grid upgrading initiatives

This chapter will provide insight into system architectures for OW. Control theory will not be explained in detail. When it comes to OW grid architecture, the elements that

are the most relevant for this chapter are the CS, OSS, and TTS. WTs, switchgear, protection equipment, and subsea cables are examples of elements that fall within OW grid architecture but are not expressly covered in this study. However, primary power electronics such as inverters/converters in WTs, and hence the electrical output from WTs, will be considered in context of the CS. In Figure 2.1 a general architecture of an OWPP from [8] is illustrated.

It can be debated whether the term "grid architecture" accurately captures the scope of this chapter or if a term such as "offshore electrical system" (OES) would be more fitting. OW grid architecture refers to, in this chapter, the design and configuration of the electrical infrastructure used to transmit electricity generated by OWPPs to the onshore electrical grid. This includes the layout of transmission cables, the location of OSSs, and the placement of any other necessary electrical equipment. In [9], it is stated that the OES in a large OWPP is defined as a system that includes "several OSSs and offshore transmission lines." The authors further clarify that the term "OES" is used in their paper to refer to this system.

When numerous OWPPs are interconnected, this is sometimes referred to as an offshore grid. An offshore grid definition may be found in [9], which states: *"An offshore grid refers to an interconnected power grid between the OWFs and the onshore power networks, in which several OWFs share one or more OSSs and offshore transmission lines to save costs and submarine corridors"*, this is illustraited in Figure 2.2 [9]. They also refer to the offshore grid as a power network in the sea. The presence or absence of an offshore grid may influence the choice of technology in the OWPP system for transmitting the generated power to the PCC. The comparison between the OES mode and the offshore grid mode in the paper shows that the offshore grid mode requires more PCCs.

2.1.1 Collection System

Underwater cabling connects all WTs within a OWPP in an array configuration, allowing electricity generated by each unit to be transmitted to its own OSS. This network of cables is known as a *collection system* or *collector system*, it is also known as an *inter-array system* [10].

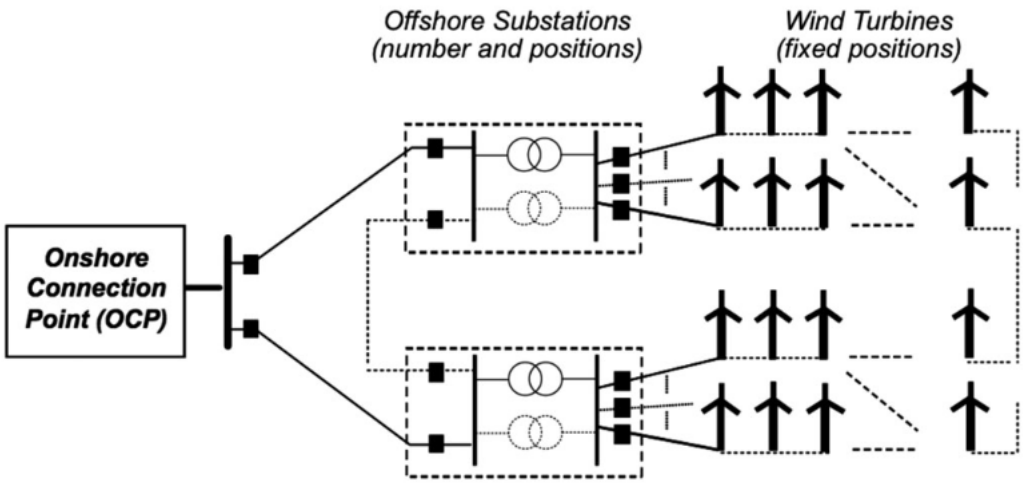

Figure 2.1: *General architecture of an OWPP from [8].*

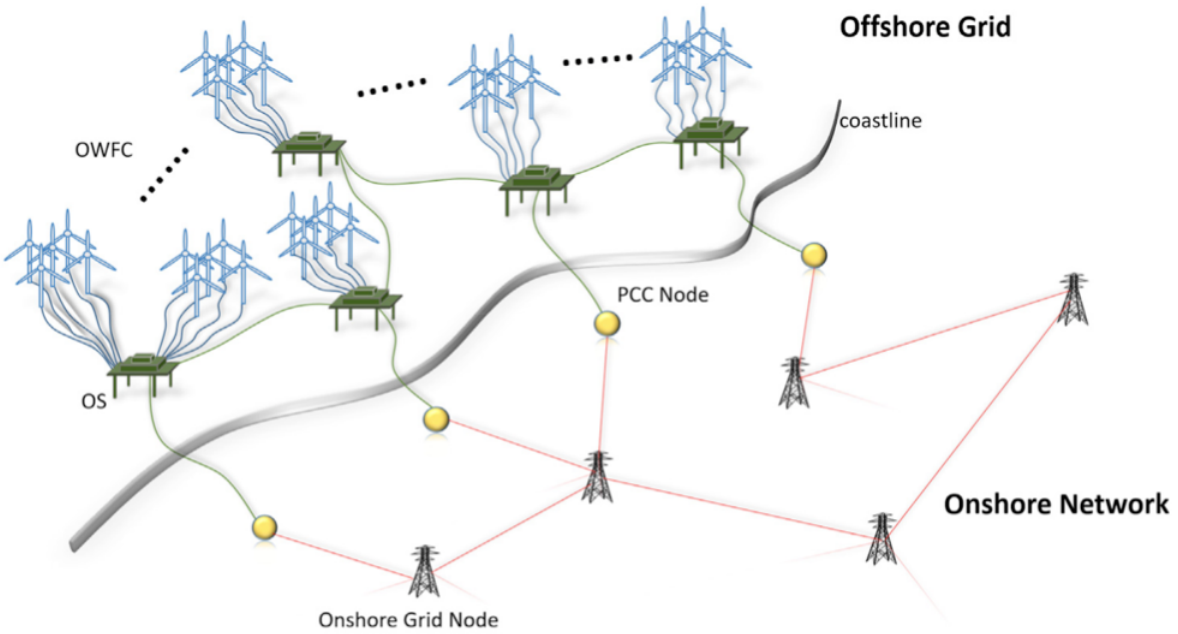

Figure 2.2: *Illustration of an offshore grid from [9].*

Due to the wake effect phenomenon, WTs are needed to be separated a particular number of rotor diameters apart from one another in OWPPs. This frequently results in enormous sites spanning tens of kilometers; such large sites will need significant cable routes to link all turbines to its belonging OSS. Because the CS cabling span the whole site, losses connected with the CS account for a large amount of overall OWPP losses [10].

As a result, it is critical to limit losses generated by the CS since reducing these losses can considerably lower overall electrical power losses across the OWPP, resulting in a more efficient OWPP and more power provided. This boost in output power will result in higher profits for site owners in the long run. These losses can be decreased simply by for example rearranging the CS cabling configuration [10].

For the OWPP CS to be constructed, the WTs and the OSSs must all be properly positioned. Engineers must go through various stages while developing an OWPP construction, one of which is the CS design. This is a challenging optimization challenge in which engineers attempt to strike a compromise between minimizing CS cable losses and minimizing development expenses associated with subsea cabling [10].

The CS must be developed to fulfill the general requirements outlined below [10]:

- the system must be constructed in such a manner that the risk of negatively impacting personnel and public health and safety is minimized, and it must meet all applicable health and safety regulations.
- compliance with all applicable codes and standards, such as IEC and IEEE, as well as national grid codes, distribution codes, and System Operator-Transmission Owner Code (STC).
- export capacity must equal at least 100% of OWPP output.
- reduce CAPEX (material and installation expenses).
- reduce OPEX (losses and maintenance expenses).
- maximized availability and reliability.
- as low environmental impact as possible

- robust component supply chain.
- redundancy against single faults to supply power to auxiliary loads.

The adequacy of the OWPP electrical infrastructure becomes crucial as the power capacity of OWPPs grows. The total efficiency, reliability and cost-efficiency of the OWPP will be heavily influenced by the CS architecture. The overall role og the electrical CS is to gather power from individual WTs and maximize total energy output. Depending on the size of the OWPP and the required level of reliability, a CS may be configured in a variety of ways. Various OWPP CS typologies are now in use in OWPPs, while others are in the design phase [10]. Radial design, single-sided ring design, double-sided ring design, and star design are some examples of existent structures. These all have unique strengths and disadvantages. Some of them will also be covered further later.

Offshore WTs are currently based on designs for onshore usage, delivering an alternating current output for direct connection to the electrical grid and complying with appropriate grid codes for power quality and fault response. To understand how WT generator technology may impact control techniques, the OWPP electrical system as a whole must be considered [10]. Figure 2.3, provided by Aker Solutions in [11], aims to illustrate a realistic CS for OWPPs that includes both bottom-fixed and floating turbines and OSSs.

2.1.2 Offshore Substation

The primary function of an OSS is to step up the voltage from the CS level to a higher level suited for exporting offshore power to the grid. The term "collection platform" will also be used in this chapter, reffering to a smaller platform for collection purposes only, as for example a T-branch. Because OWPPs are frequently placed far from shore, the voltage must be increased to prevent losses caused by long transmission lengths. OSSs are common for large scale OWPPs and those located more than 15 kilometers from shore [10]. The OSS of a large scale OWPP usually represents around 7% of the total cost. There is here no strict definition of what constitutes a "large scale" OWPP. However, factors like the number and capacity of WTs and other considerations like location and technology may be considered. A single OSS could typically support up to 500 MW. The

Figure 2.3: *A CS for an OWPP, with both bottom-fixed and floating WTs connected to OSSs via underwater cables. The OSSs are either floating or bottom-fixed, depending on the water depth [11].*

number of OSSs may rise as the size of the OWPP grows. The need for additional power capacity is typically the cause for having several OSSs [10]. OWPPs will typically have more than one OSS if it is financially feasible in order to increase the export reliability of the OWPP. An OSS is normally delivered by a supplier as a single component and weighs between 1800 and 2200 tonnes, for a 500 MW OWPP. These OSSs are typically not service-based, however often have a small work-shop inside. The key electrical system components of an OSS are as follows [10]:

- transformer, this is the main component of the OSS and also the main reason for the complexity that comes with an OSS.
- a backup diesel generator, in the event of a power outage via the export cable.
- switchgear, which is used in OSSs to distinguish between export cables (for TTS) and CS cables.
- converters are also placed at the OSS if the onward TTS utilizes HVDC.
- reactive power compensation equipment is utilized to offer the best reactive power

compensation for maximum power transmission to the onshore grid. These are typically depicted as items such as a reactor bank or a STATCOM.

- the OSS is earthed appropriately to guarantee power safety in the event of a safety concern or short circuit.

When planning a CS, the placement of any OSS is critical. This position has a large influence on the arrangement of the cabling and hence has a large impact on the costs of the project. OSSs should ideally be positioned in the OWPP to reduce the quantity of CS cables connecting all turbines. The number of OSSs will be decided by criteria such as the size of the OWPP, which will define the overall length of the CS cables, as well as the voltage level, which will determine the maximum possible length of cable. The maximum capacity of the OWPPs transformers and cables will also have an impact on the selection [10]. Lastly, the OWPP's necessary or desired reliability will impact this decision.

In Figure 2.4 an illustration of a floating OSS provided by Nexans in [12] can be seen. When the water depth approaches 50 to 70 meters, constructing OSSs on the sea floor becomes more difficult and expensive [12]. These OSSs can collect and transmit electricity from OWPPs, allowing wind power to be harnessed even in deeper waters.

2.1.3 Transmission to Shore

Cabling systems are critical in connecting an OWPP into a national grid or power transmission network since they transport large amounts of electricity over great distances to thousands of houses and millions of people. The cabling sector has grown significantly over the years as demand for subsea cables has increased continuously. Many nations pledge to invest in OW and connect it to their national power grids. As more OWPP projects in deeper oceans with changing climatic conditions are planned, improved cabling technologies will be necessary to build higher capacity and larger diameter power lines [13].

In view of international promises to considerably enhance OW capacity, the OW sector has identified CS and export cabling systems as critical areas where relevant cost savings

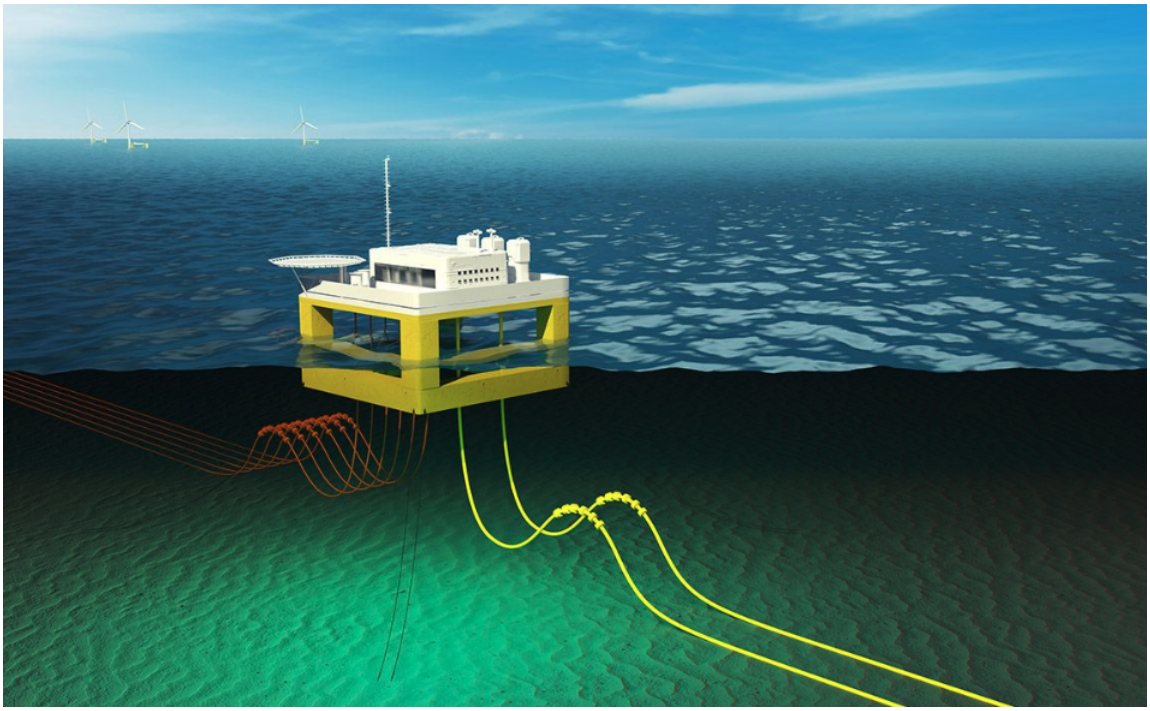

Figure 2.4: *An illustration of a floating OSS provided by Nexans in [12].*

should be examined. The cable installation technique, sequencing, and failure avoidance can further reduce lifetime costs for a specific OWPP, particularly for CSs and export cables. These are influenced by a number of factors, including OWF and coastal architecture, water depth, WT size, fixed or floating foundation type, environmental sea state and seabed conditions, and building, transportation, and installation arrangements [13].

In Figure 2.5 an illustration provided by Ørsted in [14] illstrated a simplified grid architecture for an OWPP including TTS between the OSS and the OCP.

2.2 Reliability and Availability in Offshore Wind

Due to the focus on reliability, the availability of OW will be discussed in this report. There is a need to define technical availability in this regard. As a percentage of the theoretical maximum, system availability is the percentage of time an individual WT or OWPP is available to generate electricity [15]. There is also another internationally agreed definition of commercial availability, however, the technical availability is the definition that will be used here. In Figure 2.6, a model that has been created by a group from International Electrotechnical Commission illustrating the availability of a WT in

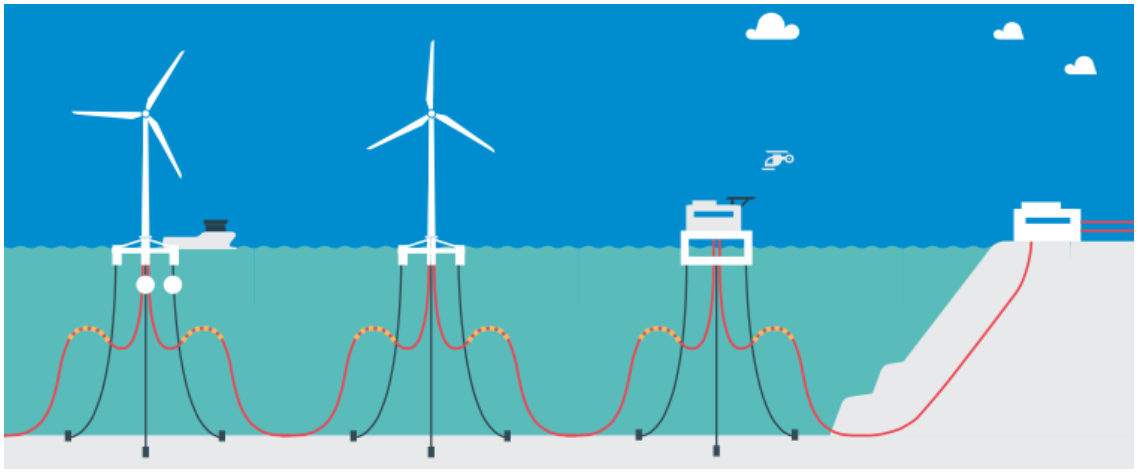

Figure 2.5: *An illustration of an offshore grid architecture provided by Ørsted in [14]. Here, floating OWTs connected to a floating OSS with TTS and connection to the PCC.*

terms of time and energy output is shown.

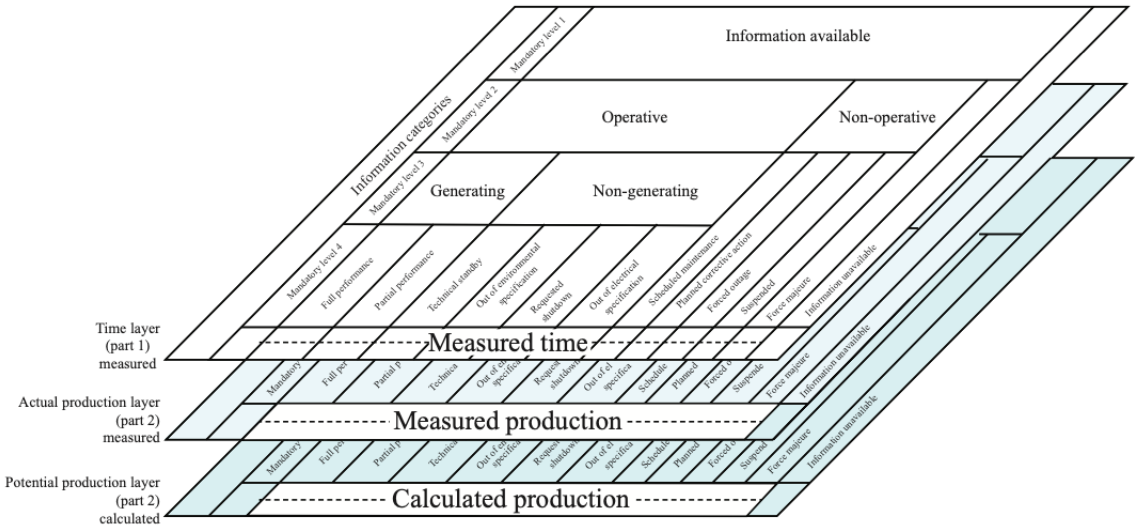

Figure 2.6: *A model from IEC 61400-26-1 (2019) found in [15] describing the availability of a WT in terms of time and energy output.*

Figure 2.7 shows how the availability of a WT varies depending on the machine's characteristics, its accessibility, and its maintenance procedures [15]. In respect to the theoretical availability and maintainability that will be impacted by all external circumstances, this figure illustrates the real availability of a WT or OWPP.

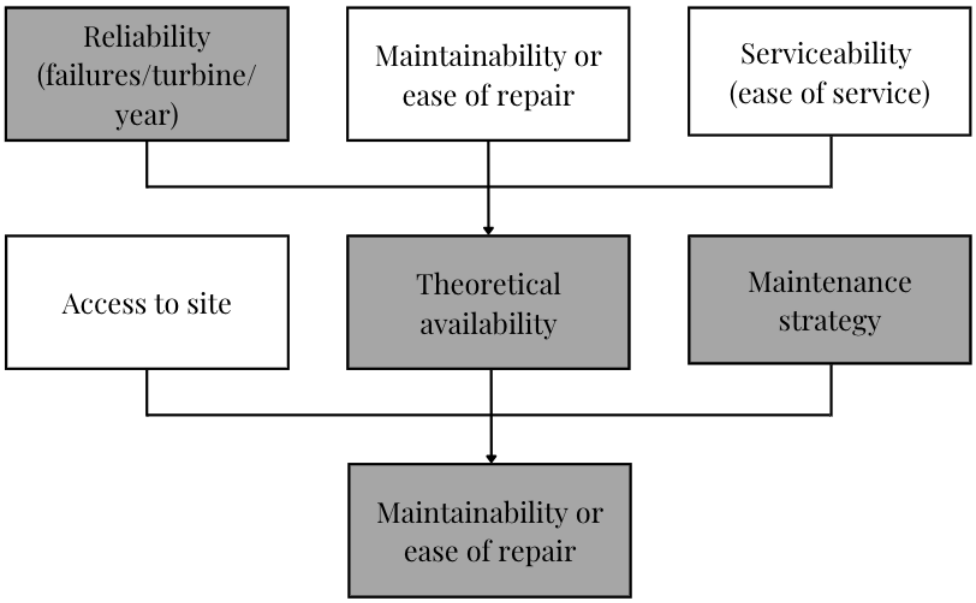

Figure 2.7: *Availability in relation to machine characteristics, location accessibility, and maintenance tactics, recreated from [15].*

In relation to reliability, the following will be used in this report [15]:

$$
\begin{aligned}
MTTF &: \text{Mean Time To Failure,} && \text{[hours]} \\
MTBF &: \text{Mean Time Between Failures} \approx MTTF, && \text{[hours]} \\
MTTR &: \text{Mean Time To Repair,} && \text{[hours]} \\
\lambda &: \text{Failure rate, } \lambda = 1/MTBF && [hours^{-1}]
\end{aligned}
$$

Also, Energy Not Supplied (ENS) needs to be addressed for later [16]

$$ENS = MTTR \cdot rGl \tag{2.1}$$

Where,

ENS :	Energy Not Supplied,	[MWh/year]
$MTTR$:	Mean Time to Repair,	[hours]
r :	failure rate,	[year/km]
G :	lost generation as a result of cable failure,	[MW]
l :	cable length,	[km]

The Average System Availability Index (ASAI) of an electric distribution system is often presented as a percentage and can be defined as [17]:

$$ASAI = \frac{S}{C} \tag{2.2}$$

Where,

S :	customer hours of available service,	[hours]
C :	customer hours demanded,	[hours]

Some elements are necessary to understand in order to comprehend the reliability and availability difficulties with OW. An important factor in this is how weather affects the reliability and availability of OW. It is also crucial to realize that only a limited amount of reliability data on the layouts and grid connections of OWPPs is available [15].

The entire quantity of electricity that may be transmitted can be limited by the size of the offshore transformer. It may be feasible to link more than one substation transformer in parallel to provide increased OWPP production capacity for OWPPs with capacities in the range of more than 500 MW. This will also increase wind power availability since, in the event of a transformer failure due to a fault, at least a small amount of the power can be transmitted [10].

2.3 Efficiency in Offshore Wind

The efficiency of OWPPs is important to their success. It not only affects the profitability of the project, but it also plays an important part in lowering the environmental effect of wind energy. The design of the WTs, the choice of CS and its topology, the OSSs, and the TTS are all elements that can impact the efficiency of OWPPs. The various technologies that will be reviewed in this paper will have varying efficiencies for different projects. In this report, efficiency refers to performance-efficiency.

For a variety of reasons, offshore and onshore wind power plants can have varying degrees of efficiency. Wind speed and direction, WT design and grid architecture are all important aspects that can impact the effectiveness of wind power plants. The wind speed and direction are significant differences between offshore and onshore wind. OWs are often stronger and more constant than onshore winds, which can increase the efficiency and power output of offshore WTs. The best option for an OWPP may not be the same as the best option for an onshore wind power plant. DC collecting methods, for example, may be more efficient for large scale OWPPs but may not be appropriate for smaller onshore wind power plants. OWPPs in general may require more complex and costly grid architectures to enhance efficiency when compared to onshore wind power plants.

Although this chapter will not be specifically about WTs, but the gird architecture of an OWPP, the power generated in a WT is the basic of this and will be used later. The power generated for different wind speeds for a WT is given by [18]:

$$P_{gen_{wt}}(v_w) = 0.5\rho A C_p v_w^3 \tag{2.3}$$

Where,

v_w : wind speed,	$[m/s]$
ρ : air density,	$[kg/m^3]$
A : area swept by turbine blades,	$[m^2]$
C_p : power coefficient	

The yearly energy generated by WTs is estimated by multiplying the power generated as a function of wind speed, the probability of the wind speed occurring, and the number of hours in a year [18]. Hence:

$$E_{gen_{wt}}(v_w) = N_{wt} \int_{V_{min}}^{V_{max}} (P_{gen_{wt}}(v_w)) f(v_w) 8760 dv_w \tag{2.4}$$

$$f(v_w) = \frac{k}{c}(\frac{v_w}{c})^{k-1} e^{-(\frac{v_w}{C}^k)} \tag{2.5}$$

Where,

f_{WB} : Weibull probability distribution function

V_{min} : cut in wind speed, $[m/s]$

V_{max} : cut out wind speed, $[m/s]$

N_{wt} : number of WTs

k : Weibull shape parameter, $k = 2$

c : Weibull scale parameter, $c = 9.5$

Other key equations and viewpoints on the efficiency of the various technologies will be discussed further in the efficiency section for each of the technologies.

3 State of the Art Literature Review on Offshore Wind Grid Architectures

This chapter is replicated almost in its entirety from the previously mentioned specialisation project report [3], written in Autumn 2022. The only modifications made include the removal of content not further relevant to this Master's project work, and the editing of some sentences, including the appropriate re-numbering of references, to indicate the relevant transition from the specialisation project report to this Master's thesis.

Both AC and DC are currently being considered for offshore transmission in both CSs and TTS [19]. High Voltage DC (HVDC) is traditionally used for long distances due to lower power loss costs compared to High Voltage AC (HVAC). However, HVAC is also being considered for longer distances through the use of higher voltage AC cables and mid-cable reactive power compensation [19]. The ability to efficiently collect and transfer the electricity produced by individual WTs to shore will be a barrier for future development of OWPPs farther offshore [1]. Multiple OSSs would be needed to shorten the cable length in order to collect power in a large scale OWPP, say 2 GW in size, with numerous WTs. Operating CSs at a higher collecting voltage, such as 66 kV AC, as an alternative to the existing 33 kV AC voltage level for offshore CSs has been a subject of debate over the past years [1]. Moving the CS voltage level from 33 kV to 66 kV might save 1.5% of the cost of electricity, according to Trust-funded research in the United Kingdom [1].

HVAC and HVDC are currently the most often used technologies for offshore transmission [19]. The majority of OWPPs are connected by HVAC, however as transmission undersea cables become more distant, HVDC is being evaluated as a practical solution in a number of projects [20] and for the future of large scale OW. Other technologies have been proposed for the future of large-scale OW in addition to each of these well-functioning alternatives that has been used on land for a long time. A potential solution that might lower overall expenses and increase the total supplied active power to shore is LFAC.

When it comes to the CS, a DC CS is a relatively new option for the wind sector that may

be able to reduce total expenses. The technology is still in the research phase [21]. The LCOE for OW may decrease as a result of the potential of this system to remove some of the most expensive components of the CS. A DC CS is typically used in conjunction with a HVDC TTS. The potential for combining the technologies reviewed in this chapter could be further explored. In this section, the efficiency, reliability, and cost of each of these technologies will be reviewed.

3.1 HVAC

HVAC technology is arguably the most common choice for transmitting the power produced in the OWPP to shore, both in the CS and for the TTS. In the CS, the most typically employed voltage level is 33 kV. This option is restricted by existing technology as well as power capacity, cable length, and losses [22]. Higher voltage levels improve transmission capacity and maximum cable length. OWPPs with greater voltage level in their CS can be directly linked to shore, without the need of a complex OSS. It can be argued that achieving this using a conventional 33 kV system would be implausible unless the distance between the OWPP and the shore is significantly shortened. Hence, a higher voltage level enhances the potential of linking small OWPPs located further out from shore and large OWPPs located closer to shore without the need of an OSS. Longer CS cables can be realized for OWPPs covering a broad area with greater voltage, reducing the demand for more than one OSS [10]. This section will review the options for the use of AC systems, with a focus on unconventional, increased voltage levels, in the CS, such as 66 kV and even 132 kV.

OWPPs running at greater CS voltages than the standrad of today can save up to 1.5% on energy costs [16]. Higher voltage in CSs possibly has the potential to minimize the number of cable strings entering a platform as more wind turbines can be linked per string, reduce system losses, boost availability, reduce total cable length, and reduce the number of OSSs. This significantly reduces the cost of designing future OWPPs. Furthermore, when the power rating of current turbines improves, the cost savings from a 66 kV CS, or even higher, increase even more, implying that the switch to higher voltage is a rational decision [16].

The majority of the existing literature on the benefits of increasing the voltage in HVAC OWF architectures looks at the potential of increasing the CS voltage to 66 kV, whereas 132 kV is a state-of-the-art issue that is not widely covered in today's academia.

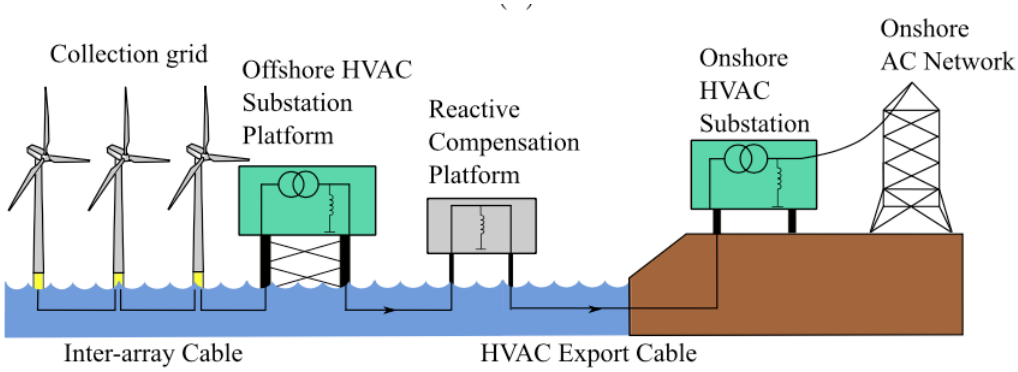

Figure 3.1: *Possible offshore topology with an HVAC grid [20].*

A medium voltage AC (MVAC) CS, one offshore substation with transformers, switchgears, and reactive power compensation make up the HVAC topology shown in Figures 3.1 and 3.2. In addition, the topology includes a platform for compensating reactive power in the center of the link to the coast; the presence of this component depends on the distance to shore.

3.1.1 Collection System

As the power capacity of OWPPs and turbines has expanded, collecting voltage levels have risen from 11 kV to 33 kV [10] and 66 kV [23] today. However, according to one research, stepping up the voltage from 33 kV to 132 kV offshore is most cost effective for longer distances, because the cost of the offshore substation is less significant when compared to the cable expenses, and the losses are substantially lower [10]. It should be

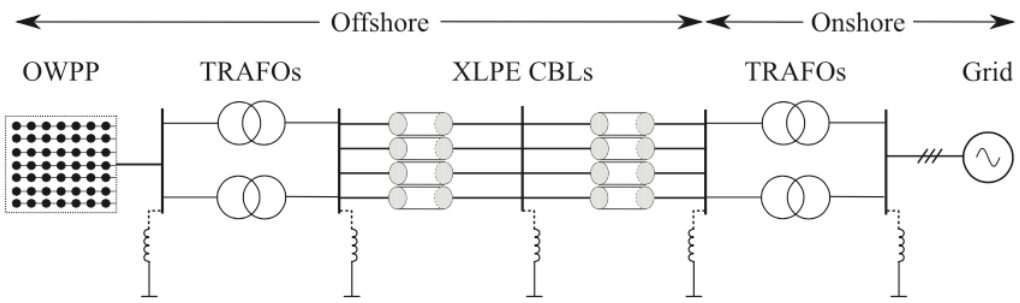

Figure 3.2: *Possible offshore grid topology with HVAC [20].*

noted that 66 kV OWPPs were just achieved. According to [24], ABB's new WindSTAR transformer is the first transformer in the world that can fit inside the tower or nacelle of a WT and boost the voltage level up to 66 kV for up to 9 MW WTs. One of the OWPP that is running today and utilizes 66 kV in its CS is Borssele 1 and 2 [23].

There are numerous ways of designing the CS in an OWPP. Redundant string cluster topology is one of them, this design is illustrated in Figure 3.3. It is built with a single loop and a switch. This provides some redundancy by allowing WTs to feed on-shore through redundant cable links. It is economical, but it requires the installation of a switch in a WT or substation. Some OWPPs are using this method [25].

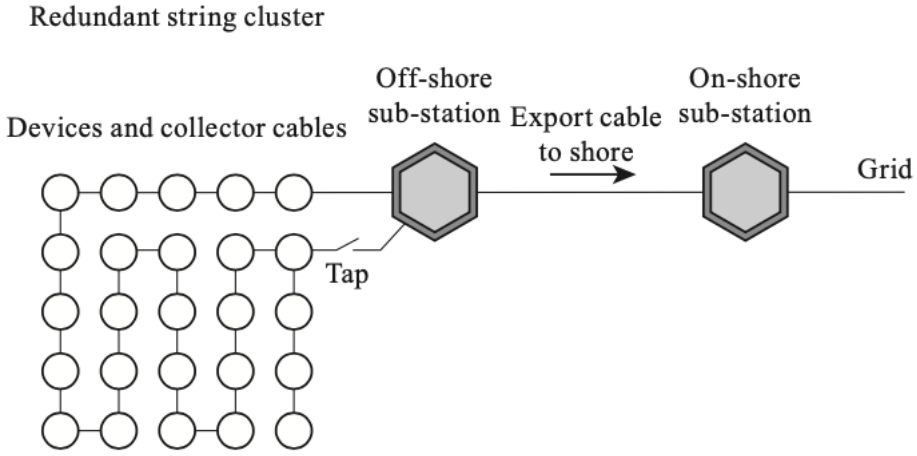

Figure 3.3: *Redundant string cluster CS from [25].*

A comprehensive comparison of 33 kV AC (rated at 36 kV) radial and ring CSs was conducted in [16], together with 48 kV AC (rated at 52 kV) and 66 kV AC (rated at 72.5 kV) radial and ring CSs. This included analysis and design work for all of the essential technical components of the system, such as cables, switchgear, transformers, WT topologies, and OSSs. The CS designs were compared and optimized. To compare the systems, a comprehensive cost-efficiency analysis was performed. For an OWPP with a lifetime of 25 years, this covered CAPEX, O&M, system losses, and cable failure losses. A qualitative comparison was carried out to discover additional risks and advantages, such as supply chain, health and safety, and O&M factors. Moving to 48 kV or 66 kV indicated a significant improvement in total life costs as compared to 33 kV. However, the results for 66 kV was the greatest, and the number of 48 kV equipment manufacturers is small in comparison to 66 kV, giving no incentive to select 48 kV over 66 kV [16].

Another advantage of employing higher-voltage to CSs is that they can reduce the number of cable strings required in CSs for large scale OWPPs because each cable has a larger capacity [10]. This may become an appealing alternative, particularly as WT dimensions increase. Currently, one of the problems of utilizing voltages higher than 33 kV for the CS are as follows. Commercially accessible "dry-type" transformers rated over 33 kV and capable of stepping up from an appropriate generating voltage, such as 3.3 kV, are in short supply. They are also more costly than 33 kV transformers, which are more accessible [10]. Furthermore, collection cables with a voltage of 33 kV or less can be of the 'wet design,' which eliminates the need for metallic moisture barriers to surround the cable as an outer sheathing layer or around the insulated core (s). Higher-voltage underwater cables are already available in a 'dry design,' with a lead sheath acting as a water barrier. Their disadvantages include greater cable capital costs and perhaps higher installation costs owing to the added weight, and the lead sheath is prone to stress failure whenever movements or vibrations occurs [10].

A full cost-efficiency analysis (cost, supply chain, certification, insurance, etc.) is necessary for a given project to make an educated choice on whether to utilize 33 kV or higher-voltage collecting cables because the influence on the total OWPP design might be significant [10].

3.1.2 Substation

Because HVAC is the most commonly used technology in OWPP TTS, the majority of what is discussed in 2.1.2 also applies to an HVAC OSS. However, this HVAC part investigates the options for boosting the voltage level in the CS. Switchgear, transformers, cables, and related accessories are the key substation components connected to upgrading CS voltage [26]. It can be argued that increasing CS voltage would be a greater challenge for turbine manufacturers than OSS manufacturers, because an increased voltage step would be necessary at the turbine, but not certainly on the OSS, depending on the TTS voltage.

Some of the major manufacturers in the industry (ABB, Siemens, Schneider, and others) currently provide 66kV switchgear systems [26]. Dry type transformers are typically em-

ployed in OW applications, with their more robust features and environmentally friendly attributes justifying the greater cost of this equipment. These are usually found in the nacelle. Dry type transformers have not been widely available above 33 kV, although some manufacturers (ABB, CG) are supplying transformers insulated with biodegradable synthetic ester oils for 66kV LV applications. These would be more suited for placement near the base of the turbine tower, where vibration levels are lower [26].

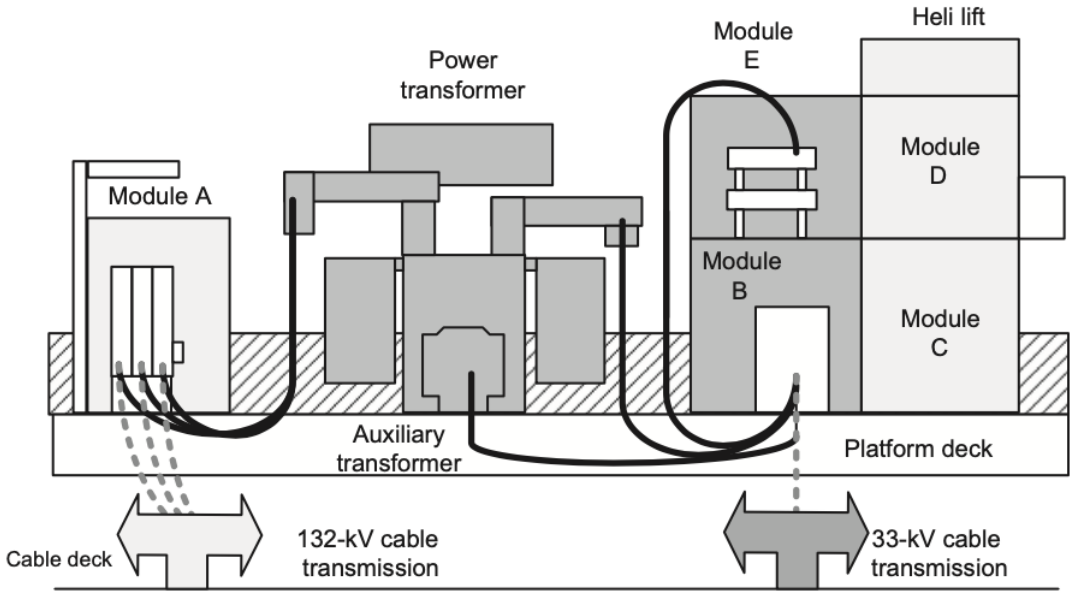

Figure 3.4: *A typical layout of an 33/132 kV AC OSS [10].*

In Figure 3.4, a typical HVAC OSS is depicted. The details are unimportant here, however it is clear that the transformer is a crucial component of the OSS. When the size of the transformer is compared to the size of the heli lift, it is obvious that it is large and complex.

3.1.3 Transmission to Shore

HVAC TTS has long been regarded as the industry standard for transferring electricity from an OWPP to shore. However, as previously said, the OWPPs are positioned further offshore, and HVAC has become a viable option to HVDC for long transmission distances also for OW.

In Figure 3.5, a typical operating 33 kV OWPP CS configuration is depicted, which is the London Array in the United Kingdom. It is a large scale OWPP with an AC radial

structure, including independent redundant string clusters and 150 kV HVAC export cables for TTS. Each radial branch is a loop with switches at the end of the loop and at the OSS to offer redundancy in the case of an CS cable failure [25]. This is even another example of the redundant string cluster shown in Figure 3.3.

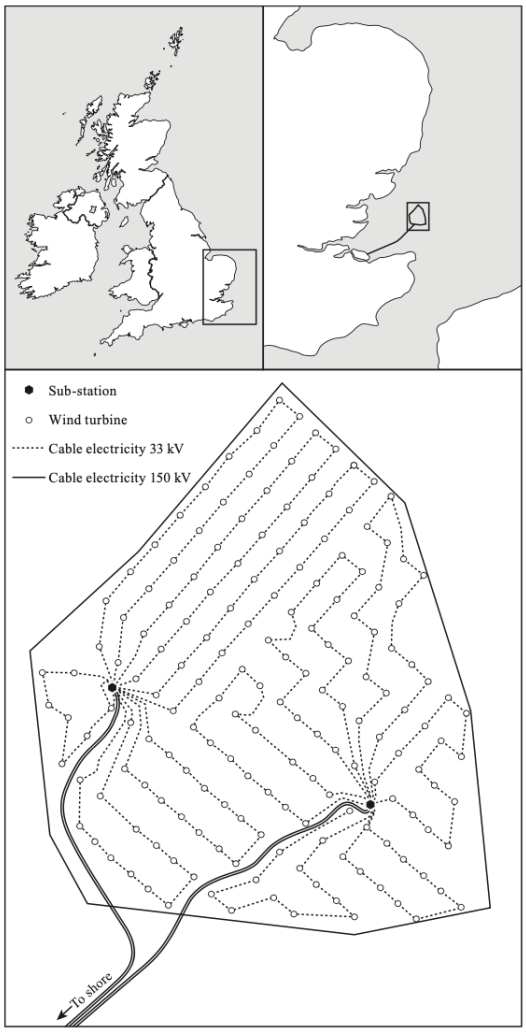

Figure 3.5: *Layout of the OWPP London Array [25].*

The London Array has an installed capacity of 630 MW distributed on 175 WTs with a capacity of 3.6 MW each. The CS has a total length of 200 km with AC cables and a voltage level equal to 33 kV. The CS is connected to two OSSs with transformers stepping up the voltage to 150 kV AC. The TTS has a total length of 53 km with double lines and is connected to the 400 kV main grid at shore [25].

3.1.4 HVAC in terms of Reliability

OWPP availability is determined by the availability of both generators and auxiliary equipment as cables, transformers, and switchgear. The generator availability was assumed to be 100% for the studies indicated in 3.1, since it was crucial to focus on the differences between systems at different voltage levels. Hence, a difference in the generator availability would have contributed with a higher uncertainty to the study. The reliability of cables was the most essential component in terms of availability, and the one that might possibly alter the most between the basic case and the higher voltage systems. This was due to differences in the lengths of the radial threads between the basic case and the higher voltage design. To comprehend the impact of cable availability, the Mean Time to Repair (MTTR) and failure rate of the cable have to be determined. It was discovered that life cycle cost is highly sensitive to cable failure rate estimates, hence a broad range was chosen. On a 1 GW OWPP with 200 wind turbines and 200 km of cable installed, the worst failure rate anticipated three failures per year. On the same OWPP, the best failure rate anticipated one failure per six years. Eq. (2.1) was used to calculate the reliability of the CS, taking into consideration the cable failure rate and the mean time to repair.

It was estimated that the cable would fail halfway down the string, resulting in slightly more than half of the generators in a string being lost on average. Furthermore, the best case MTTR values were one month, two months, and three months, with the worst case being three months. While for the transformer, the estimated availability in terms of MTTR was best case 10 days, 20 days, and worst case 30 days.

Benefits in reliability for the high voltage case could be seen when comparing the 66 kV voltage level case to the 33 kV voltage level case. This included all possible scenarios, from greatest availability to worst.

3.1.5 HVAC in terms of Efficiency

As previously stated, the purpose of this HVAC section is to shed light on the possibilities and obstacles of boosting the system voltage for an OWPP linked to shore through

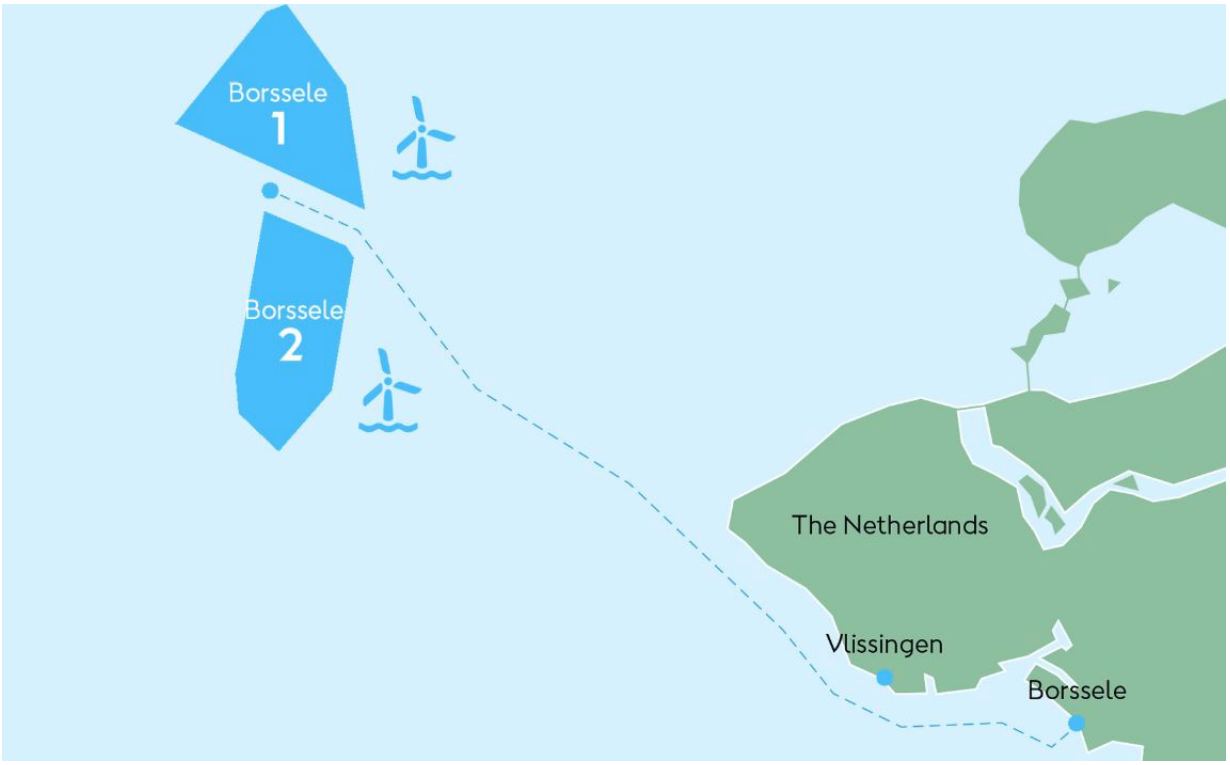

Figure 3.6: *An overview of the OWPP Borssele 1 and 2 from [23].*

HVAC. The fundamental reason for this has already been mentioned: reduced energy losses, particularly from the CS. The sub sections 3.1.1 and 3.1.3 is also considering some efficiency perspectives of the CS and the TTS of AC systems.

A study in [27] is looking at the OWPP Borssele Wind Farm. An overview of Borssele 1 and 2 can be seen in Figure 3.6. Borssele 1 and 2 is located around located around 23 kilometers off the Dutch coast in 14 to 36 meters deep water. The two OWPPs contains a total of 94 wind turbines providing 752 megawatts (MW) of power [23]. Hence around 8 MW installed capacity for each WT. However, according to the data used in [27], one hundred 7 MW WTs in each CS are analyzed, for a total of two CSs. Other wind resource data was also supplied, but it is not relevant here. The CSs for both 33 kV and 66 kV can be seen in Figure 3.7. There are 430 km of inter-array cables for 33 kV and 310 km for 66 kV in the analyzed case.

In Figure 3.8, a plot of power losses in the CS of the OWPP Borssele calculated in [27] can be seen. The CS exists of two clusters. Logically, power losses in the CSs are reduced by 66 kV compared to 33 kV. Some more detailed results can be seen in Table 3.1. These results has been found by finding the probabilistic expected values from Eq. (3.1) and

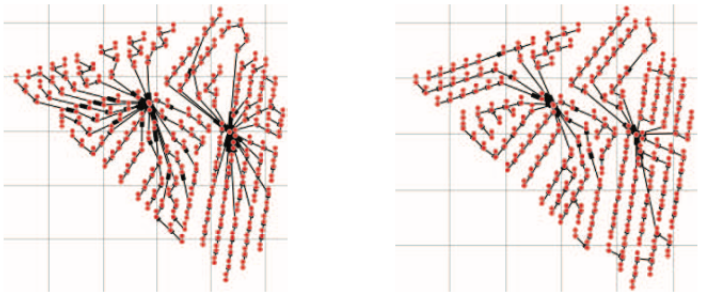

Figure 3.7: *CS architectures for 33 kV and 66 kV for the case in Borssele Wind Farm from [27].*

annual produced energy of the OWPP from Eq. (3.2) [27]. The losses for the 33 kV CS are twice as high as the losses for the 66 kV CS.

$$E[Y] = \int_{v_{min}}^{v_{max}} Y(v) * f_{WB}(v)dv \tag{3.1}$$

$$E_{annual} = T \int_{v_{min}}^{v_{max}} P_{PCC}(v) f_{WB}(v)dv \tag{3.2}$$

Where,

Y : produced power

v_{min} : cut in speed

v_{max} : cut out speed

f_{WB} : Weibull distribution function

p_{PCC} : power at the PCC

T : expected produced power at the PCC

3.2 LFAC

A design that may lower the overall cost of current transmission lines has been proposed using LFAC technology. Comparing HVAC systems to HVDC systems, a cost decrease

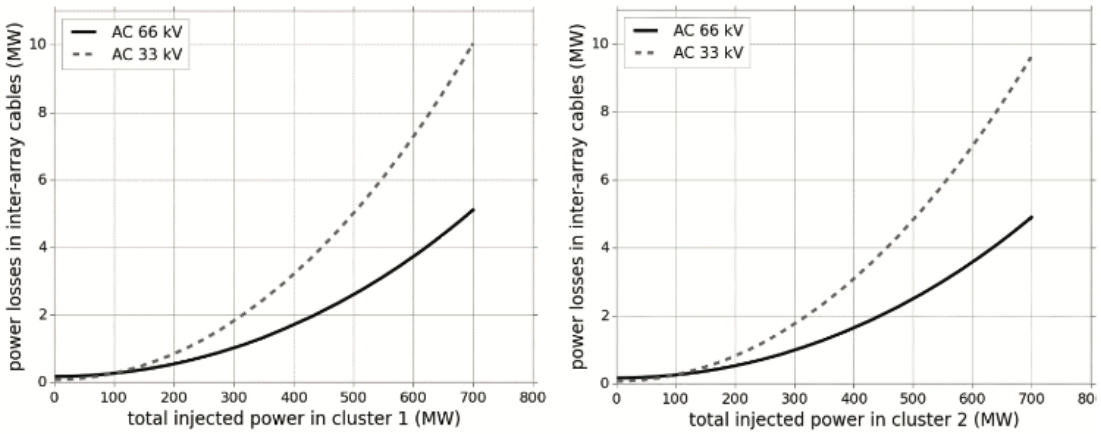

Figure 3.8: *Losses in both clusters for 33 kV and 66 kV from the case in [27]. Cluster 1 to the left and cluster 2 to the right.*

Table 3.1: *Results from case study in [27] on power losses in CS.*

Cluster	**Wind turbines Mean annual produced power (MW)**	**Voltage level (kV)**	**Mean annual inter-array power losses (MW)**	**Losses percentage of mean annual produced power**
Cluster 1	335	33	3.77	1.13 %
		66	1.98	0.59 %
Cluster 2	335	33	3.62	1.08 %
		66	1.90	0.57 %

might be made by eliminating the offshore converter and boosting the HVAC cable ability to deliver power while running at low frequency. Since a century back, Central and Northern European railway networks have used LFAC, which is normally 16.7 Hz [20]. The requirement for long-distance railroads and the existence of significant eddy current losses caused by normal AC frequencies were the driving forces behind the introduction of low frequency. Therefore, LFAC technology has been suggested in the literature as an alternative to conventional HVAC and HVDC transmission systems for OWPP integration [20]. LFAC may be a relevant technology for use in both the CS and the TTS for several OWPPs in the future.

As mentioned and opposed to HVDC, LFAC does not require offshore converter stations, which is one of its key advantages. By eliminating this need, the grid complexity is decreased [28]. One of the other key benefits of the described transmission system is the expansion of the maximum transmission range due to the enhanced power transfer capacity of the HVAC cables working at lower frequency. A significant voltage drop along the cable and cable current carrying capacity are the two factors that restrict the amount of power that may be sent. Active and charging current, which are influenced by frequency, transmission distance, and cable capacitance, define this current capacity. Low frequency operation of cables results in decreased charging current, which in turn results in less reactive power generation, increasing the maximum amount of active power that may be delivered over the cable [20].

In general, wind farms that are located further offshore than 80 km utilise, and are expected to utilise HVDC transmission to shore [28]. As a result of several influencing factors, such as water depth, wave conditions, grid stability and reliability, this number will vary. An examination of this will be conducted in more detail.

In Figure 3.9 and Figure 3.10, the topology of an LFAC transmission system is depicted. A CS that can operate at different system frequencies is connected to a converter. The converter is an AC/AC converter, which is said to have been created utilizing a Back-to-Back (B2B) architecture with Voltage Source Converters (VSCs), is used to run the system at low frequency at all times. The offshore substation would include LFAC transformers and also switchgears connected to the onshore substation through e.g. XLPE cables. The B2B converter and transformers has the potential to work at grid frequency

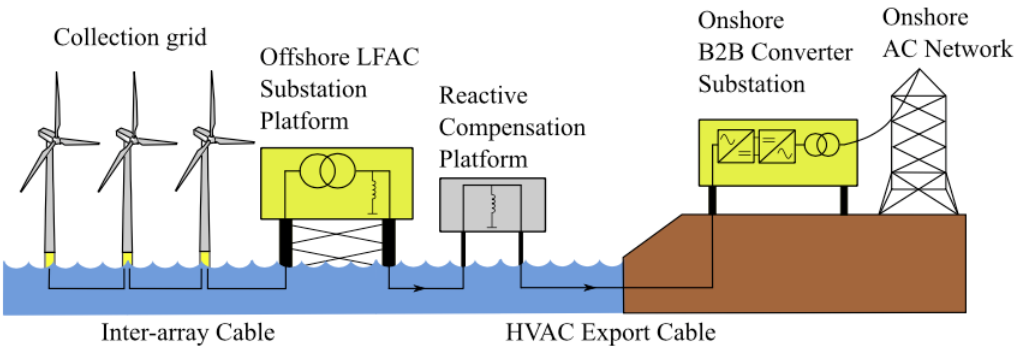

Figure 3.9: *Possible offshore topology with an LFAC grid [20].*

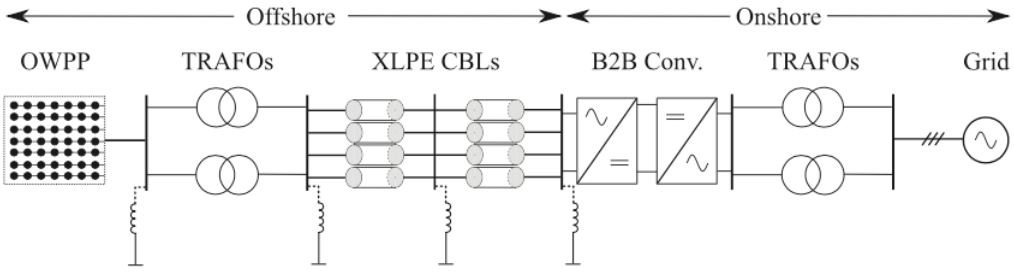

Figure 3.10: *Possible offshore grid topology with LFAC [20].*

and are located at the onshore substation. Switchgear and LFAC transformers linked to the onshore substation through e.g. XLPE cables might be part of the OSS. The onshore substation house the B2B converter and transformers, which have the capacity to operate at the grid frequency. In order to specify the combinations shown in Figure 3.10, reactive power compensation could be installed on both substations and in the center of the cable. Reactive power regulation is not necessary on the onshore grid side since the B2B converter can also control reactive power [20].

In addition to the offshore converter station being eliminated, the adoption of LFAC has significant effects on the offshore infrastructure. The size of the transformers and reactors will likely rise due to the lower frequency, which will also have an impact on the size of the OSSs.

3.2.1 Collection System

In literature, different CS possibilities for use with LFAC transmission have been looked into; these include using a network that transmits LFAC at the same frequency or pro-

ducing LFAC using a DC CS and an offshore inverter [20].

Using DC CSs was primarily done to avoid redesigning the WT to produce low frequency. The low frequency voltage waveform must be produced by an offshore inverter station, though. Since there is still an offshore conversion step that adds to the transmission system's total cost, reliability, and efficiency, the offshore inverter may make this form of LFAC transmission system less favorable. Additionally, the offshore inverter adds harmonics to the LFAC transmission system that must be removed before the onshore converter [20]. It has been discovered that when LFAC transmission is utilized with a DC CS, it performs comparable to HVDC and conventional AC systems in terms of cost and reliability [20]. It is clear that the type of CS used and whether an offshore inverter is necessary are the primary factors influencing any reliability differences.

Due to the absence of an offshore converter and the consequent reduction in overall interruption time, analysis has revealed that the reliability issue is considerably altered when considering an LFAC offshore CS, leading to a more reliable supply of electricity from the OWPP. This shows that an LFAC CS should be the preferred design option for OWPPs connected to LFAC transmission, despite the knock-on effects of size and expense for frequency dependant components at the turbines.

Due to the larger size of the transformer stated above, LFAC could also call for a redesign of the offshore WT. The transformer and converter are now located in the nacelle of the turbine, however under these circumstances and as the WTs themselves become bigger, the transformer will become progressively larger and heavier. Due to space and weight restrictions in the nacelle of upcoming huge offshore WTs, it could be more practical to place the transformer in the base of the WT [28].

When selecting a generator type, a number of generator types have been assessed with LFAC. For fixed speed generators connected directly to the grid, the gearbox ratio must be reduced to provide the appropriate frequency. According to simulations, the generator type and LFAC had unsteadiness during startup. A redesign would likely be required to securely attain 16.7 Hz at the turbine output, which would need a sizable inertia. The size of the fixed speed machine will thus rise. The amount of space needed in the WT is significantly enhanced if this is added to the demand for a larger WT transformer [28].

When used in conjunction with an LFAC transmission system, a doubly fed induction generator (DFIG) has demonstrated the ability to satisfy the criteria for reactive power production from grid codes in a manner similar to that of a 50 Hz DFIG. However, the size of the turbine would still increase if a DFIG was to be used in conjunction with LFAC.

The generator size and weight should be kept to a minimum in future WT systems. Compared to DFIGs or fixed speed turbines, Permanent Magnet Synchronous Generator (PMSG) systems are expected to be lighter and require less maintenance. Due to its reduced space requirements compared to regular WTs and just requiring a full converter reconfiguration, PMSG WTs are recommended as the best alternative for producing wind power at 16.7 Hz. The WT transformer, which scales by the same factor as the previously stated AC platform transformer, is the sole component that requires more space [28].

3.2.2 Substation

The size advantage of the low frequency system over its HVDC equivalent may be its most significant benefit. This platform simply includes the appropriate AC switchgears and the AC transformer in the LFAC system. The transformers, reactors, and OSS are only a few of the components of the offshore network that are significantly impacted by changes in frequency. The low frequency transformer is bigger than at 50 Hz, which is one drawback of LFAC. The reason for this is that an LFAC transformer has to be developed with a larger core cross-sectional area to make up for the decreased frequency in order to maintain the same amount of power. This can be seen in Eq. (3.3). The core cross-sectional area is inversely proportional to the frequency according to Eq. (3.3) assuming no other changes. Hence, the core cross-sectional area of a 16.7 Hz transformer would need to be three times bigger than a 50 Hz transformer. Additionally, the solution of the LFAC switchgear would be larger than the 50 Hz switchgear, which might result in higher manufacture and installation costs [28].

$$A_{core} = \frac{E}{4.44 f N B_{sat}} \tag{3.3}$$

	Cycloconverter	Matrix converter	Back to Back VSC
Semiconductor	Thyristor	Bilateral monolithic switch	IGBT
Conversion type	AC–AC	AC–AC	AC-DC-AC
Power Control	P only	Q control depends on $P > 0$	Independent P and Q
AC filters	Large (3^{rd}–13^{th} harmonic)	Small	Small (31^{st}–35^{th})
Black start capability	No	No	Yes
Weak system performance	Requires strong grid (commutation failures)	Good (no commutation)	Good (no commutation)
Fault ride through capability	Not decoupled	Not decoupled	Decoupled
Power factor	0.78 lagging	Controllable	Controllable
Frequency response	Only from Wind farm	Only from Wind farm	From both Wind farm and DC capacitor
Voltage control	Needs external equipment e.g. SVC	OK (limited output – 0.866 of input)	Independent Q control

Figure 3.11: *A comparison of three different converter options at the PCC [28].*

Where,

A_{core} : core-cross sectional area of transformer, $[m^2]$

E : Rated voltage, [V]

f : Frequency, [Hz]

B_{sat} : Saturation flux density, [T]

N : Number of turns

A Cycloconverter (thyristor-based converter) or a VSC are the two major alternatives for efficiently connecting LFAC to the grid [29]. Although the cycloconverter is the less costly alternative on its own, the technical requirements of main grid connection and compliance would need additional expenditures in the form of additional filtering and reactive compensation. Alternatively, with dynamic control over both active and reactive power and a more advanced switching pattern that eliminates the need for lower order harmonic filters, the VSC will reduce technical problems when connecting to a main grid [29].

3.2.3 Transmission to Shore

Among other requirements, a converter must be able to satisfy the grid code specifications at the PCC. As a function of this, it makes sense to examine a few different converters at the OCP to determine their strengths and limitations. The literature has already done this, as shown in Figure 3.11. It summarizes the key comparative factors and compares the three converter alternatives, Cyclocoverter, Matrix converter and B2B VSC.

Active power control may be provided via the cycloconverter control, and based on the system frequency, control techniques can be created to give frequency response. The onshore converter of an OWPP must have control over reactive power in order to maintain the voltage in the onshore grid at the OCP. The power factor of 0.78 for the cycloconverter, that can be seen in the mentioned figure, would require reactive power compensation [28].

Traditional matrix converters have some limitations, but reactive power can be controlled to a larger extent. The capacity to compensate for reactive power is constrained by the topology; it is not feasible to generate reactive power when active power is zero. The B2B converter in contrast does not have this constraint because of its built-in energy storage. It may deliver reactive power at zero output current, that is, when the active power is zero. This is a significant benefit when taking into account the connectivity to a weak network, where management of reactive power and voltage is essential to maintaining the stability of the network stability [28].

3.2.4 LFAC in terms of Reliability

Offshore sites might provide challenges for reliable operation. Because of the limitations in reaching offshore infrastructure, the repair time for offshore components is sometimes quite long [29].

Since LFAC aims to compete with HVDC for distances in the range of 100 km - 200 km according to Figure 3.13, it would be interesting to compare numbers in terms of reliability and efficiency for these technologies. In [29], a case study for comparison of VSC-HVDC and LFAC was done. The relevant research focuses on two configurations, as shown in Figure 3.12, a 50 Hz CS with VSC-HVDC transmission and a 16.7 Hz CS with LFAC transmission.

The LFAC CS is assumed to use the same 33 kV AC cables operating at a frequency of 16.7 Hz and the same B2B converter as the 50 Hz CS. For this analysis, full converter wind turbines are employed, and it is assumed that the full converter can provide AC at a frequency of 16.7 Hz for the LFAC system [29]. An overview of all the components in the system can be seen in Table 3.2. The study developed analytical loss models for all

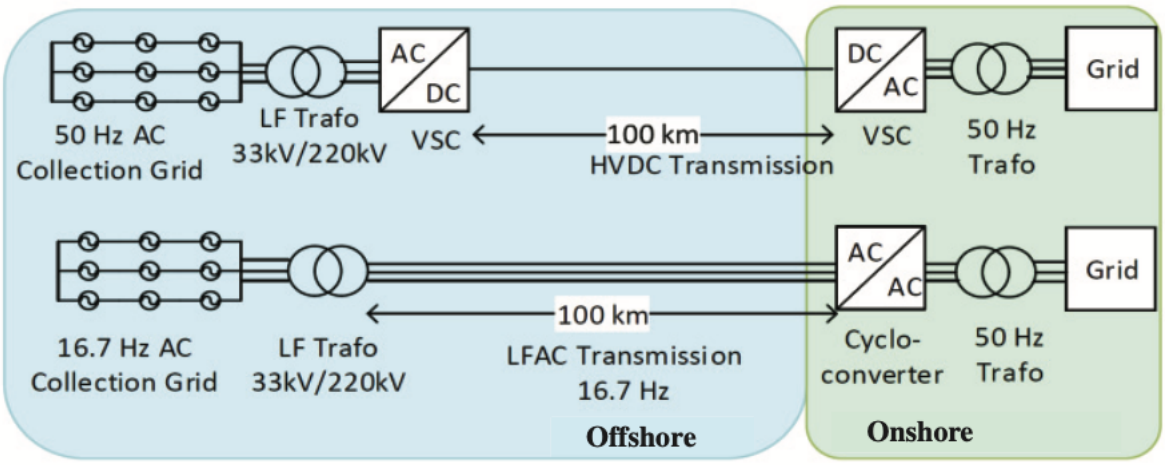

Figure 3.12: *Case from [29] comparing HVDC TTS with 50 Hz MVAC CS with 16.7 Hz LFAC CS and LFAC TTS.*

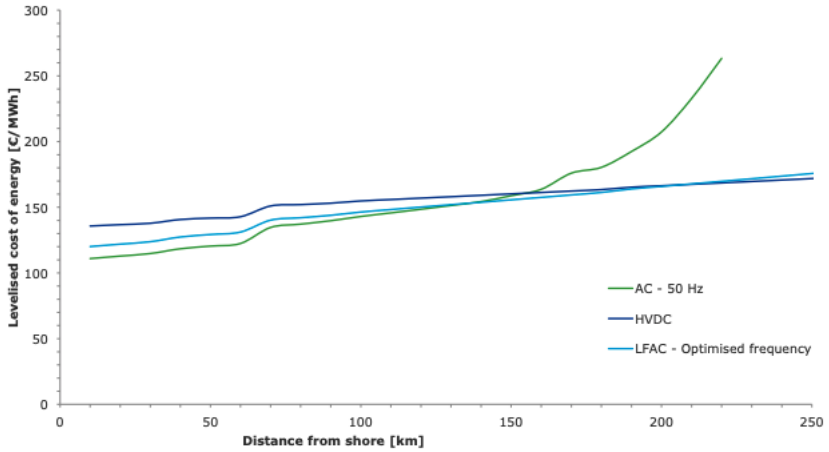

Figure 3.13: *Estimations of LCOE based on transmission distance done in [30].*

of the listed components; these models will not be discussed further here.

To simplify a comparison based only on transmission, OWPP availability is assumed to be 100% in the study. Additionally, is is assumed that each OSS has a backup transformer. This was done for redundancy purposes [29]. In Table 3.3 an overview of the failure rates and MTTR for all components is given. Also, in Figure 3.14, a plot of the efficiency in the transformers used in the study is shown. One can see that the cycloconverter has, in general, a higher efficiency than the Load Commutated Inverter (LCI). However, both han an increasing efficiency for an increase in load.

An energy capture analysis was carried out at a OWPP in the Irish Sea located about

Table 3.2: *Table from [29] illustrating the system components for the case study.*

LFAC	VSC-HVDC
16.7 Hz Wind Turbine Transformers	50 Hz Wind Turbine Transformers
16.7 Hz CS	50 Hz CS
16.7 Hz Transformer	50 Hz Transformer
-	Offshore Converter (VSC)
16.7 Hz Transmission Cable	HVDC Transmission Cable
Onshore Cycloconverter	Onshore Converter (VSC)

Table 3.3: *Failure rates and MTTR for the components in the study from [29].*

Component	$\lambda(failures/yr.)$	MTTR (hrs)
CS	0.008	2160
Circuit Breakers	0.032	720
Offshore Transformer	0.03	4320
Transmission Cable	0.08	720
VSC Onshore	0.05	720
VSC Offshore	0.05	50
Cycloconverter	0.101	50
Onshore Transformer	0.02	1440

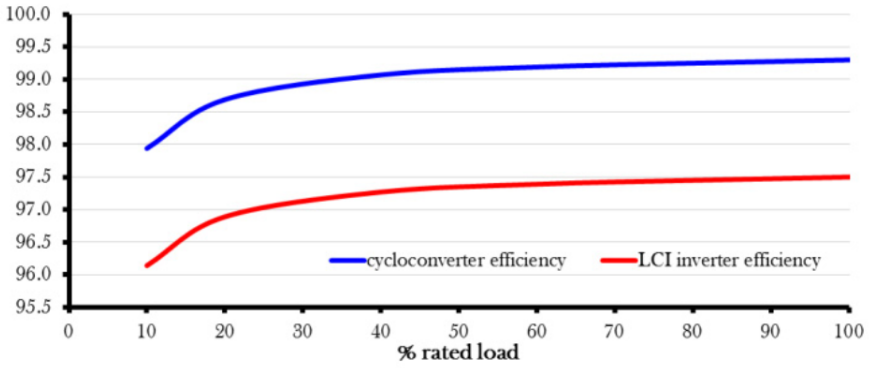

Figure 3.14: *A plot of the efficiencies for the cycloconverter and the LCI inverter used in the study from [29].*

Table 3.4: *Results from the research in [29] for both VSC-HVDC and LFAC.*

	VSC-HVDC		LFAC	
	Total Energy Capture (MWh)	**Total losses (MWh)**	**Total Energy Capture (MWh)**	**Total losses (MWh)**
2010	952 397	119 620	972 323	99 693
2011	981 249	124 732	1 002 056	103 925
2012	953 261	120 152	973 317	100 096
2013	994 655	119 879	1 010 758	103 776

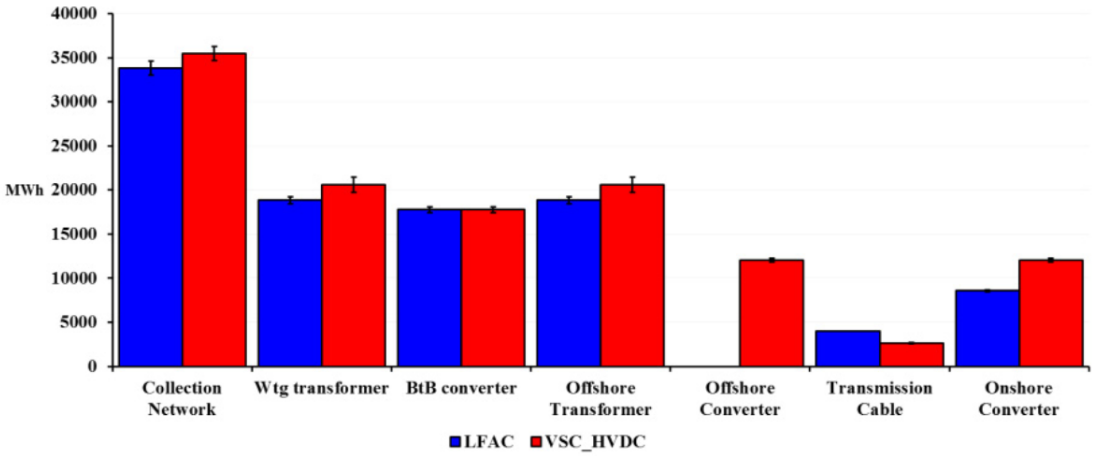

Figure 3.15: *Breakdown of losses from the results in the research done in [29].*

100 kilometers from PCC onshore. The OWPP had an installed capacity of 200 MW distributed across 40 turbines. Each turbine had a 5 MW installed capacity and where Type 4 WTs with full conversion capabilities linked in a radial CS [29].

The findings of the research in [29] are shown in Table 3.4. It is a result of an energy capture analysis done on the VSC-HVDC transmission system and the LFAC system with a cycloconverter during a four-year period, 2010-2013 with real wind data from the relevant OWPP in the Irish Sea. Because of the elimination of the offshore converter and reduced losses at lower frequencies of the CS and transformers, LFAC captured more energy and had less losses than the VSC-HVDC design.

In Figure 3.15, the losses that are shown in Table 3.4 are broken down to its components. For the four years, the error bars show the standard deviation within each component. The error bar is the little line that appears at the top of each bar. It can be seen that the CS is the largest source of the energy losses, as mentioned earlier. The transformer losses are larger for the 50 Hz transformers than for the LFAC transformers, both in the WT and on the OSS. The TTS for LFAC leads to higher losses than for the HVDC TTS.

Table 3.5: *Numbers from the research in [29] with different combination of transmission technologies and converters.*

	Unavailability (hrs)	**EENS (MWh)**	**Total Losses (MWh)**
LFAC_Cycloconverter	174.2	19 679	121 551
VSC_HVDC	207.9	23 034	144 129
VSC_MMC_HVDC	207.9	23 034	132 383
LFAC_VSC	207.9	19 434	124 953
LFAC_VSC_MMC	171.6	19 434	118 761

However, the onshore converter has, as expected, higher losses for the VSC-HVDC than the LFAC cycloconverter.

The research in [29] also found numbers for other combinations of the technologies with the choice of transformers. It looks like other wind data was taken as base in this calculation, however, it was not provided or specified. The results from this contains numbers for the capital costs, unavailability, EENS and total losses and is listed in Table 3.5. Future VSC implementations will most likely be built on Modular Multi-level Converters (MMCs) rather than 2-level VSC converters, which will further minimize VSC losses. The sole difference anticipated between the two-level converter and the MMC converter is efficiency, which deserves more investigation [29].

When the cycloconverter for LFAC is replaced with an MMC-based VSC, a boost in reliability can be seen since the VSC is more reliable than the cycloconverter onshore. Also, an increase in efficiency can be seen because the MMC technology is more efficient at lower loads than the cycloconverter [29].

The results from [29] agree with the earlier statement that one of the largest benefits of utilising LFAC is the opportunity to remove the offshore converter. Another advantage of using LFAC is the increased reliability brought in by the absence of the offshore converter station. Because of the lack of the offshore converter, this research implies that LFAC is more reliable than VSC-HVDC, and that LFAC with a VSC linked is the most reliable design [29]. Another advantage of LFAC over VSC-HVDC is the reduction in overall losses; it can be shown here that (assuming MMC), utilizing LFAC with a cycloconverter lowers losses by 8.2%, and using a VSC instead of a cycloconverter reduces losses by

10.3% [29].

3.2.5 LFAC in terms of Efficiency

In terms of efficiency, LFAC has various benefits over other choices such as increased voltage HVAC and DC CS. For example, it is less sensitive to long-distance losses, which can assist to optimize the quantity of power provided to the grid. Furthermore, LFAC systems may be designed to operate at lower voltages, reducing the requirement for expensive high-voltage equipment and improving overall system efficiency. In Section 3.2, it was mentioned that there are, in general, two limiting factors that limit the possible power transfer capability of an HVAC cable. One is maximum allowable voltage deviation at the receiving end of the cable, the other is the cable current carrying capability. This cable current carrying capability is affected by both the active and the reactive current, also called charging current. The charging current is a function of the length and capacity of the cable and the frequency [28]. The mathematics behind the limiting factor of cable current carrying capability can be described through the following equations. The expression for the charging current is shown in Eq. (3.4). It can be seen that if the frequency decreases, the charging current decreases. As a consequence, the reactive power shown in Eq. (3.5) also decreases and hence, the active power delivered through the cable increases as can be seen in Eq. (3.6) [28].

$$I_C = 2\pi f l C E \tag{3.4}$$

$$Q_C = I_C E \tag{3.5}$$

$$P_R = \sqrt{S^2 - {Q_C}^2} \tag{3.6}$$

Where,

I_C	: charging current,	[A]
f	: frequency,	[Hz]
l	: length of cable,	[km]
C	: shunt capacitance,	[F]
E	: rated voltage,	[kV]
Q_C	: reactive power,	[VAr]
P_R	: active power transmission capability,	[W]
S	: apparent power,	[VA]

In [31], the author of this Master's thesis, together with a co-author, *William Blytt*, performed some very simple calculations A.1 on the efficiency of LFAC versus 50 Hz HVAC for the OW site in Utsira Nord in Norway. Figure 3.16 represents a plot of the provided active power to the OCP for both technologies. This calculation is simply based on Eqs. 3.4, 3.5 and 3.6, with no regard for OSSs. This is purely for illustrative purposes. Relevant assumptions for the calculations:

V	: transmission voltage,	300 kV
C	: capacitance in cable,	$0.13\mu F$
l	: length of cable,	50 km

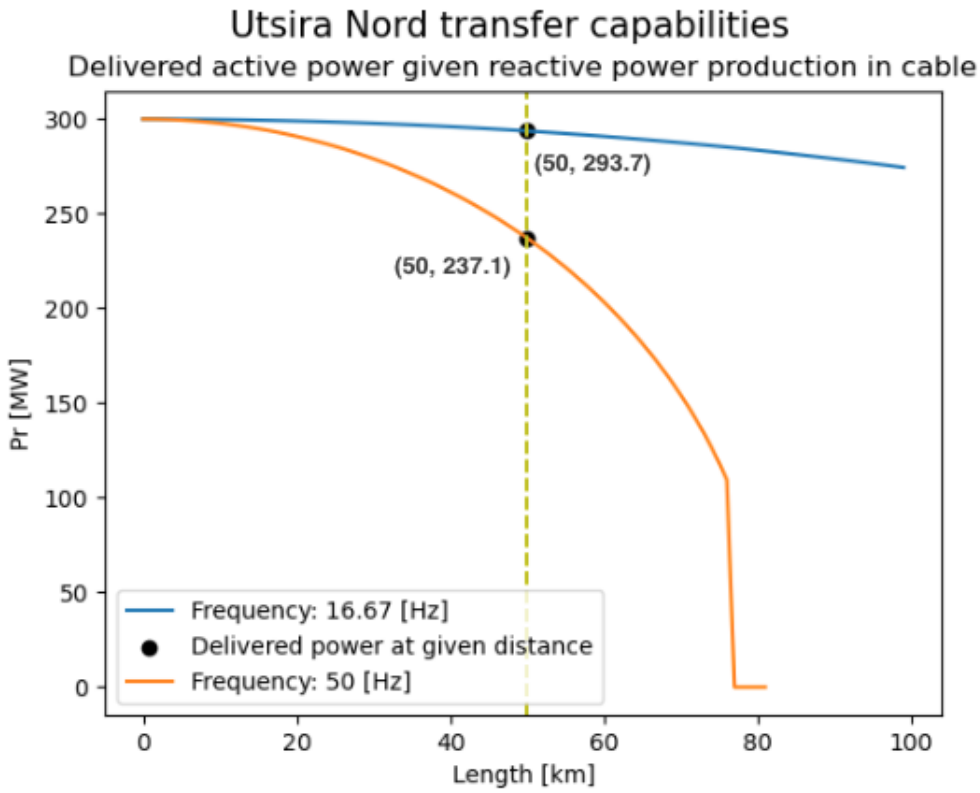

Figure 3.16: *Delivered active power given LFAC connection to Utsira Nord compared to conventional 50 Hz HVAC.*

The voltage level of 300 kV was a fitting choice for a OWPP with a total capacity of 300 MW and a 1000 A cable. The figure clearly shows that active power losses vary greatly. The LFAC transmission was predicted to have a total loss of 6.3 MW. A total loss of 62.9 MW was calculated for the typical HVAC, 50 Hz transmission. To put it another way, provided active power to shore at $f = 16.67Hz$ was about 293.7 MW, but delivered power at $f = 50Hz$ was approximately 237.1 MW, resulting in a significant difference between the two transmission options. In comparison to reality, this was a fairly simplistic computation. A closer examination at the scenario in 3.2.4 would offer a more complete picture of the efficiency and hence losses in an LFAC system rather than an HVDC system for a certain OWPP.

4 Supplemental Theory

This chapter aims to cover fundamentals that are pertinent for this thesis, but were not covered in the earlier research contributing to this topic. Firstly, the two relevant CS topologies for the case study are briefly presented. Secondly, the theoretical aspects of two out of the three performance efficiency methodologies that are relevant to the case study in this work, are focused upon. In particular, the fundamentals of a load flow analysis, based on a BFS algorithm will be thoroughly examined. In addition, the fundamentals of a combinatorial approach of calculating the power losses in a CS of an OWPP will be presented. The chapter continues by delving more into the concepts of performance efficiency. Lastly, in the context of reliability, this chapter presents an overview of the fundamentals of approximate system reliability evaluation and the calculation of ENS.

Load flow analysis is carried out in power systems to gain insights into the characteristics of the installed network. Load flow analysis is concerned with analyzing various forms of AC power, such as voltages, voltage angles, real power, and reactive power [32]. This type of analysis is conducted during normal steady-state operation of power systems. To explore various approaches of evaluating performance efficiency and reliability in offshore wind electrical systems, the NR methodology offers a valuable basis for comparison. To investigate a distinctive approach of analyzing the CS in an OWPP, the BFS algorithm-based DSA presented in [4] will be examined. This section will cover the mathematical foundations of the DSA methodology. A more detailed description of the application of this methodology in this project work will be presented in Section 5.1. Also, basics of the NR methodology will be explained in the mentioned section.

4.1 Relevant Collection System Topologies

This section will present two relevant CS topologies for the subsequent case study. While the literature review in Section 3 briefly introduced various CS topologies, including the radial topology, this section aims to provide a concise overview of the two relevant CS topologies without going into extensive detail. The two relevant topologies in this study are the radial topology and the single-sided ring topology, as discussed in [33]. To visually

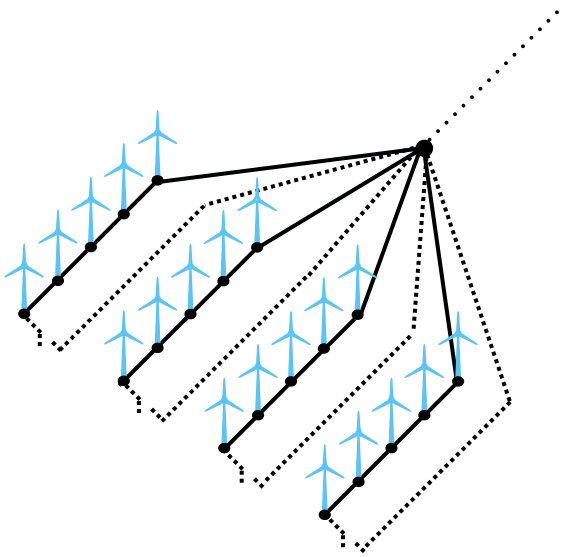

Figure 4.1: *Visual illustration of a radial CS topology.*

present these topologies, Figures 4.1 and 4.2 were created, taking inspiration from the figures in [34].

The radial design is the most basic layout for a CS in an OWPP [33]. In this configuration, the WTs are connected in series with a specified number of WTs on each series connection. This series connection is called "string" [33], and the opposite end is linked to the OSS, such as in Figure 4.1. This design provides several advantages, including cost-effectiveness, simplified control, and reduced design complexity [33].

The single-sided ring topology is similar to the radial topology [33], but with an additional string known as the "redundancy string" or "redundancy line" in this work. It can be seen in the mentioned Figure 4.2. The presence of redundancy lines primarily offers increased reliability [33]. However, it is worth noting that this advantage comes with additional costs as a potential disadvantage.

4.2 Backward/Forward Sweep: Distribution System Analysis

To obtain the system state and compare performance efficiency outcomes, a load flow calculation will be conducted using the DSA methodology [4], which is based on the

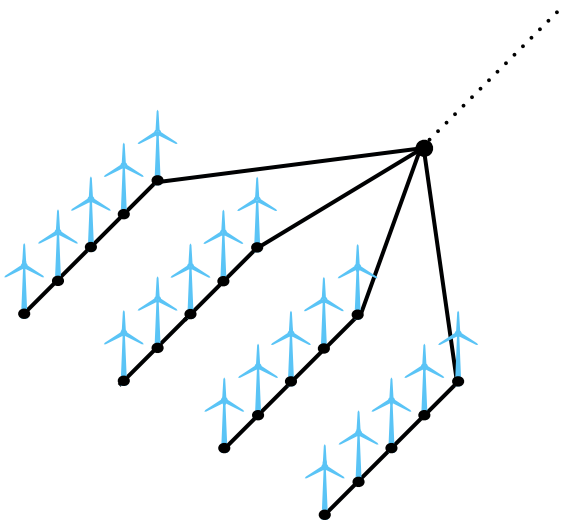

Figure 4.2: *Visual illustration of a single-sided ring CS topology.*

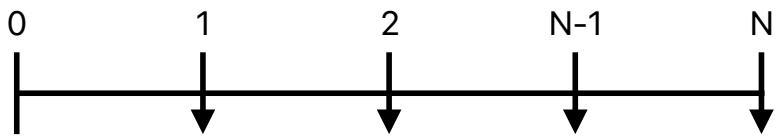

Figure 4.3: *Main feeder.*

BFS algorithm as mentioned earlier. However, distribution systems often fall under the category of ill-conditioned systems due to certain special features they possess [32]. Even though the electrical system of an OWPP differs from the normal view on what a distribution network is, it has a lot of similarities, such as being radial or weakly meshed, having an X/R-ratio smaller than 1 and having distributed generation [4]. However, the BFS algorithm is not applicable to contemporary active distribution systems [32].

A radial structure implies here, that the system does not contain any loops and each bus is connected to the substation through exactly one path.

Looking at Figure 4.4, it can be seen that the first step in the BFS method is to read the line and generation/load data. Secondly, the voltages at all buses are assumed to equal 1 p.u. The backward sweep is the next step in the method. Three distinct variants of

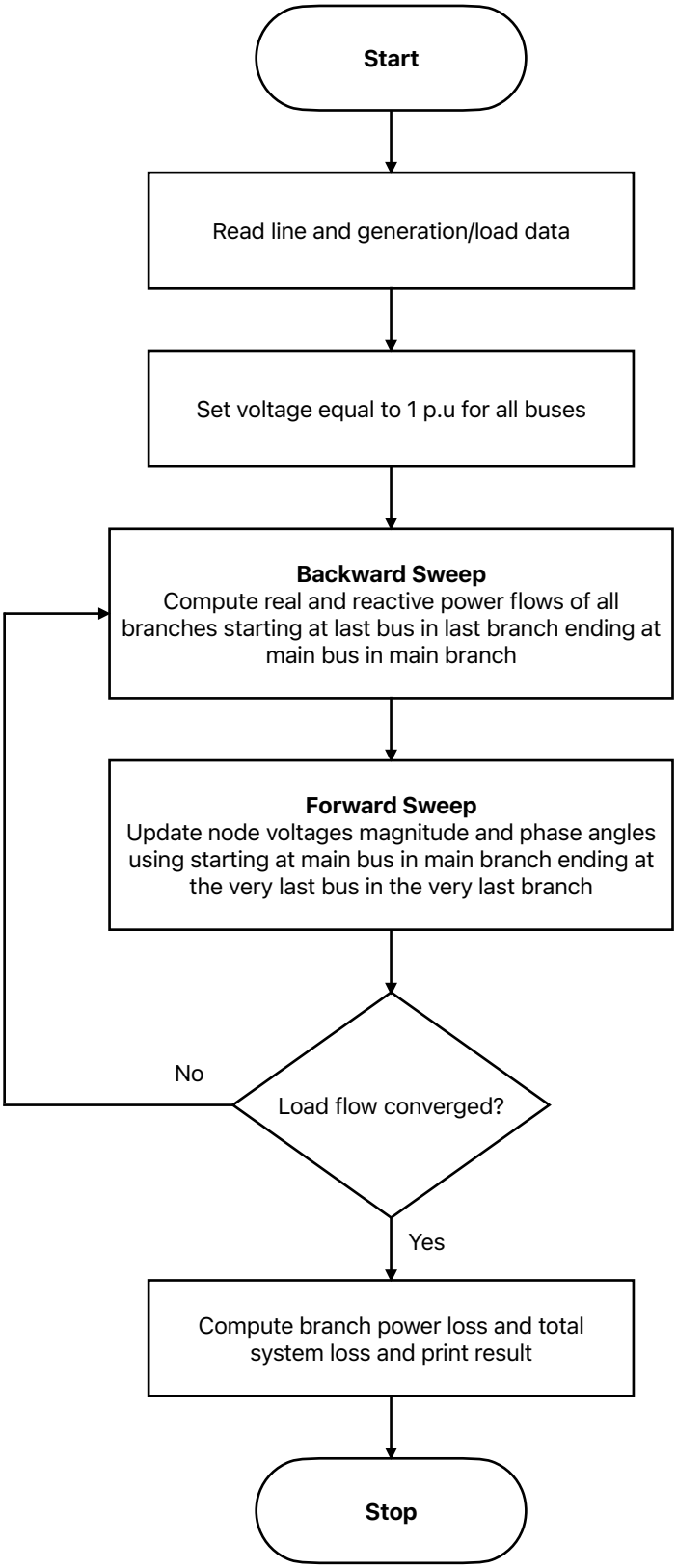

Figure 4.4: *Flow chart for the BFS algorithm, adapted for DSA [4] based on the BFS algorithm presented in [32].*

the backward sweep are well-known, as described in [32]. These variants are the current summation method, which evaluates branch currents, the power summation method, which evaluates power flows in branches, and the admittance summation method, which evaluates driving point admittance node by node. The DSA presented in [4] uses the power summation method by evaluating the power flows in the branches as follows, going backwards from the last node [32]:

$$P_k = P'_{k+1} + R_k \frac{P'^2_{k+1} + Q'^2_{k+1}}{V^2_{k+1}} \tag{4.1}$$

$$Q_k = Q'_{k+1} + X_k \frac{P'^2_{k+1} + Q'^2_{k+1}}{V^2_{k+1}} \tag{4.2}$$

Where,

$$P'_{k+1} = P_{k+1} + P_{Lk+1}$$
$$Q'_{k+1} = Q^2_{k+1} + Q_{Lk+1}$$

And where,

P_k	: real power flowing out of bus k,	[W]
Q_k	: reactive power flowing out of bus k,	[VAr]
P_{Lk+1}	: real load power at bus k+1,	[W]
Q_{Lk+1}	: reactive load power at bus k+1,	[VAr]
R_k	: resistance of line between bus k and k+1,	[Ω]
X_k	: reactance of line between bus k and k+1,	[jΩ]

Another commonly used method, the current summation method, is described in [35]. This method uses the following equation to calculate the current drawn from each bus:

$$I_i = \frac{S_i}{U_i}, i = 2, ..., N. \tag{4.3}$$

Where,

S_i : apparent power flowing out of bus i, [VAr]

U_i : voltage at bus i, [V]

i : bus number

N : last bus in the system

The current summation method calculates all branch currents as follows, by starting from the farthest nodes and moving upstream [35]:

$$I_{ij} = I_j + \sum_{m \epsilon A_j} I_{jm}, j = N, ..., 2 \tag{4.4}$$

Where,

I_{ij} : current at line between bus i and j, [A]

I_j : current out of bus j, [A]

I_{jm} : current at line between bus j and m, [A]

A_j : index set of nodes,

After calculating the real and reactive power flows of all branches by applying Eqs. 4.1 and 4.2, starting from the last bus in the very last branch and ending at the first bus in the main branch, the voltage magnitudes and angles for all buses can be updated. This is the forward sweep and it begins at the first bus in the main branch and concludes at the last bus in the very last branch. For the power summation method presented in [4], the forward sweep can be conducted through the following equation:

$$V_m = V_j - I_{jm}(R_{jm} + jX_{jm}) \tag{4.5}$$

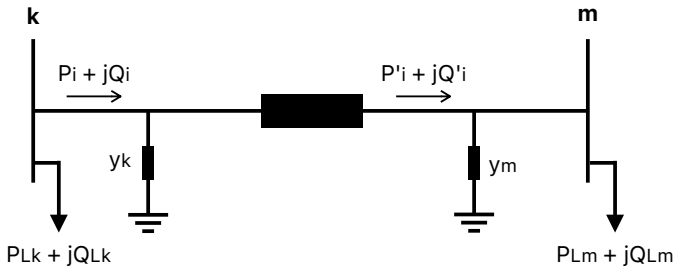

Figure 4.5: *Transmission line representation recreated from [4].*

Where,

V_m : voltage at bus m, [V]

V_j : voltage at bus j, [V]

I_{jm} : current at line between bus j and m, [A]

R_{jm} : resistance of line between bus j and m, [Ω]

X_{jm} : reactance of line between bus j and m, [jΩ]

Based on natural relationships, it is evident that there are several ways to calculate updated voltage levels using results from the backward sweep. However, the correlation described by Equation 4.5 is also presented for voltage calculation in the forward sweep of the current summation method in [35]. The paper covering the DSA methodology [4] also notes the similarities related to Figure 4.5. However, it should be noted that different notations are used in this figure and equations compared to earlier equations, and they do not refer to the same buses or similar entities. The line illustrated in the mentioned figure is based on a π-equivalent. To estimate the active and reactive losses of the distribution line "k-m", one can utilize the following equations [4]:

$$P_i^{Loss} = R_i \frac{P'^2_i + Q'^2_i}{V_m^2} \tag{4.6}$$

$$Q_i^{Loss} = X_i \frac{P'^2_i + Q'^2_i}{V_m^2} \tag{4.7}$$

The active and reactive power flow of the line before the impedance can then be expressed as [4]:

$$P_i = P'_i + P_i^{Loss} \tag{4.8}$$

$$Q_i = Q'_i + Q_i^{Loss} - V_k^2 y_k \tag{4.9}$$

Where,

P'_i : active power flow entering bus m,	[W]
Q'_i : reactive power flow entering bus m,	[VAr]
V_k : voltage at bus k,	[V]
y_k : shunt admittance	[S]

However, the flow chart presented in Figure 4.4 shows further that after updating the voltages, a check for convergence will be done by comparing the voltage of the previous iteration with the present iteration [32]. If the largest mismatch is less than the specified tolerance for voltage mismatch, convergence can be achieved [32]. Nevertheless, if the maximum voltage mismatch in the system is excessively large, the backward and forward sweeps must be repeated until convergence is achieved [32].

4.3 Combinatorial Methodology

This section will provide an overview of theory behind a combinatorial method with the purpose of analyzing the performance efficiency in the CS of the OWPP to be presented in the case study in Section 6. Only computations relating to power losses will be performed using this basic approach. As a result, it provides no results on other performance efficiency parameters like voltage magnitudes and angles.

A radial topology is presented in [36] and can be seen in Figure 4.7. A calculation for

active cable losses is also given using the following expression:

$$\begin{aligned} P_{LossesCable} &= [I^2 + (2I)^2 + (3I)^2 + ... + (nI)^2]R_{Cable} \\ &= \frac{n(n+1)(2n+1)}{6} I^2 R_{cable} \end{aligned} \tag{4.10}$$

$$R_{cable} = R * L_{cable} \tag{4.11}$$

Where,

I : rated steady state current from each WT transformer, [A]

R_{cable} : cable resistance, [Ω/m]

L_{cable} : total cable length in CS, [m]

n : number of WTs in each string

It is then reasonable to assume that the reactive losses in the cable can be written as follows:

$$\begin{aligned} Q_{LossesCable} &= [I^2 + (2I)^2 + (3I)^2 + ... + (nI)^2]X_{Cable} \\ &= \frac{n(n+1)(2n+1)}{6} I^2 X_{cable} \end{aligned} \tag{4.12}$$

(a) *Radial structure recreated from [37].* **(b)** *Equivalent representation of (a).*

Figure 4.6: *Model used in [37] to equivalence the CS of a large wind power plant.*

The mathematics behind Eq. (4.10) can be explained by referring to the content presented in [37]. Given the radial topology in Figure 4.6, the following can be obtained [37]:

$$\mathbf{I_1} = \mathbf{I_2} = \mathbf{I_3} = \mathbf{I_4} = \mathbf{I} \tag{4.13}$$

Where I is the output current from each WT. Now, expressing the total current coming fra all WTs in the CS as:

$$\mathbf{I_S} = n\mathbf{I} \tag{4.14}$$

Where n is the number of WTs i each radial. Given this, it is possible to derive the voltage drop across each impedance in Figure 4.6 as follows:

$$\begin{aligned} \Delta\mathbf{V_{Z_1}} &= \mathbf{IZ_1} \\ \Delta\mathbf{V_{Z_2}} &= 2\mathbf{IZ_2} \\ \Delta\mathbf{V_{Z_3}} &= 3\mathbf{IZ_3} \\ \Delta\mathbf{V_{Z_4}} &= 4\mathbf{IZ_4} \end{aligned} \tag{4.15}$$

Hence, the power loss across each impedance equals:

$$\begin{aligned} \mathbf{S_{LossZ_1}} &= I^2\mathbf{Z_1} \\ \mathbf{S_{LossZ_2}} &= 2^2 I^2\mathbf{Z_2} \\ \mathbf{S_{LossZ_3}} &= 3^2 I^2\mathbf{Z_3} \\ \mathbf{S_{LossZ_4}} &= 4^2 I^2\mathbf{Z_4} \end{aligned} \tag{4.16}$$

Again, given Eq. (4.14), this can be simplified as:

$$\begin{aligned} S_{TotalLoss} &= I^2(Z_1 + 2^2 Z_2 + 3^2 Z_3 + 4^2 Z_4) \\ &= I^2 \sum_{m=1}^{n} m^2 Z_m \end{aligned} \tag{4.17}$$

Where m is the sum index. Looking at this expression, it can be seen that it equals Eq. (4.10).

As for the equivalent representation in Figure 4.6b, the following can now be obtained [37]:

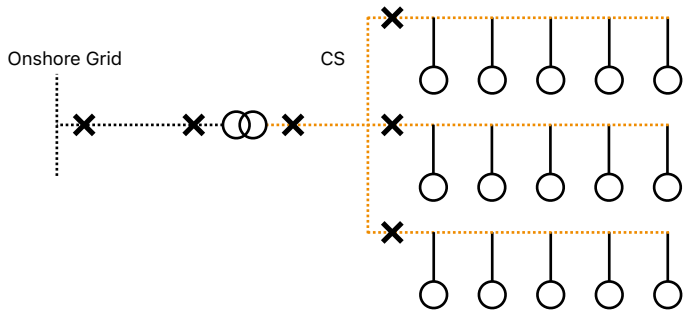

Figure 4.7: *AC radial CS topology recreated from [36].*

$$S_{TotalLoss} = I_S^2 Z_S \tag{4.18}$$

$$Z_S = \frac{\sum_{m=1}^{n} m^2 Z_m}{n^2} \tag{4.19}$$

It should be noted that the derivation is based on the following set of assumptions from [37]:

- The current injection from all WTs is assumed to be identical in magnitude and angle.
- Reactive power generated by the line capacitive shunts is based on the assumption that the voltage at the buses is one per unit.

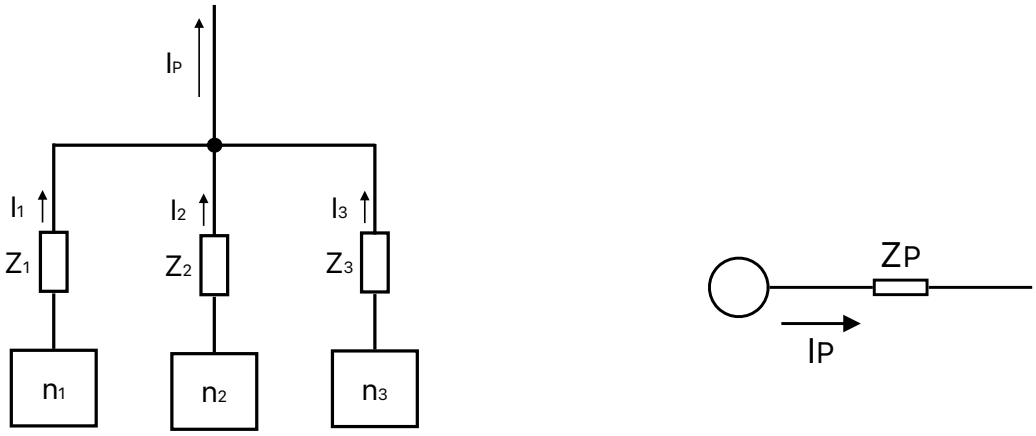

(a) *Parallel connection of three radial branches. Recreated from [37].*

(b) *Equivalent representation of (a). Recreated from [37].*

Figure 4.8: *Model used in [37] as a configuration where the radial topology is gathered through a parallel structure.*

The observation of Figure 4.8 reveals a network comprising of several radial branches merging together, which corresponds to the system topology presented in Figure 4.7. The resulting output currents from each branch can be expressed as follows [37]:

$$\begin{aligned} \mathbf{I_1} &= n_1\mathbf{I} \\ \mathbf{I_2} &= n_2\mathbf{I} \\ \mathbf{I_3} &= n_3\mathbf{I} \end{aligned} \tag{4.20}$$

Hence, the cumulative output current from the parallel branches can be expressed as [37]:

$$\mathbf{I_P} = \mathbf{I_1} + \mathbf{I_2} + \mathbf{I_3} \tag{4.21}$$

$$\mathbf{I_P} = (n_1 + n_2 + n_3)\mathbf{I} \tag{4.22}$$

Upon examination of Figure 4.8b, the following observations can be made [37]:

$$\begin{aligned} \mathbf{S_{Z_1}} &= \mathbf{I_1^2 Z_1} \\ \mathbf{S_{Z_2}} &= \mathbf{I_2^2 Z_2} \\ \mathbf{S_{Z_3}} &= \mathbf{I_3^2 Z_3} \end{aligned} \tag{4.23}$$

Leaving the total loss as [37]:

$$\mathbf{S_{Z_P}} = \mathbf{I_P^2 Z_P} \tag{4.24}$$

By combining Eq. (4.22) and (4.24), the equivalent impedance for the parallel configuration can be expressed as:

$$\mathbf{Z_P} = \frac{\sum_{m=1}^{n} n_m^2 Z_m}{\left[\sum_{m=1}^{n} n_m\right]^2} \tag{4.25}$$

The dielectric losses arising from the dielectric insulation material present in both the CS and TTS cables can be obtained through the following, as proposed in [29] and [38]:

$$W_d = 2\pi f C V^2 tan\delta \tag{4.26}$$

Where,

f	: Frequency,	[Hz]
C	: Capacitance,	[F]
V	: Voltage,	[V]
$tan\delta$	: Insulation loss factor (XLPE),	0.0004

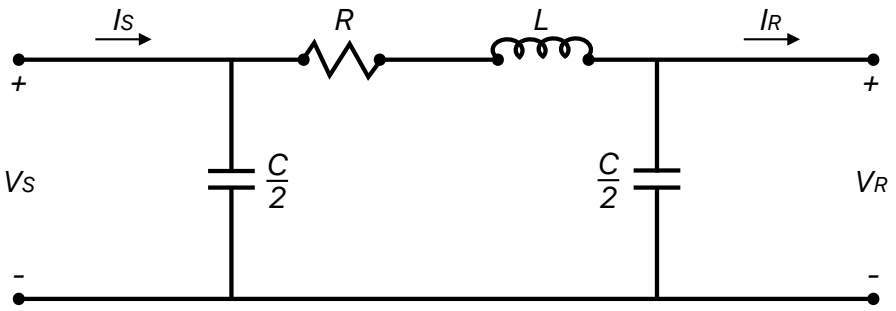

Figure 4.9: *π-equivalent of a transmission cable.*

4.4 Transmission Cable

The transmission cable can be modelled as a π-equivalent, showed in Figure 4.9 with the resistance (R), inductance (L) and shunt capacitance (C) [39][40]. The cable impedance (Z) is determined by the combination of resistance and inductive reactance, which can be expressed as:

$$Z = R + jX_L \tag{4.27}$$

In this equation, the reactance (X) is depending only on the inductive reactance of the cable. The inductive reactance is given by:

$$jX_L = j\omega L \tag{4.28}$$

Here, j represents the imaginary unit, ω is the angular frequency, and L denotes the inductance of the cable.

The shunt admittance (Y) shown in Figure 4.10 can be expressed as the sum of conductance (G) and susceptance (b) as follows:

$$Y = G + jb \tag{4.29}$$

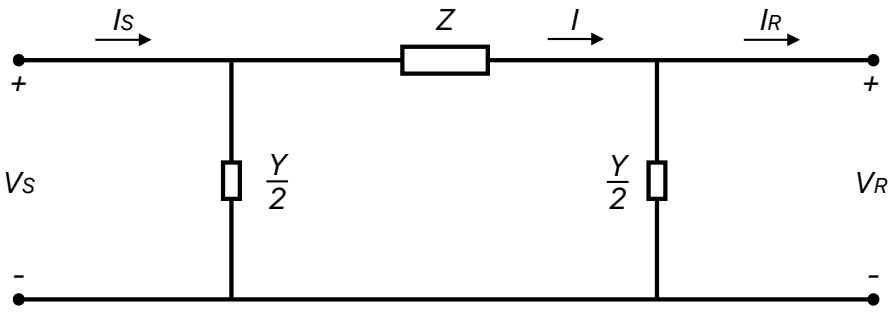

Figure 4.10: *π-equivalent of a transmission cable modeled with impedance and shunt admittance.*

Here, the susceptance (b) is given by:

$$jb = j\omega C \tag{4.30}$$

The shunt admittance represents the combined effect of corona loss and the potential difference between the lines and the cable's surroundings [41].

4.5 LFAC Transmission Cable

Considering Eq. (4.28) and the definition of capacitive reactance (X_C) as stated in [39], we have:

$$X_C = \frac{1}{j\omega C} \tag{4.31}$$

Additionally, the angular frequency (ω) is given by:

$$\omega = 2\pi f \tag{4.32}$$

By analyzing these equations, it becomes evident that when the transmission frequency is

reduced, the inductive reactance decreases. This reduction in inductive reactance results in an increased flow of active power [39]. At the same time, the capacitive reactance increases, limiting the capacitive charging current in the cable [39]. Notably, the charging currents caused by capacitance are more significant in long transmission cables, making this phenomenon more relevant for TTS compared to CSs [41]. However, it can be argued that this relevance depends on the control of reactive power in the CS.

4.6 X/R-ratio

In recent years, numerous methods for power flow analysis have been published [42]. While there is a wide range of proposed methods for distribution system power flow, the NR-based methods and the BFS-based methods have emerged as particularly popular choices [42]. However, it has been reported that several methods encounter issues when the X/R ratio decreases and the R/X ratio increases in certain cases [42]. The same issue has been reported in the case of OWPPs, as their electrical systems are often designed in a similar manner to distribution systems [43]. In OWPPs, cabling of the CS is normally achieved using long MV cables, which often has a low X/R ratio. This ratio is often such that the reactance (X) is less than the resistance (R) of the cables [43]. This situation typically results in variations in both active and reactive power within the cables, potentially causing notable voltage variations in this case [43].

The converters of modern WTs (often Type 3 or Type 4) are limiting the Var capacity by its operating boundaries [43]. The terminal voltage and active power production affects the range of Var capacity, meaning that the total Var capacity of the OWPP experiences a significant reduction when the WTs operate close to their maximum load, leading to a decrease in their ability to provide voltage support [43].

The convergence issues caused by the mentioned low X/R ratio in MV distribution systems has been reported by several authors for many different methods [42]. Nevertheless, some writers argue that the BFS algorithm solves this problem more effectively than alternative methods, such as NR-based ones. Yet, no analytical evidence was provided [42].

4.7 Reliability

4.7.1 Approximate System Reliability Evaluation

As a basis for the RELRAD-method that will be further explained in Section 5.2, an approximation of parallel components in the system will be presented here. The method, derived from [44], enables the application of the RELRAD method to systems with parallel components by estimating their failure rates and repair times. In this work, the requirement is limited to a maximum of three parallel components for approximation purposes.

In general, one can utilize the following for approximations on series systems, to obtain the system failure rate, the system repair time and the system unavailability [45]:

$$\lambda_s = \sum \lambda_i \tag{4.33}$$

$$U_s = \sum \lambda_i r_i \tag{4.34}$$

$$r_s = \frac{U_s}{r_s} \tag{4.35}$$

In contrast to series systems, extending the equations for a general n-component system from a 2-component parallel system is not possible [44]. To estimate the approximate failure rate of a 2-component parallel system, one can use the following descriptive approach cited from [44]:

"Failure of the system occurs if (component 1 fails followed by failure of component 2 during the repair time of component 1) or (component 2 fails followed by failure of component 1 during the repair time of component 2)."

This can be expressed as:

$$\lambda_p = \lambda_1(\lambda_2 r_1) + \lambda_2(\lambda_1 r_2) \tag{4.36}$$

Where λ is the failure rate and r is the repair time of the components. However, applying this logic to express the failure rate and repair time of a 3-component parallel system with component A, B and C, one can describe it as in [44]:

"Failure of the system occurs if (A fails followed by failure of B during repair of A followed by failure of C during the overlapping repair of A and B) OR (A fails followed by failure of C during repair of A followed by failure of B during the overlapping repair of A and C) OR (Plus 4 more similar statements for the failure sequences BAC, BCA, CAB, CBA)"

Mathematically, this can be expressed as follows:

$$\begin{aligned}\lambda_p = &\lambda_A(\lambda_B r_A)(\lambda_C \frac{r_A r_B}{r_A + r_B}) + \lambda_A(\lambda_C r_A)(\lambda_B \frac{r_A r_C}{r_A + r_C}) \\ &+ \lambda_B(\lambda_A r_B)(\lambda_C \frac{r_A r_B}{r_A + r_B}) + \lambda_B(\lambda_C r_B)(\lambda_A \frac{r_B r_C}{r_B + r_C}) \\ &+ \lambda_C(\lambda_A r_C)(\lambda_B \frac{r_A r_C}{r_A + r_C}) + \lambda_C(\lambda_B r_C)(\lambda_A \frac{r_B r_C}{r_B + r_C})\end{aligned}$$

This can be simplified as follows:

$$\lambda_p = \lambda_A \lambda_B \lambda_C (r_A r_B + r_B r_C + r_C r_A) \tag{4.37}$$

Assuming equal failure rates and repair times for the three parallel components, the approximate failure rate can be expressed as:

$$\lambda_p = 3\lambda^3 r^2 \tag{4.38}$$

Where λ and r equals the failure rate and repair time of the three components. Furthermore, the average repair time can be estimated as follows [44]:

$$r_p = \frac{r_A r_B r_C}{r_A r_B + r_A r_C + r_B r_C} \tag{4.39}$$

Additionally, by assuming equal repair times for components A, B, and C, the average repair time can be simplified as follows:

$$r_p = \frac{r}{3} \tag{4.40}$$

This will be used in the approximation of parallel TTS cables i the RELRAD-analysis conducted in Chapter 6.

4.7.2 Energy Not Supplied

While Eq. (2.1) presents the expression for ENS, further clarification is required to explain its utilization in this study. In [46], it is expressed as:

$$ENS = \sum L_{a(i)} U_i \tag{4.41}$$

Where,

$L_{a(i)}$: average load connected to load point i, [MWh]

U_i : annual outage time of load point i, $[\frac{hours}{year}]$

And the annual outage time again is expressed as:

$$U_i = \lambda_i r_i \tag{4.42}$$

Also, [46] expresses ENS by the following:

$$ENS = \sum L_C d \tag{4.43}$$

Where,

L_c : load curtailed, [MW]

d : duration of interruption, $[\frac{hours}{year}]$

However, this viewpoint is primarily focused on the load aspect. In this work, there will be only one load bus and several generation buses. Hence, an interpretation of these expressions in the context of this work can be outlined as follows:

$$ENS = \sum U_i * L_i \tag{4.44}$$

Where L_i is the load curtailed due to an outage of component i in MW and U_i is the unavailability (or annual outage time) of that curtailed load in hours. L_i can be calculated by subtracting the power delivered to the load point in the faulted condition from the average power delivered in a fault-free condition. While not entirely identical, a comparable interpretation is made in [47]. The usage of this will be further explained in Section 6.2.2.

5 Methodologies: Performance Efficiency and Reliability Analysis of Offshore Wind Power Plants

Based on the supplemental theory presented in the previous chapter, the present chapter will outline the methods that will be employed for the case study analysis. As previously mentioned, the focus of this Master's project is to explore strategies/methodologies for analyzing these case systems. Additionally, the objective is to evaluate the performance efficiency and reliability of different system configurations. To that purpose, this section will provide an overview of the three primary methodological approaches — DSA, NR, and the combinatorial method — selected for the performance efficiency study. The subsequent examination will go into the use of these strategies and give an extensive overview of how they have been implemented in Python for this work. In the context of reliability analysis, the DSA algorithm and the RELRAD methodology hold significant relevance. The RELRAD methodology will be explained later in this chapter. Regarding the application of LFAC to the case study, minimal alterations are expected within the methods. Nonetheless, the forthcoming sections will explicitly highlight any changes made and their corresponding effects, if any.

5.1 Performance Efficiency

5.1.1 Applying Distribution System Analysis Methodology

The DSA methodology, which is derived from the BFS algorithm discussed in Section 4.2, retrieves the system state in terms of line flows and voltage properties, encompassing both magnitude and angle. The DSA method necessitates input data consisting of net active and reactive powers at each bus within the system. Additionally, an initial guess of the voltage properties is also required, as mentioned earlier. The basics of the method are explained thoroughly in Section 4.2.

In addition to the given Python data files related to the DSA algorithm [4] that can be accessed through [5], some additional scripts were developed for this work by the author

of the thesis. The additional scripts can be found in Appendix B.1. This appendix serves as a resource for the additional scripts used for the DSA analysis.

The input data for this method is sourced from various Python files, such as *IEEE69-BusDist.py* and *UtsiraNordCase.py*. The required input data should encompass all buses in the system, including their respective active and reactive net power injections. Additionally, a complete listing of all lines, along with their corresponding total resistance and reactance, and the corresponding bus numbers indicating the origin and destination of each line is essential. By default, these lines are assumed to be connected. However, if there are any lines for backup supply with an open switch, such cases need to be explicitly specified. The arrangement of these buses and lines involves adding them to two respective lists along with other buses and lines in the system. This structure simplifies the organization and allows for easier management and access to the interconnected elements of the system.

Through the utilization of defined classes and their associated methods, the script attains a certain level of organization, reusability, and maintainability. The *DistribObjects.py* file encompasses various classes, including Bus, Line, DistLoadFlow, Statcom, SVC, Battery, and Capacitor. Given the significance of the Bus, Line and DistLoadFlow classes within this script, their organization, comprising member variables and methods are listed in Figure 5.1. It should be mentioned that other member variables and methods do exist in the script, however, the most relevant are included in this overview.

Several member variables and methods depicted in Figure 5.1 are self-explanatory, but some require further clarification. Within the Line class, it is worth mentioning that the "Ibstat" variable indicates the connectivity status of the line. For instance, if the line is intended for backup supply or faulted, it would be set to "False". Additionally, the "RedLine" variable signifies whether the line serves as a "Redundancy-Line" for backup supply or not.

The most important contribution from this work in terms of in house code to support this existing tool are the two methods "CheckOutage()" and "Outage()" that can be seen in the mentioned appendix. Looking at the "CheckOutage()" method: this method iterates through the BusList and LineList of the system to verify whether any normally

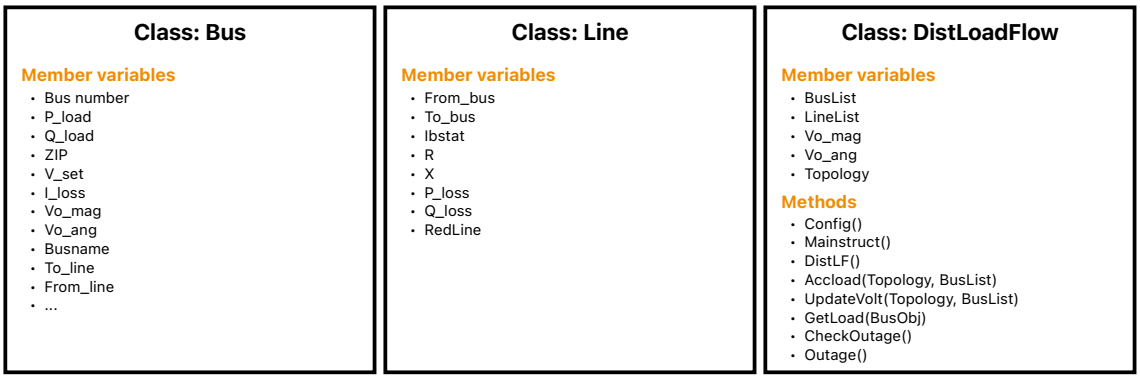

Figure 5.1: *Overview of classes in DSA: Bus, Line and DistLoadFlow with belonging member variables and methods, based on figure from [4] and new methods created in this work.*

functioning lines are disconnected. If a line is found to be disconnected, the "Outage()"-method is ran. This results in the disconnection of the remaining string of lines connected to that point. As a consequence, the system topology is changed. The execution of these methods are done early in the method, ensuring that the system topology, once determined, does not include the faulted buses.

5.1.2 Applying Newton Raphson Methodology

One of the three methods to be used to investigate the performance efficiency in this work is the NR load flow methodology. The utilized python scripts are taken from previous work and are not a part of this Master's work. As the development of the NR load flow solver in Python is not within the scope of this work, the methodology will not be extensively explained. The author considers it less crucial compared to the alternative method in terms of time utilization. While the mathematics of the algorithm itself may not hold crucial importance in this work, the utilization of the NR method will be explored and compared to its alternative methods within this work. Furthermore, potential applications of the NR methodology in this context will be discussed in Chapter 7.

The NR methodology is primarily an iterative approach used to solve a system of si-

Table 5.1: *Simple description of methods used in DistLoadFLow.*

Method	Input	Output	Description
CheckOutage()	-	-	Systematically scans the LineList of the system to identify disconnected normally operating lines.
Outage()	-	-	If any disconnections are found in CheckOutage(), the affected line causes the remaining portion of the system beyond it to become disconnected, resulting in changes to the system's topology.
Config()	-		Facilitates the establishment of connections between two buses by assigning the corresponding line to the destination bus. It also prepares a list of branching connections from the originating bus, ensuring a comprehensive representation of the system's topology.
Mainstruct()	-	Topology	The algorithm constructs a tree structure using topology information derived from instances of a node class. The main path can contain an arbitrary number of branchings on a bus. Multiple branchings can also exist within sublists. The fundamental principle involves inserting a sublist until reaching the element where the branching occurs. The output is assigned to the self.topology member variable.
DistLF()	Maximum nr. of iterations	-	The algorithm resolves the distribution load flow problem through a specified number of iterations. It utilizes a combination of forward sweeps for voltage updates and backward sweeps for load updates and loss calculations.
Accload()	Topology, BusList	Pload1, Qload1 Ploss1, Ploss2	Used in DistLF() to compute the cumulative downstream active and reactive load at all buses, as well as the active and reactive losses of lines. Additionally, it determines the cumulative equivalent load at the buses.
GetLoad()	BusObj	PloadAct, QloadAct dPdV, dQdV	The algorithm calculates the net voltage-corrected load at the bus using a simple ZIP model. Used in Accload() to update the accumulated equivalent load at the buses.
UpdateVolt()	Topology, BusList	-	Used in DistLF() to updates the voltage profile based on the accumulated load at each bus.

multaneous nonlinear equations involving an equal number of unknowns [48]. In each iteration, the nonlinear problem is approximated through linear matrix operations [48], where it can be argued that a Jacobian matrix is an important part of those calculations, the details of how the jacobian matrix is built can be seen in [48]. Based on power flow equations and an initial guess of the voltage properties in the system, the power voltage (angle and magnitude) mismatches at each bus within the system can be found through the mentioned matrix operations. The steps in the NR methodology are in [48] explained through the following steps:

Step 1: Guess values for voltage angle and magnitudes at each bus.

Step 2: Use initial voltage properties to calculate powers at each bus, including power mismatches and Jacobian elements.

Step 3: Obtain voltage magnitude and angle mismatches through matrix operations.

Step 4: Find new values for voltage magnitudes and angles.

Step 5: Use new values as starting values for the next iteration and continue until convergence is achieved.

Convergence is obtained when the calculated mismatches are small enough.

5.1.3 Applying Combinatorial Methodology

The application of the combinatorial methodology is solely based on an interpretation of the way of calculating power losses though the methodology presented in Section 4.3. It will be used in the Case study as a base for comparison to the two other performance efficiency methodologies. The simplicity of the NR method, in comparison to the other two methods, will serve as a valuable foundation for engaging comparisons in the discussion section of Chapter 6. The methdology was conducted through a python script, which can be found in Appendix B.2. The script includes certain unused methods that were initially intended for implementation in these analyses. However, they ultimately became irrelevant and were not utilized.

5.2 Reliability: Applying RELRAD Methodology

In terms of reliability, the relevant method of obtaining reliability indicies in this work is the RELRAD methodology, based on the work done in [45]. This section aims to offer an explanation of the relevant methodology, along with an adapted interpretation specific to a scenario involving a single load point and multiple power supplies. This interpretation is a result of limited information in the literature [45], leading the author to to propose a practical application of the method in the specific context of OWPP CSs. The application focuses on multiple generators, particularly wind turbines, and a single load.

The objective of the RELARD methodology is to assess the reliability of a radial power system. In cases where necessary, an approximate system reliability evaluation, as described in Section 4.7.1, can be employed. This enables the estimation of parallel system properties such as failure rates and repair times [45] that can be utilized within a radial system, where components are connected in series. Frequently, the RELRAD methodology, as demonstrated in [45], is employed to calculate the unavailability of a system using Eq. (4.42). Nevertheless, determining the unavailability of the entire system is not always a straightforward task. In such cases, the RELRAD methodology can be applied to obtain the unavailability for the system as a whole.

To illustrate the construction of the methodology, an example based on the work in [45] can be utilized. Figure 5.2, which is based on a figure in the mentioned reference, represents a system with four different sections, line 1, line 2, line a and line b. Also, it consist of two different load points, Load Point A and Load Point B. There is a supply coming into section 1 with a circuit breaker close to this supply at section 1. The RELRAD methodology aims to assess the unavailability of the system by systematically examining different failure states and aggregating the resulting unavailabilities for each load point. The RELRAD methodology is described in [45] as follows:

"The algorithm (then) accumulates reliability indices for each load point from each component, giving outages to the load point. Finally, when the fault contribution from every component is investigated, the total accumulated indices are available."

Considering a switching time of 0.5 h and the component data presented in Table 5.2,

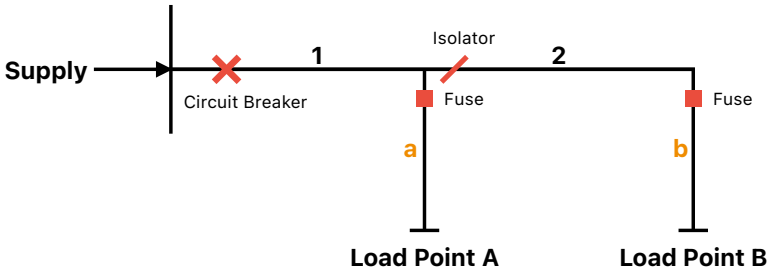

Figure 5.2: *Used to illustrate the construction of RELRAD through an example based on [45].*

Table 5.2: *Component data for RELRAD example.*

System Section	λ $[\frac{failures}{year}]$	**r** $[\frac{hours}{failure}]$
1	0.1	5.0
2	0.2	3.0
a	0.3	4.0
b	0.3	4.0

Table 5.3: *RELRAD analysis example based on [45] with different component data and similar methodology.*

System Section	Load Point A			Load PointB		
	λ $[\frac{failures}{year}]$	r $[\frac{hours}{failure}]$	U $[\frac{hours}{year}]$	λ $[\frac{failures}{year}]$	r $[\frac{hours}{failure}]$	U $[\frac{hours}{year}]$
1	0.1	5.0	0.5	0.2	5.0	1.0
2	0.1	0.5	0.05	0.2	3.0	0.6
a	0.3	4.0	1.2	-	-	-
b	-	-	-	0.3	4.0	1.2
Total	0.6	3.75	2.25	0.6	3.83	2.3

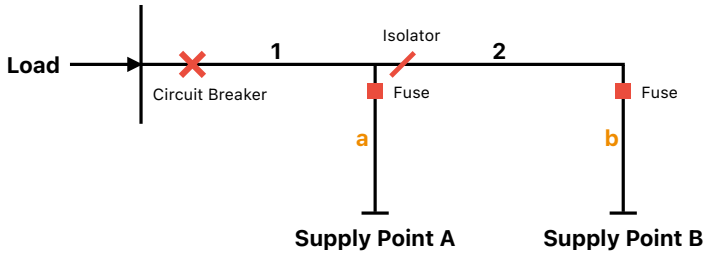

Figure 5.3: *Interpretation of RELRAD methodology.*

which includes failure rates and repair times belonging to the example based on the work in [45], the following results can be obtained:

Calculations not specified here that are used to obtain the results in the model can be explained through Eqs. 4.33, 4.34 ad 4.35.

Based on the resulting ENS obtained from the results from the example provided in Table 5.4, various other reliability indices can be derived, including ASAI. However, this specific approach does not fully address the scenario of having multiple power supplies and only one load point, which is often encountered in OWPPs. Due to the absence of any explanations in the literature, the author has therefore taken the liberty to interpret this scenario based on the existing methodology and theory. Based on the interpretation of the system in Figure 5.3, the following results can be calculated from the system:

Where L_c is the load curtailment due to the given failure and the total load curtailment

Table 5.4: *Interpretation of RELRAD analysis.*

System Section	Load Point A				
	λ $[\frac{failures}{year}]$	**r** $[\frac{hours}{failure}]$	**U** $[\frac{hours}{year}]$	L_c **[MW]**	**ENS [MWh]**
1	0.2	4.0	0.8	4	3.2
2	0.1	4.0	0.4	2	0.8
a	0.2	2.0	0.4	2	0.8
b	0.6	2.0	1.2	2	2.4
Total	1.1	2.55	2.8	2.6	7.2

is assumed to equal the system ENS divided by the system unavailability. The system ENS is calculated through Eq. (4.44). The system unavailability now represents the total number of annual hours in which the full load cannot be supplied. Furthermore, it should be noted that the failure rate and repair time used in the analysis do not correspond to the conventional system repair rate and repair time. A more detailed discussion on these properties will be presented in Chapter 6.

6 Case Study: Utsira Nord

This Chapter presents the execution and outcomes of the conducted case study in this Master's work. It begins by introducing the selected case site of Utsira Nord, providing all necessary case site and input information. Subsequently, it explains the application of the three methods (DSA, NR, and the combinatorial method) used in the performance efficiency and reliability analysis of the pertinent OWPP. Lastly, the comprehensive results obtained through these analyses is presented and thoroughly discussed.

The components listed in Table 6.1 will be considered within the two system configurations of the case site OWPP:

Table 6.1: *System components that will be regarded in performance efficiency and reliability analysis.*

HVAC	**LFAC**
50 Hz WT Transformer	16.7 Hz WT Transformer
50 Hz CS	16.7 Hz CS
50 Hz Offshore Transformer	16.7 Hz Offshore Transformer
50 Hz Transmission Cable	16.7 Hz Transmission Cable
-	16.7 Hz B2B Converter
50 Hz Onshore Transformer	16.7 Hz Onshore Transformer

The performance efficiency analysis focuses on the assessment of power losses within the system, encompassing both active and reactive power. Furthermore, it evaluates the voltage magnitude and angle of the buses within the system. The analysis was performed individually for the CS, the TTS, and the complete system comprising both the CS and TTS. Therefore, the results for each component will be presented accordingly. Results are provided for both the AC-configuration and the LFAC-configuration of the system in the performance efficiency analysis for all relevant cases. Furthermore, apart from analyzing the performance efficiency of the system, the results obtained from the various methods will be compared and extensively discussed.

The reliability analysis evaluates and compare the results of the RELRAD methodology

applied to both the radial CS topology and the single-sided ring CS topology. However, the analysis will solely consider the AC-system, as including the LFAC-system would consume valuable time that could be better allocated to other essential analyses. The RELRAD methodology allows for the determination of the ENS, which is the most significant output result for the two mentioned system configurations. Furthermore, the contribution of each component to the overall ENS will be presented. The RELRAD analysis exclusively relies on outputs from the DSA and does not incorporate results from the NR method or the combinatorial method in its calculations. In other words, this reliability analysis is more about comparing the two different CS topologies and their reliability itself than comparing the different methodological approaches presented. Furthermore, this study seeks to assess the potential of RELRAD, as well as other comparable reliability analyses such as approximate system reliability evaluation for offshore wind analyses.

6.1 Case Site and Input Data

This subsection provides the pertinent details regarding the case site and OWPP, along with the input data for all system components. Moreover, any assumptions made will be explicitly stated here or in more appropriate sections. The data provided primarily consists of cable and transformer data based on primary impedances, and reliability data, including failure rates and repair times. Furthermore, this section includes visual representations of the CS, the TTS, and the full system through various figures.

A representation of the CS in the selected case site at Utsira Nord can be seen in Figure 6.2, comprising a configuration of 33 15 MW state-of-the-art WTs, each with an active power output of 15 MW and a reactive power output of 0.15 MVA. The cable distance between two WTs was assumed to be 2.5 km and the specific cable distances from the OSS to the first WT in each radial can be seen in Figure 6.1. The total cable length within the CS is 92 km. This length encompasses two specific types of 66 kV cables as depicted in Figure 6.2b. Further details regarding their specifications will be provided later in this section.

Through the case study, the assumed apparent power base value is 500 MVA, and the

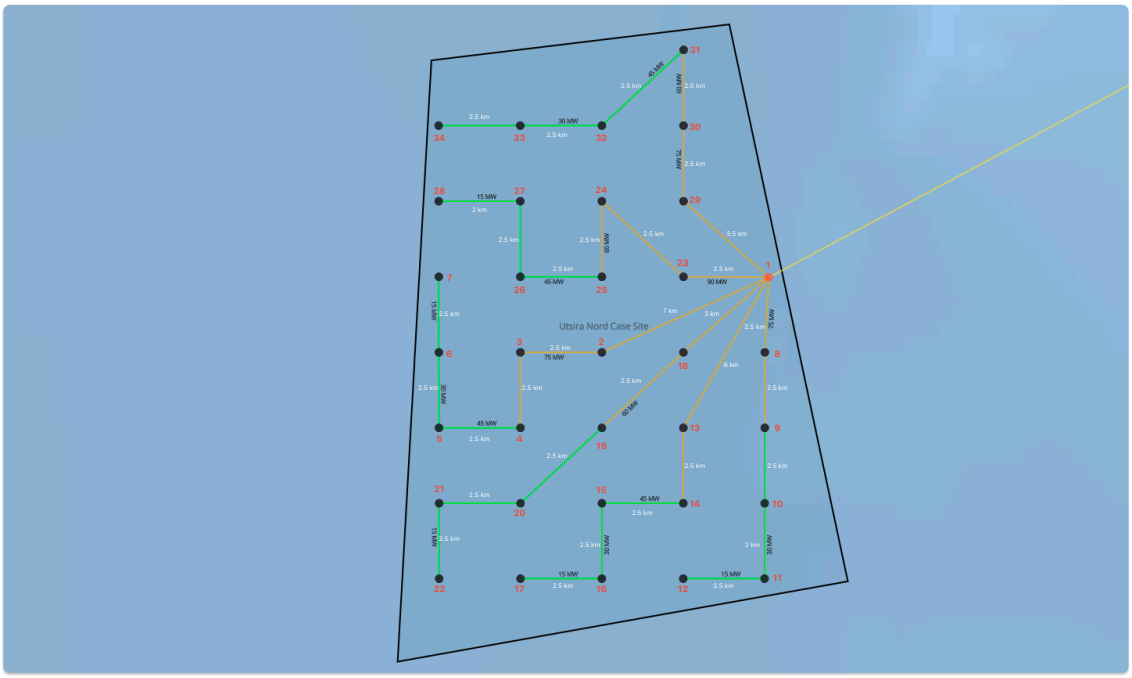

Figure 6.1: *Case site CS overview with distances and power flows given no losses, produced using Vind [49].*

Table 6.2: *Input cable type data used in the case for all systems analysed.*

Cable type	Voltage level [kV]	Resistance $[\frac{\Omega}{km}]$	Inductance $[\frac{mH}{km}]$	Frequency [Hz]	Reactance $[j\frac{\Omega}{km}]$	Impedance $[\frac{p.u}{km}]$
Three core (XLPE) 500mm^2	66	0.15	0.34	50	0.107	0.0172 + j0.0123
Three core (XLPE) 800mm^2	66	0.09	0.32	50	0.101	0.0103 + j0.0115
Three core (XLPE) 1000mm^2	220	0.0224	0.35	50	0.110	0.0002 + j0.0011
LFAC Three core (XLPE) 500mm^2	66	0.15	0.34	16.67	0.036	0.0172 + j0.0041
LFAC Three core (XLPE) 800mm^2	66	0.09	0.32	16.67	0.034	0.0103 + j0.0038
LFAC Three core (XLPE) 1000mm^2	220	0.0224	0.35	16.67	0.037	0.0002 + j0.0004

voltage base values are as follows: 66 kV on the CS side of the offshore transformer, 220 kV on the TTS, and 420 kV on the PCC side of the onshore transformer.

CS cable data is presented in Table 6.2 and consists of a combination of information obtained from assumptions and actual data from [50]. The inductance values used are sourced from [50], providing reliable and validated information. However, it is important to note that the resistance values for the specific cross-sectional area at the 66 kV voltage level were not directly obtained from available sources. In the absence of specific data for this state-of-the-art combination, reasonable assumptions were made based on comprehensive research conducted on other voltage levels and various cross-sectional areas. As for the TTS cable data, this was entirely obtained from [51].

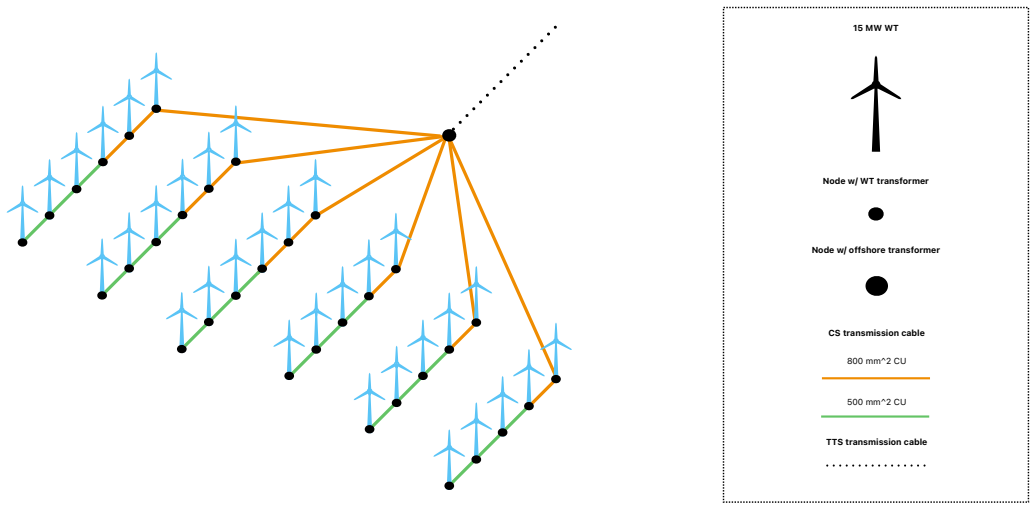

(a) *Case CS at Utsira Nord.* **(b)** *Legend case CS at Utsira Nord.*

Figure 6.2: *CS created for the case study at Utsira Nord. Topology in (a) and legend in (b).*

It is worth mentioning that neither the DSA nor the NR load flow analysis takes into account the shunt capacitance. However, the shunt capacitance plays a significant role in determining the performance efficiency, especially for the TTS. To address this, the same python script mentioned in Section 3.2.5 will be utilized to calculate the reactive power production (due to the capacitance) within the TTS cables. This straightforward calculation is based on Eqs. (3.4), (3.5), and (3.6). It is important to clarify that the only effort to this, done in this thesis work was changing the input values to obtain the desired output. The intention is not to present any new information that was not already provided in Section 3.2.5, but rather to highlight the significance of this phenomenon and emphasize that it is not accounted for in the other analyses. The input parameters used in the analysis comprise a combination of assumptions and data sourced from [50]. Specifically, the equivalent cable capacitance is set at 0.19 μF. The current flowing through the cables is assumed to be 2.188 kA, while the transmission voltage is maintained at 220 kV across the 34 km TTS.

The reactance values in Table 6.2 are obtained through the basics of Eqs. 4.27 and 4.28. The LFAC impedance values are assumed to be equal except frequency changes and hence, according to Eq. (4.28) reactance changes, leading to an increased active power flow, as mentioned earlier in Section 4.5. The assumed power capacity for the cables is

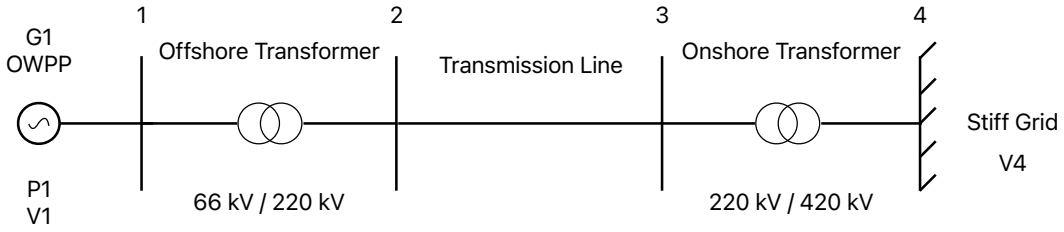

Figure 6.3: *Transmission to shore system for Utsira Nord case site. Used in performance efficiency of TTS through DSA.*

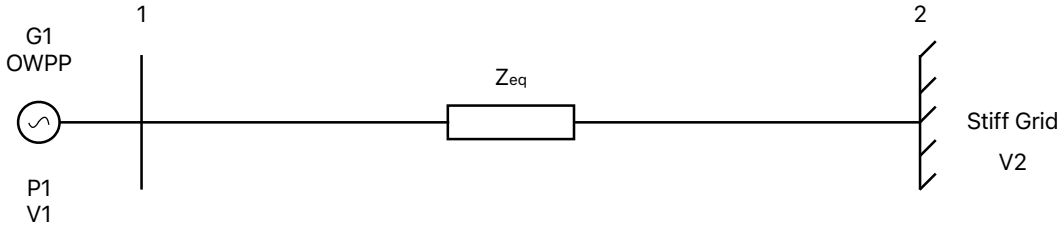

Figure 6.4: *Transmission to shore system with equivalent impedance for Utsira Nord case site. Used in performance efficiency analysis of TTS through NR.*

50 MVA for the three-core 500 mm^2 CU cable and 90 MVA for the 800 mm^2 CU cable [52]. This means that the 500 mm^2 CU cable can handle the power transmission from the three outer WTs, while the inner part of each radial from WT number three requires an 800 mm^2 CU cable. As previously mentioned, the total cable length amounts to 92 km, consisting of 45 km of 500 mm^2 cables and 47 km of 800 mm^2 cables. It is essential to note that numerous site-specific factors impact the abilities of the cable, including its current carrying capacity and fault conditions. However, since these aspects are not the primary focus of this work, emphasis is placed on the importance of simplicity in this part of the process. Moreover, the aim is to facilitate the incorporation of new, state-of-the-art component input data for potential future work in this area.

The TTS system for the case site can be seen in Figure 6.3. The cable input data is listed in Table 6.2 as already mentioned.

The author of this thesis initially attempted to locate current and reliable information

Table 6.3: *Equivalent impedances for offshore transformers, onshore transformers, and cycloconverter for LFAC system.*

	Voltage [kV]	**Frequency [Hz]**	**Equivalent Impedance [p.u]**
Offshore Transformer	66 / 220	50	0.001 + j 0.050
Onshore Transformer	220 / 420	50	0.0025 + j 0.070
LFAC Offshore Transformer	66 / 220	16.67	0.001 + j 0.017
LFAC Onshore Transformer	220 / 420	16.67	0.0025 + j 0.023
Cycloconverter	220	16.67	0.0025 + j 0.010

concerning the equivalent impedance of transformers for modeling purposes. However, this proved to be a difficult task, and rather than compromising accuracy, simple assumptions were made, resulting in the equivalent impedance values in Table 6.3. These selected values have implications for the overall losses in the system and ultimately affect voltage magnitudes and angles. Based on these assumptions, it was determined that including WT transformer losses in the analysis of CS performance efficiency would only obscure the results, and thus, there was no justification for their inclusion.

During the analysis of the TTS system, an equivalent impedance is used to represent the combination of the three parallel transmission cables, the offshore transformer, and the onshore transformer. Additionally, for the LFAC configuration of the system, the cycloconverter equivalent impedance is also taken into account. The LFAC transformers are assumed to have unchanged resistance compared to the conventional AC transformers. However, the reactances are assumed to be divided by three, as can be fairly reasoned though the literature review from Chapter 3.

To analyze the performance efficiency of the TTS, the cable data from Table 6.2 and transformer impedance data from Table 6.3 were utilized as input for both the DSA and NR analysis. However, in the case of NR analysis, the transformer impedance data was used to represent the equivalent impedance of the TTS system. Furthermore, the system state resulting from the DSA conducted on the entire system (CS and TTS combined) was interpreted as the initial condition at the offshore substation bus (Bus 1 in Figures 6.3 and 6.4) for the TTS analysis.

The case site with both CS and TTS can be seen in Figures 6.5 and 6.6. The PCC for

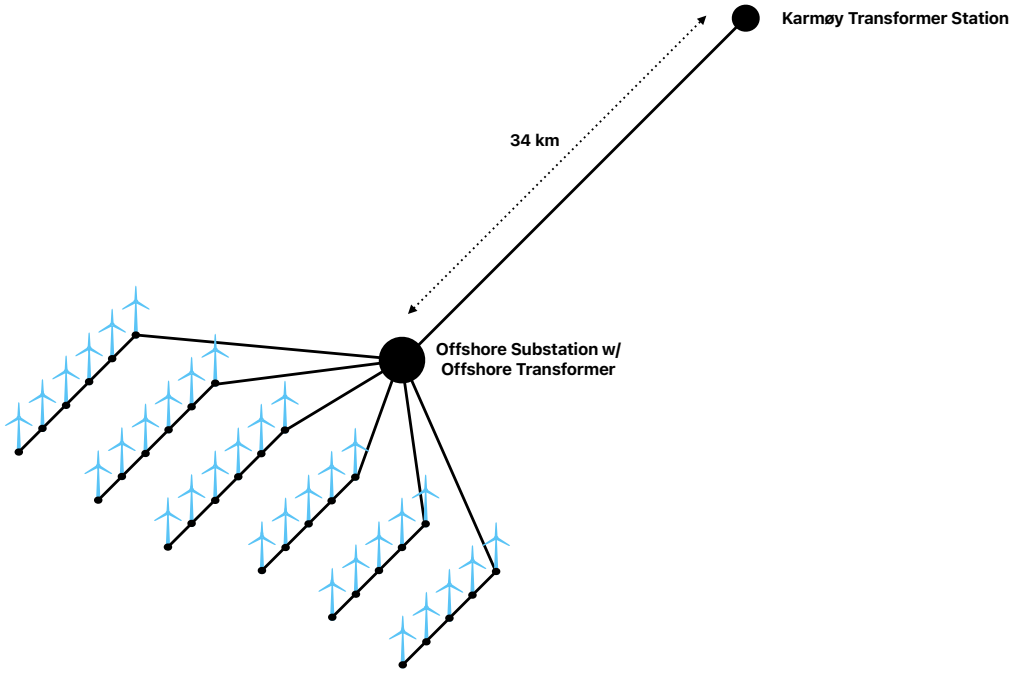

Figure 6.5: *CS + TTS in Utsira Nord Case Site.*

the TTS was assumed to be located at Karmøy Transformer Station, resulting in a total transmission distance of 34 km from the OSS to the PCC. Bus number two in Figure 6.6 is included provide insight to the voltage properties at the midpoint of the TTS in the DSA.

Regarding the combinatorial method, the cable impedance was assumed to equal the average impedance of the system, equaling an impedance of $0.0161 + j0.0122/km$ for the AC-cables and $0.0161 + j0.0041/km$ for the LFAC-cables. Also, the output current from each WT was assumed to equal 230 A, based on simple calculations including the power rating of the transformer and the system voltage.

6.1.1 Reliability-Relevant Input Data

In addition to the presented input data for the performance efficiency analysis, Table 6.4 contains pertinent input data for the reliability analysis. The data is sourced from [29] and [53] and contains failure rates and repair times for all system components.

To assess the approximate system reliability of the transmission cables in the TTS, Eq.

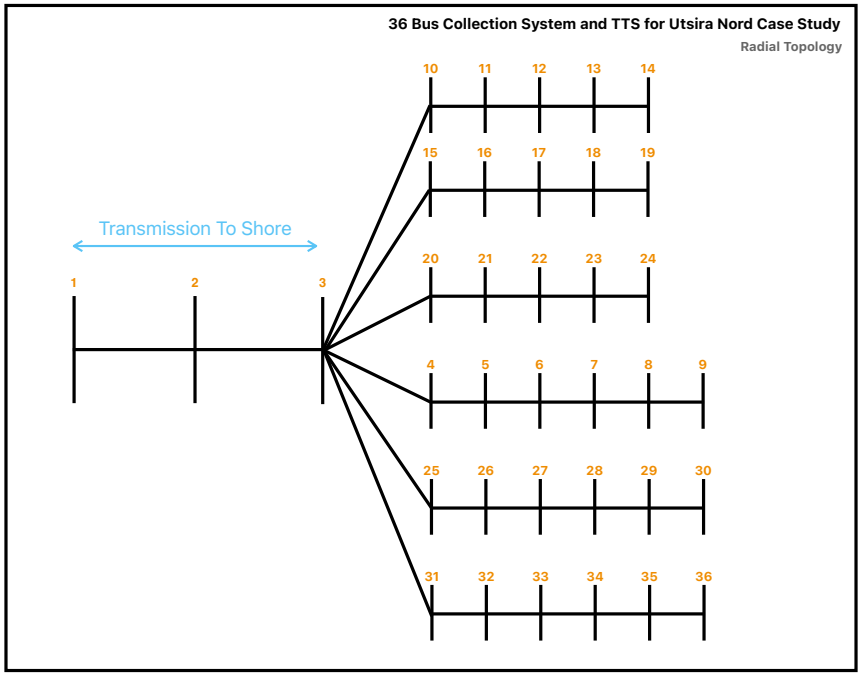

Figure 6.6: *CS + TTS Utsira Nord case with bus numbers corresponding to DSA analysis and results. CS with radial topology.*

Table 6.4: *Failure rates and repair times of system components from [29] and [53].*

	Failure rate, $\lambda[\frac{occ}{year}]$	**Repair Time, r $[\frac{hours}{occ}]$**
CS Cable	0.015/km	1440
Offshore Transformer	0.03	4320
TTS Cable	0.015/km	1440
Onshore Transformer	0.02	1440

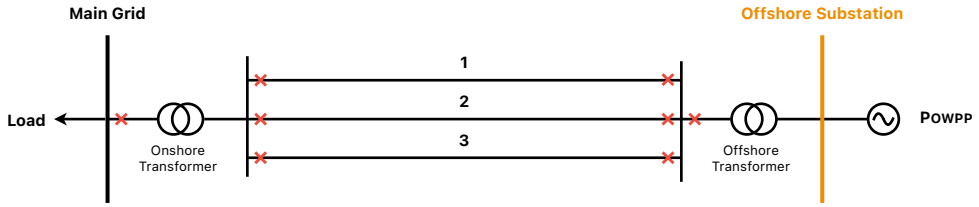

Figure 6.7: *TTS cables to be approximated for RELRAD-study.*

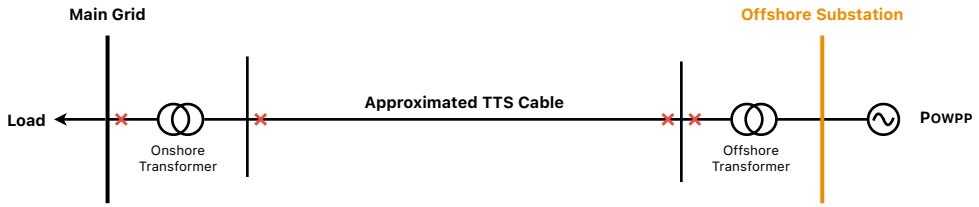

Figure 6.8: *Approximated system reliability evaluation of the TTS cables. Approximating the failure rate and repair time of three parallel cables.*

(4.38) was employed alongside the provided component data, which includes the failure rate and repair time. By applying this, the approximate failure rate of the TTS cables used was 0.0024 [$occ/year$] and repair time 480 [$hours$]. The approximation of the TTS cables can be seen in Figures 6.7 and 6.8.

The circuit breakers are assumed to be perfect (i.e. never faulted) and the switching time is assumed to equal 0.5 hours. Only single faults are taken into account in this study, thereby disregarding the possibility of multiple faults occurring simultaneously, except in the case of approximate system reliability evaluation, for parallel subsystems.

6.1.2 Energy Production

In order to facilitate the analysis of energy production, simplifying assumptions were made. On April 25, 2023, the Norwegian Water Resources and Energy Directorate (NVE) released a publication titled "Identification of investigation areas for offshore wind," translated from Norwegian. In this publication, a new area suited for offshore wind called "Vestavind F" was identified, which includes the original Utsira Nord site

area. Detailed data for Vestavind F can be found on the NVE website [54]. NVE has estimated the operational time for a project in this area to be around 5300 hours per year. Additionally, the average wind speed at a height of 150 meters above sea level has been calculated to be 10.2 m/s. Based on this wind speed, it is assumed that the wind turbine will have an electrical efficiency of 85%. In this context, when referring to the "electrical efficiency" of the WT, it specifically denotes the percentage of its maximum installed capacity that it is expected to generate on average.

6.2 Execution

While considerable information has been provided regarding the methodologies employed in this case study, this section will serve as a simple description outlining the approach and strategy for conducting the performance efficiency and reliability analyses. In addition, this section aims to address any assumptions and provide clarifications regarding the execution of the analyses that have not been previously mentioned.

6.2.1 Performance Efficiency Analysis

The results will be obtained using the three methods that have been thoroughly explained in this report. The DSA will serve as the primary foundation for this case study, as it has consistently proven to be well-suited for the conducted analyses throughout the work. Also, it provides all the performance efficiency output data that the two other methods also provide. However, these alternative methods will also be utilized as comparative foundations for the analysis. As mentioned earlier, Figure 6.6 illustrates the complete case system, which also is interpreted into the DSA.

The results obtained from the methods, which are interpreted and executed in Python, will form the foundation for the subsequent analysis. However, these results will also be utilized for conducting comparisons and creating plots and visualizations. This will facilitate a deeper understanding, comparison, and further discussion of the results. The discussion will be presented in Section 6.4, which follows the results section.

The NR load flow analysis is interpreted with a convergence threshold of 10^{-5}, indicating

that it will continue iterations until the active and reactive power errors are below or equal to the specified threshold. In other words, the analysis will iterate until the found values of active and reactive powers have converged within the given error limit.

6.2.2 Reliability Analysis - RELRAD

The reliability analysis will be carried out using the RELRAD methodology, utilizing results obtained from the DSA. The fault scenarios considered in the analysis include all lines within the entire system, encompassing both the CS and the TTS. This encompasses offshore and onshore transformers as well. It will be specified when new results was obtained from the DSA except from performance efficiency results utilized. Due to the extensive amount of output data collected, not all Python output results could be included in Appendix. However, the most pertinent outputs are available in Appendix and referenced accordingly in the relevant sections.

When obtaining the ENS through Eq. (4.44), L_i can be determined by subtracting the active power delivered despite the presence of a faulted component from the average load (L_a). This calculation enables the assessment of the relative impact that the fault has on the average load, thereby contributing to the ENS.

The case site used for the reliability study is depicted in Figure 6.9 with a radial topology of the CS, while Figure 6.10 represents the system with the scenario of a single-sided ring topology. As explained in Section 4.1, each string in this topology is equipped with redundancy lines, which serve as backup cables in the event of faults occurring in the normally connected cables. These are separated from the normally operating strings through circuit breakers.

The switching time was disregarded in the RELRAD-analysis for the radial topology, as it is significantly smaller compared to the repair times of the components. It was included for the CS circuit breakers in the single-sided ring topology as this was the only contribution to ENS in this case. However, the results indicated that this inclusion could have been easily disregarded without affecting the analysis significantly. In the RELRAD-analysis for the single-sided ring topology, some other assumptions were made.

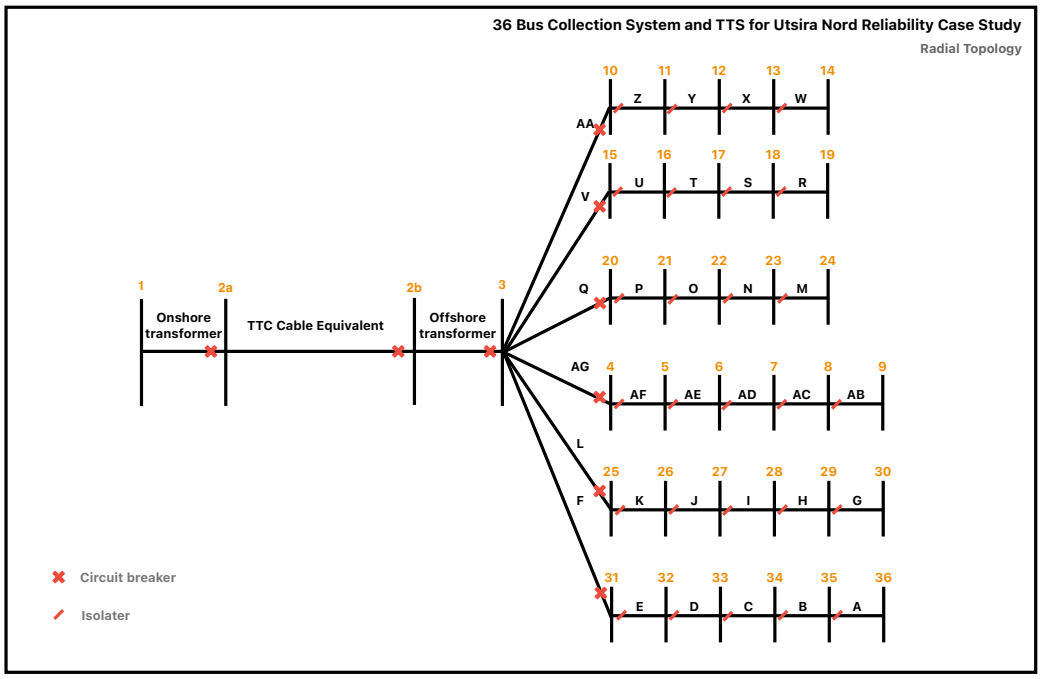

Figure 6.9: *Case site including CS and TTS for reliability analysis with radial topology, hence including circuit breakers and switches.*

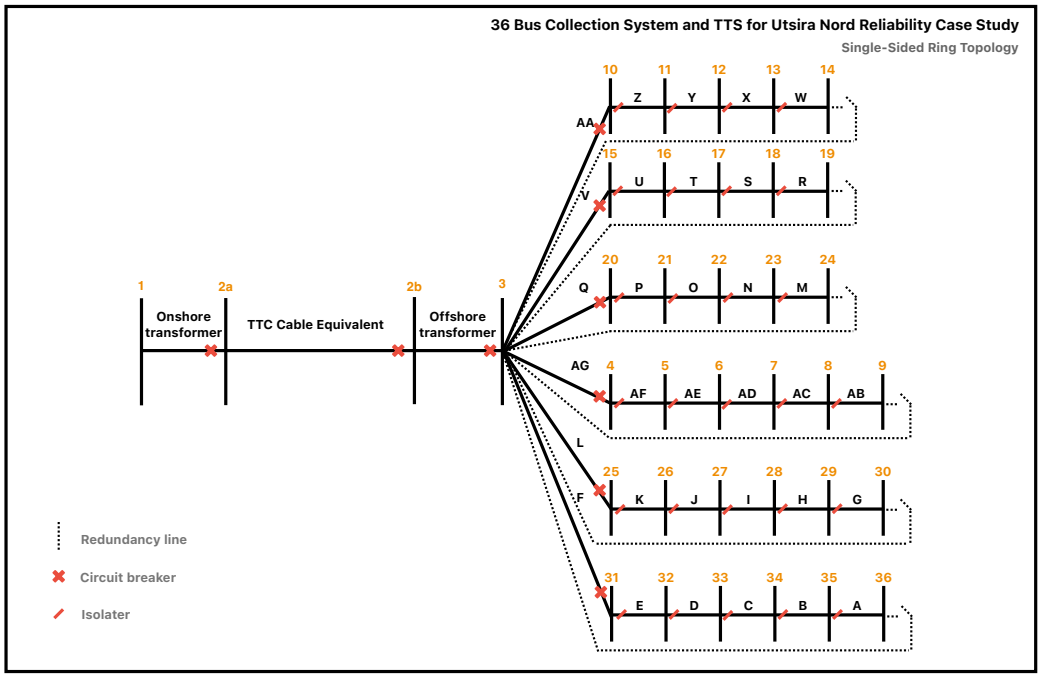

Figure 6.10: *Case site including CS and TTS for reliability analysis with single-sided ring topology, hence including circuit breakers, switches and redundancy lines.*

The contributing methods from this work in the DSA tool cannot handle faulted lines together with connected redundancy lines. Hence, it was assumed that no additional power losses occurred during the rerouting of power through the redundancy cables in the event of a CS cable fault.

6.3 Results

In this section, the results and findings from the case study are discussed. The performance efficiency analysis begins with the presentation of results for the CS, followed by the TTS, and concludes with comprehensive results for the full system configuration. Lastly, the findings from the reliability analysis using the RELRAD methodology will be presented. The subsequent section will involve a detailed discussion of the presented results. Therefore, the main objective of this subsection is to provide comments on the results in order to facilitate a comprehensive discussion of their implications and significance.

All relevant python outputs and results from the performance efficiency and reliability analysis can be found in Appendix C. Tables, plots and figures will be made for the most relevant results. In cases where additional figures are needed, references will be made to the corresponding figures in the appendix.

Based on the wind condition assumptions made in Section 6.1.2, the active power delivered from the WTs to the CS was estimated at 2230.0 GWh. This value serves as the reference for all energy-based results involving power losses, such as in GWh. Also considering results from the DSA with an 85% electrical efficiency in the WTs. It can be seen in Figure C.39 in Appendix C.7.1, that the active power delivered to the TTS from the CS was estimated to be 0.8316 p.u. This equals 2203.7 GWh and is used as basis for all energy-loss estimations in the TTS for the performance efficiency analysis. For a better reference basis of power losses, the energy delivered to both the CS and the TTS in the LFAC case will be assumed to be equivalent to the energy in the normal AC system case.

Based on the assumptions in Section 6.1.2, the active power delivered to the main grid

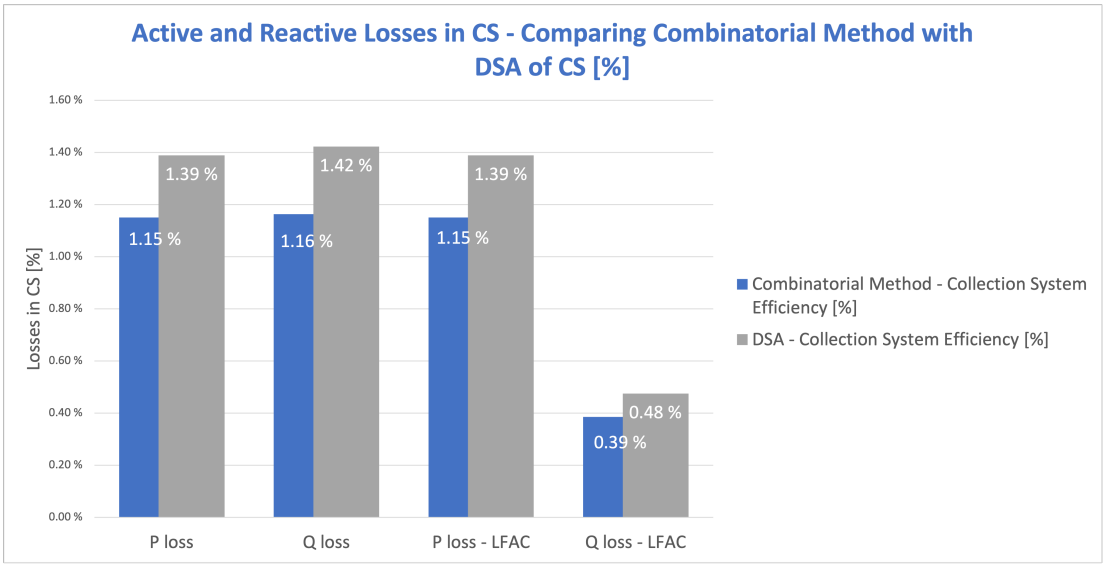

Figure 6.11: *Comparing active and reactive losses in [%] from combinatorial method with DSA of CS. Displaying result for both AC- and LFAC-system.*

was calculated, considering results from the DSA with an 85% electrical efficiency in the WTs. It can be seen in Figure C.39 in Appendix C.7.1, that the active power delivered to the main grid equaled 0.8274 p.u. Based on the given wind condition assumptions and this result, the total active power delivered to the grid was estimated at 2192.6 GWh, also known as the average load (L_a).

6.3.1 Performance Efficiency: Collection System

The CS was analyzed using all three relevant methods. However, most of the results obtained from the DSA of the CS are included in the comprehensive evaluation of the full system, which is discussed in Section 6.3.3. This approach is adopted to enhance the visual representation of the results, as standalone presentation may not provide the same level of information without the opportunity for comparison. However, a comparison of the DSA of the CS and the combinatorial method will be provided in this section. The absence of results from the NR methodology in this section is due to its failure to converge. This issue could be attributed to the X/R ratio mentioned in Section 4.6; however, a detailed discussion on this matter will be presented in the subsequent discussion section.

Figure 6.11 shows the active and reactive losses computed using the DSA and combina-

torial methodology. In the AC-configuration, the combinatorial methodology resulted in 1.15% active losses for the CS, while the DSA calculated 1.42%. In the LFAC-configuration, the combinatorial methodology resulted in 1.15% active losses, compared to 1.39% for the DSA. For reactive power losses in the LFAC-configuration, the combinatorial methodology showed 0.39%, whereas the DSA analysis resulted in 0.48%.

6.3.2 Performance Efficiency: Transmission to Shore

The performance efficiency analysis of the TTS was conducted using both the DSA and NR methods. The results encompass active and reactive power losses, as well as voltage magnitudes and angles, for both the AC and LFAC configurations of the system. Furthermore, plots illustrating the variations in the results are generated to provide a visual representation of the differences. The execution of these analyses was done assuming 100% electrical efficiency of the WTs. The power coming from the CS into the OSS is considered as the PV bus generating 0.9763 p.u active power and 0.0318 p.u reactive power. For the LFAC-configuration of the system, the active power injection at Bus 1 equals 0.9764 p.u and the reactive power injection equals 0.0767 p.u. These values are obtained from the execution of the DSA on the full system (AC and LFAC) and are used for both the DSA and the NR analyses and can be seen in Figure C.28 and Figure C.11 in Appendix C.4.

In Appendix C.4, it can be seen that the total losses of the TTS calculated through both the NR load flow and the DSA equals 0.58% in terms of active losses and 12.63% in terms of reactive losses.

Table 6.6 shows the resulting voltage magnitude and angle from the DSA and NR method. The PV bus is represented by Bus 1, while the slack bus represents the stiff grid at the PCC. Some variations are observed in the results obtained from the two different methods. In the NR analysis results, the voltage magnitude seems to remain constant, but there are variations in the voltage angle. Comparing the two results, it can be observed that the voltage angle of Bus 1 differs by only 0.02 degrees. Nevertheless, the DSA analysis reveals a voltage decrease of 0.0018 p.u across the TTS cables, which is equivalent to a voltage drop of 396 V. The results for the LFAC-configuration of the system are displayed

Table 6.5: *Results from performance efficiency analysis of the TTS with DSA and NR. Active and reactive power of the AC-system.*

Method	Bus	Active power [p.u]	Active power [MW]	Reactive power [p.u]	Reactive power [MW]
NR	**Bus 1 (PV - OSS)**	0.9763	488.15	0.0185	9.25
	Bus 2 (Slack - Stiff Grid)	-0.9705	-485.25	0.1082	54.1
DSA	**Bus 1 (PV - OSS)**	0.9763	488.15	0.0157	7.85
	Bus 2 (Slack - Stiff Grid)	-0.9705	-485.25	0.0945	47.25

Table 6.6: *Results from performance efficiency analysis of the TTS with DSA and NR. Voltage magnitude and angle of the AC-system.*

Method	Bus	Voltage Magnitude [p.u]	Voltage Magnitude [kV]	Voltage Angle [deg]
NR	**NR: Bus 1 (PV - OSS)**	1.0000	220.00	7.45
	NR: Bus 2 (Slack - Stiff Grid)	1.0000	220.00	0.00
DSA	**DSA: Bus 1 (PV - OSS)**	1.0018	220.39	7.43
	DSA: Bus 2 (Slack - Stiff Grid)	1.0000	220.00	0.00

in Figure 6.8. Similarly, a comparable trend is observed, with a higher voltage drop of 0.0092 p.u, corresponding to 2024 V. However, the voltage angle of Bus 1 is lower in the LFAC-configuration compared to the AC-configuration, measuring 4.10 degrees as per the DSA analysis.

Active and reactive power at the buses in the TTS analysis can be seen in Table 6.5 and 6.7. Upon comparing the results obtained from the two different methods, variations in both active and reactive power become evident. A noticeable difference lies in the considerable deviation observed in reactive power when comparing the two methodologies, particularly in the LFAC case. These discrepancies will be thoroughly analyzed and discussed in the subsequent discussion section. However, Figure 6.12 visually illustrates the active and reactive power outcomes for the DSA analysis. Similarly, Figure 6.13 presents the corresponding data from the LFAC-configuration of the system. These figures aims to facilitate for a better comparison of the active and reactive power within the system for both system configurations.

Figure 6.14 presents the charging currents in the TTS. This figure is derived from previous work, as mentioned earlier in Section 3.2.5. The primary purpose of this plot is to emphasize the significance of considering charging currents, particularly in the TTS. The input parameters used are partly based on the results obtained from the DSA analysis

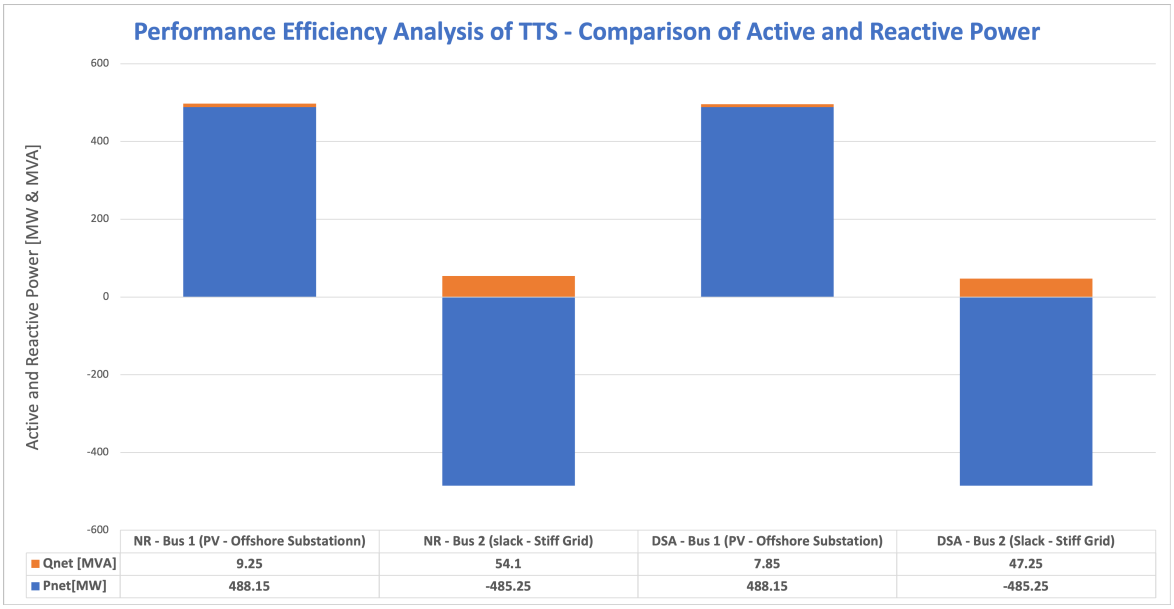

Figure 6.12: *Plot of active and reactive power in the TTS based on performance efficiency results with DSA and NR.*

Table 6.7: *Results from performance efficiency analysis of the LFAC TTS with DSA and NR - active and reactive power.*

Method	Bus	Active power [p.u]	Active power [MW]	Reactive power [p.u]	Reactive power [MW]
NR	Bus 1 (PV - OSS)	0.9764	488.20	-0.0545	-27.25
(LFAC)	Bus 2 (Slack - Stiff Grid)	-0.9698	-484.90	0.1255	62.75
DSA	Bus 1 (PV - OSS)	0.9764	488.20	0.0011	0.55
(LFAC)	Bus 2 (Slack - Stiff Grid)	-0.9699	-484.95	0.0453	22.65

Table 6.8: *Results from performance efficiency analysis of the LFAC TTS with DSA and NR - voltage magnitude and angle.*

Method	Bus	Voltage Magnitude [p.u]	Voltage Magnitude [kV]	Voltage Angle [deg]
NR	NR: Bus 1 (PV - OSS)	1.0000	220.00	4,18
(LFAC)	NR: Bus 2 (Slack - Stiff Grid)	1.0000	220.00	0
DSA	DSA: Bus 1 (PV - OSS)	1,0092	222.02	4,10
(LFAC)	DSA: Bus 2 (Slack - Stiff Grid)	1.0000	220.00	0

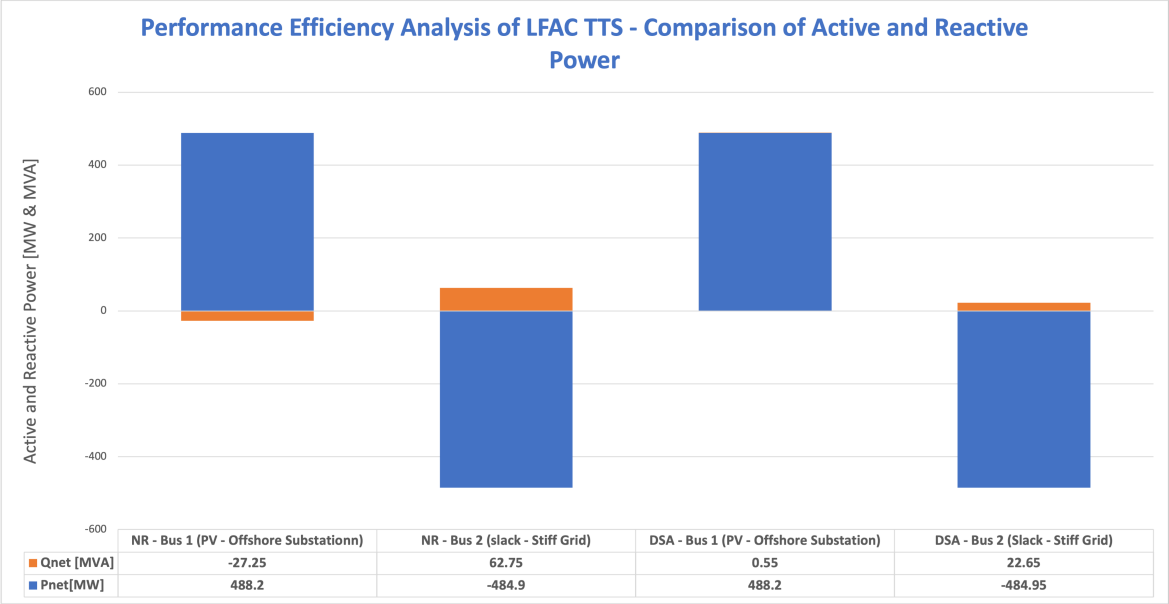

Figure 6.13: *Plot of active and reactive power in the LFAC TTS based on performance efficiency results with DSA and NR.*

of the entire system. In the AC-configuration of the TTS, the charging currents lead to a reduction of approximately 10.13 MW in the available active power delivered to the stiff grid. Conversely, in the LFAC-configuration of the TTS, the charging currents only account for around 1.12 MW of the available active power delivered to the grid. The significance of considering charging currents will be elaborated upon in the following discussion section.

6.3.3 Performance Efficiency: Full System

This subsection presents the results obtained from the analysis of the entire system, encompassing both the CS and the TTS components. In this analysis, both the DSA and NR load flow methods are employed, similar to the previous TTS analysis. Here, results of power losses and voltage properties within the system are presented. Furthermore, this section presents comparisons between the utilized methods and the two system configurations, namely AC and LFAC. Additionally, the discussion delves into the implications of conducting separate analyses for the CS and TTS components through the DSA. As previously stated within this section, all energy-based calculations assume an electrical efficiency of 85%. This implies that the power output is 85% of the maximum capacity

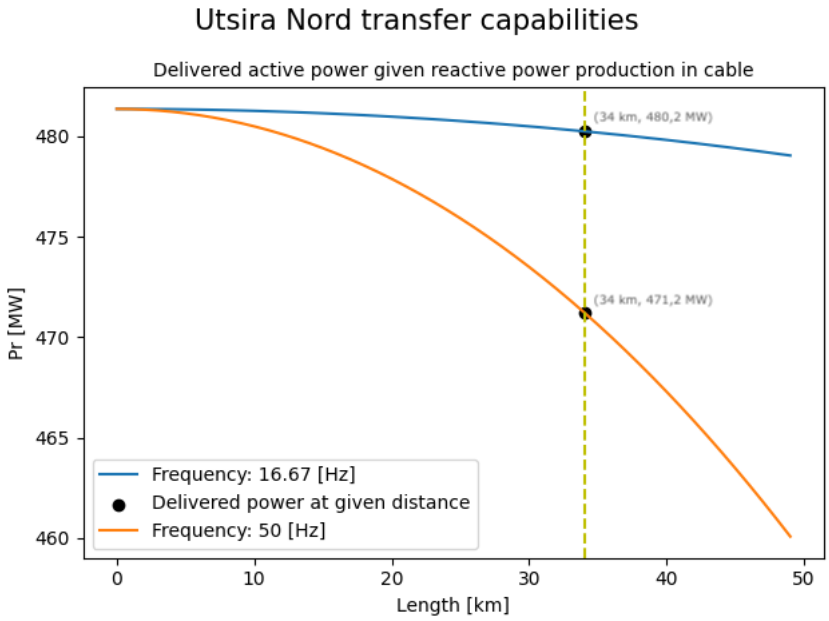

Figure 6.14: *Reactive power production in TTS due to charging currents.*

of the wind turbines, which is 15 MW for power output and 1.5 VAr for reactive power.

The power losses calculated through the DSA of the full system equals 1.94% in terms of active losses and 13.94% in terms of reactive losses, as can be seen in Appendix C.5. In the LFAC-configuration of the system, the total active power losses were 2.17% and the reactive losses were 5.57%, as calculated using the DSA for the full system (see Appendix C.6). This resulted in approximately 5 GWh higher losses in active power compared to the AC-configuration. The AC-configuration, on the other hand, had around 7.8 GVArh higher losses in terms of reactive power.

Figure 6.15 illustrates the overall energy losses within the system obtained with DSA, presented as active and reactive losses for each respective system component. It illustrates the total losses calculated for the CS alone, the TTS alone, the combined losses of both components together with the transformer losses, and the resulting losses for the entire system. It can be seen that the power losses of the entire system (CS + TTS) differs from the total of the other components losses obtained separately with 470 MWh for active energy and 950 MVArh reactive energy.

Figures 6.16 and 6.17 depicts the contribution from each system component on respectively active and reactive losses calculated through the DSA, where the results are based

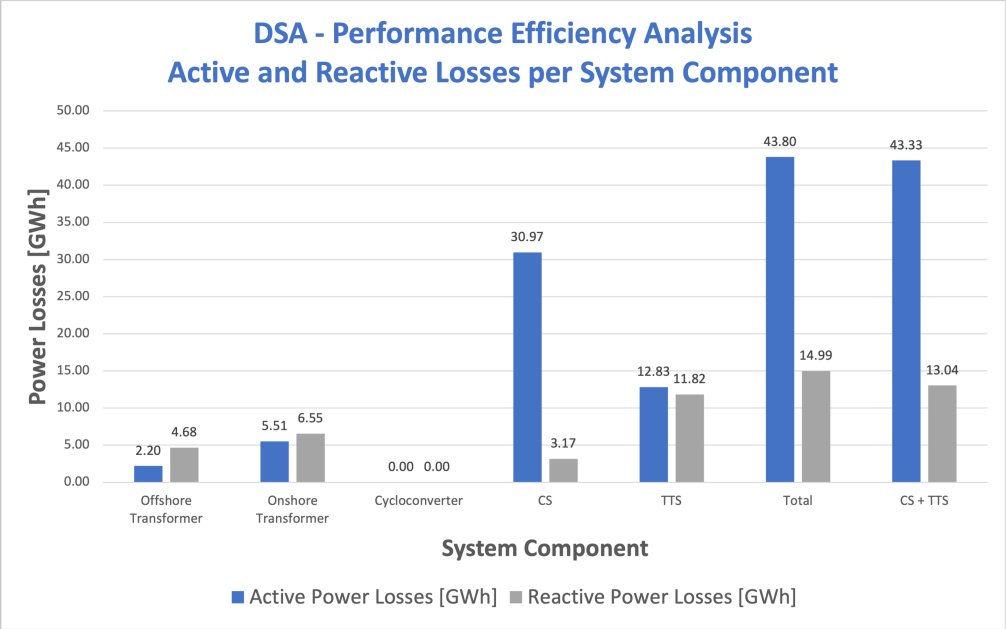

Figure 6.15: *Active and reactive losses in [GWh] per component computed for the AC-system in DSA.*

on the CS and TTS results presented in earlier sections. The analysis reveals that the CS accounts for 60% of the total active losses in the system, whereas it contributes only 12% to the reactive losses. On the other hand, the TTS represents 45% of the reactive losses, making it the largest contributor to reactive losses within the system. While the TTS only accounts for 25% of the active losses in the AC-configuration of the system.

Similar to the aforementioned figures, Figures 6.19 and 6.20 illustrate the contribution of each component to the active and reactive losses, respectively, in the LFAC-configuration of the entire system. For this system, the cycloconverter contributes to both active and reactive losses. The cycloconverter accounts for 9% of the active power losses and 9% of the reactive power losses. The results also indicate that the CS component is responsible for 50% of the active power losses and only 5% of the reactive power losses. On the other hand, the TTS component contributes to a total of 48% of the reactive power losses and 29% of the active power losses. These results could lead to some interesting questions and reflections and will be explored in the subsequent section.

Figure 6.18 illustrates the power losses in the LFAC-configuration of the system. Similar to Figure 6.15, it presents a comparison of the calculated power losses for each individual component with the overall system analysis conducted through the DSA. Interesting

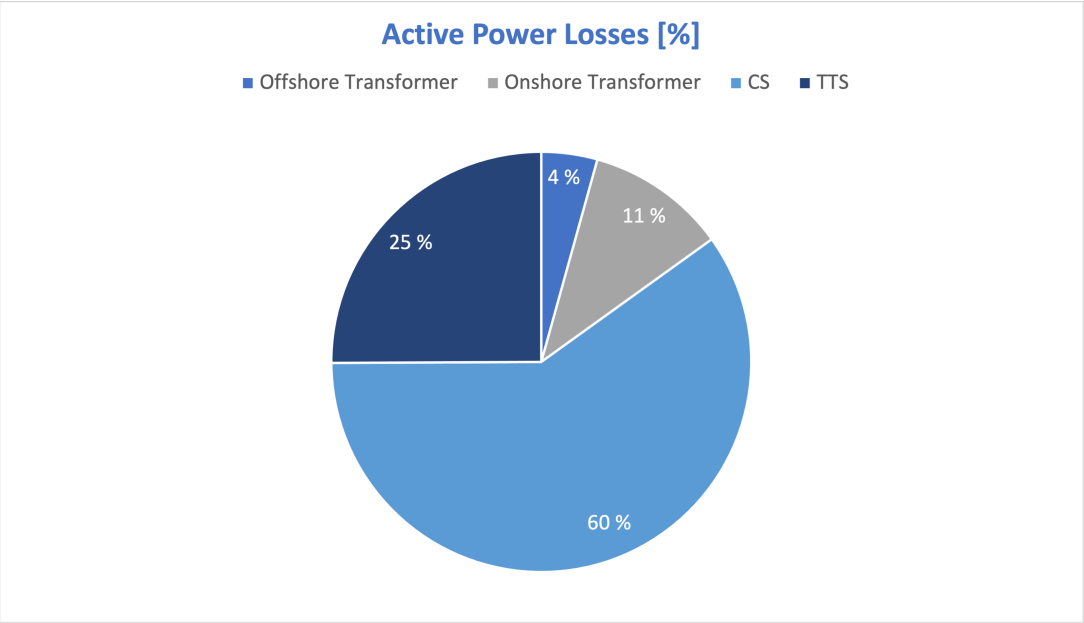

Figure 6.16: *Active losses in [%] per component computed in DSA.*

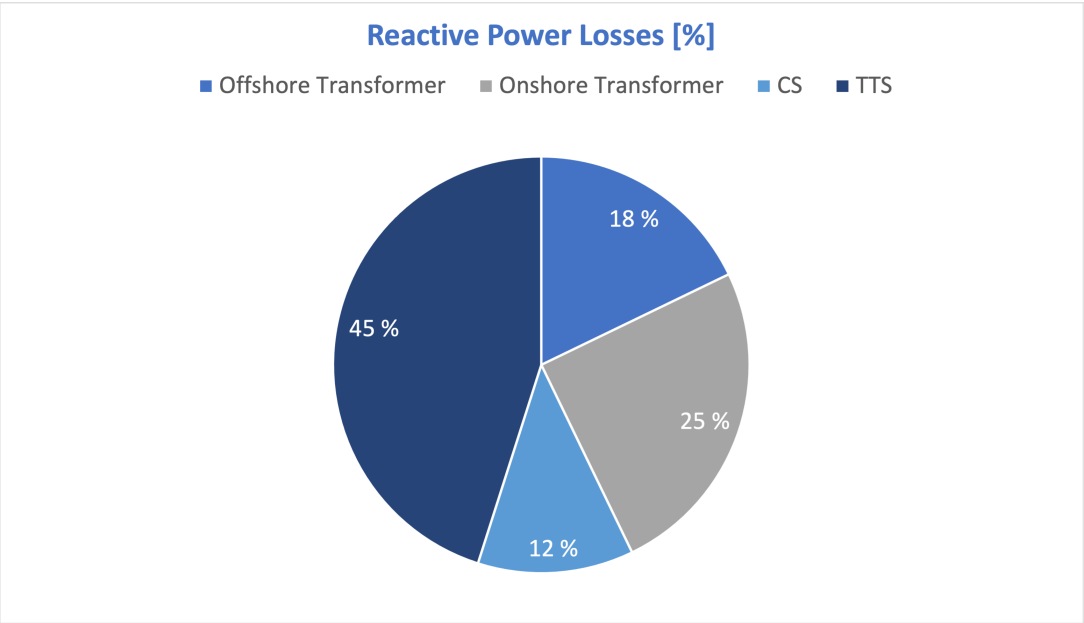

Figure 6.17: *Reactive losses in [%] per component computed in DSA.*

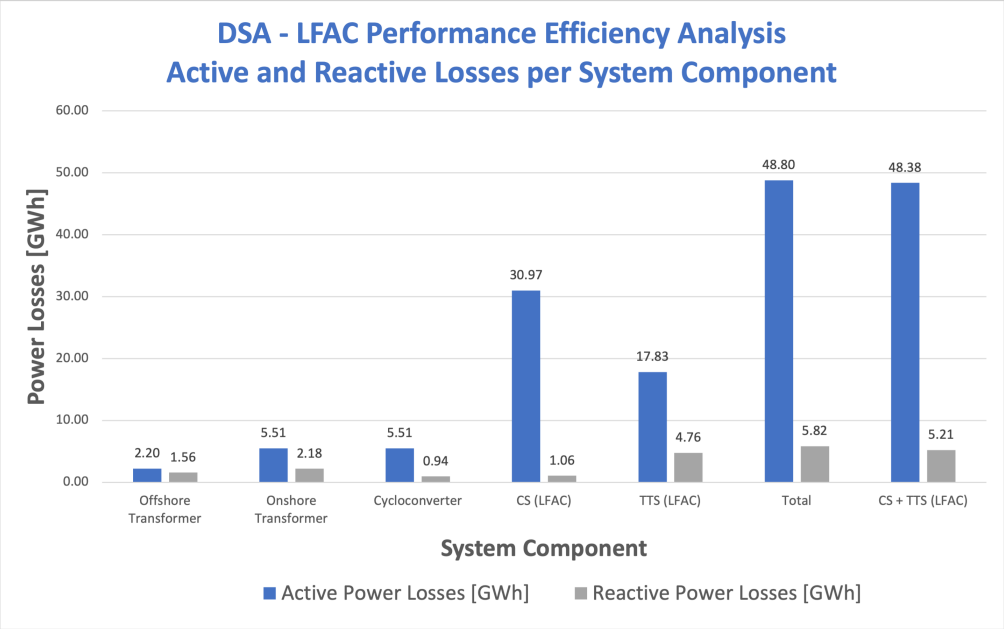

Figure 6.18: *Active and reactive losses in [GWh] per component computed for the LFAC-system in DSA.*

findings within these results will be further discussed.

In relation to the voltage profiles observed in the system through the performance efficiency analyses, the following figures aims to illustrate how the voltage differs within the system. Also, they aim to highlight the differences that that can be observed between the AC and the LFAC configurations of the system. The relevant figures provide the DSA results for both the voltage magnitude and voltage angle.

The evolving voltage profile of the full system in p.u is presented in Figure 6.21. It presents the voltage magnitude of both system configurations. It can be clearly observed that the voltage increases towards the outer WTs in each string. In addition, Bus 9, which has to longest cable distance to the OSS and hence the PCC, shows to achieve the highest voltage magnitude, equaling 1.0382 p.u equaling 68.52 kV. This can also be seen in Table 6.9, who includes the full voltage result output from the DSA of the full system. The data in the table is based on the figures in Appendices C.5 and C.6 on voltage properties. The decision has been made not to provide similar tables for other cases, as the author finds it more appropriate to refer to the Appendix in a general basis. Furthermore, the line flows specific to this case can also be found in Appendices C.5 and C.6. The voltage profile of the LFAC-configuration of the full system can be observed

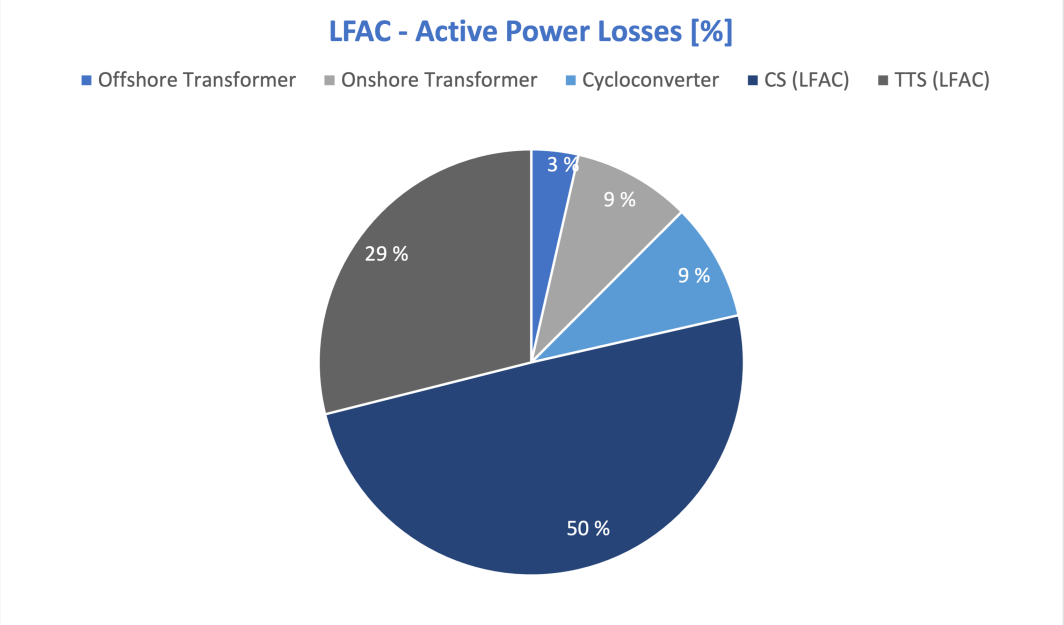

Figure 6.19: *Active losses in [%] per LFAC component computed in the DSA.*

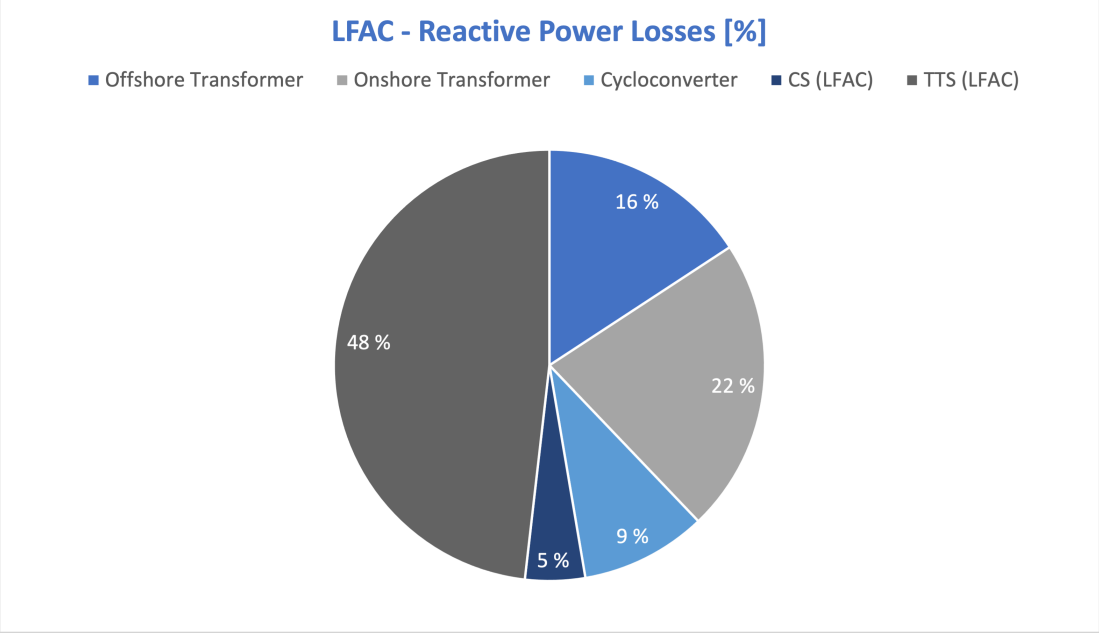

Figure 6.20: *Reactive losses in [%] per LFAC component computed in the DSA.*

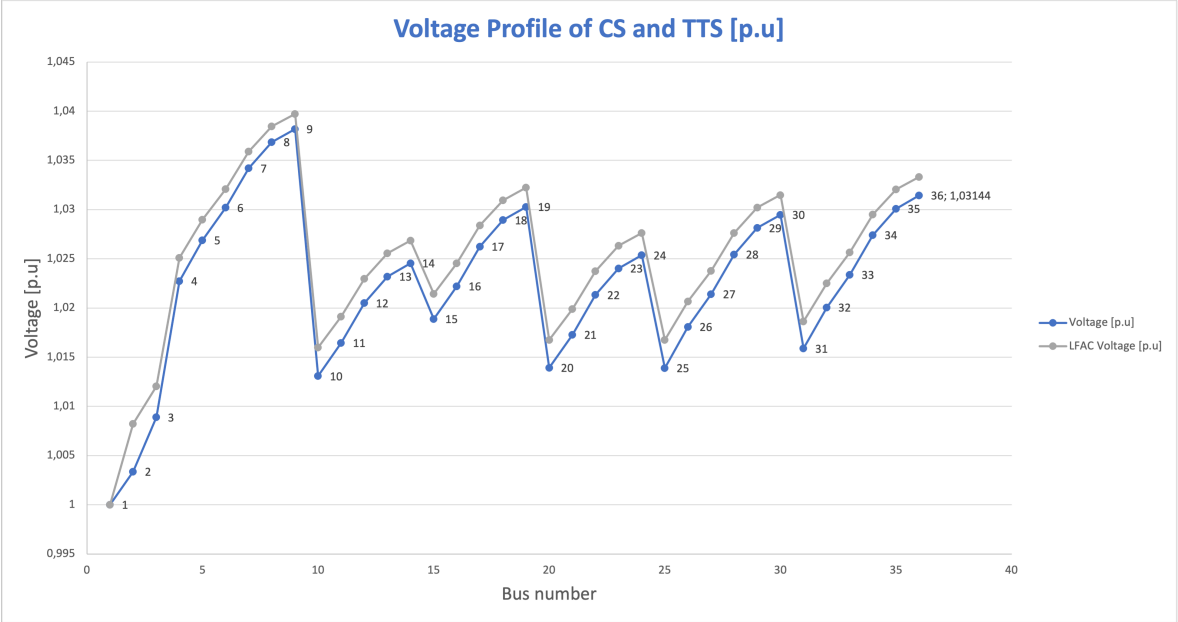

Figure 6.21: *Voltage profile in [p.u] of each bus in the case system for both AC and LFAC obtained through the DSA.*

with an increased voltage magnitude throughout the whole system. The voltage profile of the full system contains interesting information and will serve as an important source to reflection within the discussion of the results in the coming section.

A similar pattern to the voltage magnitude of the system can be seen for the voltage angle in Figure 6.22. Both the voltage angles in the AC- and LFAC-configuration of the system are presented. The AC-configuration of the system shows a noticeable trend of angles generally being 3.5-5.0 degrees higher than the LFAC-configuration, this can be seen in Figure 6.23. Moreover, there is an observed increase in the internal angle difference within the AC-configuration in Figure 6.22. More specifically, a difference of approximately 0.45 degrees between the inner and outer bus of the five WT radials and approxiamtely 0.6 degrees for the six WT radials in the AC-system. While in the LFAC-system, the variations are typically in the range 0.1-0.2 degrees for each string. According to the data presented in Figure 6.22, it is evident that the TTS experiences the greatest internal voltage deviation in terms of angle for both system configurations.

Similar to Figure 6.24, Figure 6.24 presents the difference in voltage magnitude, when comparing the AC- and LFAC-configurations of the system. It was obtained through subtracting the voltages of the LFAC-system from the voltages of the AC-system. It can

Table 6.9: *Resulting voltage output from DSA of full system. Provided for this case execution only, based on figures in Appendices C.5 and C.6. As mentioned, for information regarding other cases and the line flows of this execution, please see Appendix C.*

Bus number	Voltage [p.u]	Voltage [kV]	Theta [deg]	LFAC Voltage [p.u]	LFAC Voltage [kV]	LFAC Theta [deg]
1	1.00000	220.00	0.00	1.00000	220.00	0.00
2	1.00337	220.74	4.25	1.00823	221.81	1.94
3	1.00889	66.59	7.36	1.01205	66.80	2.96
4	1.02274	67.50	8.09	1.0251	67.66	3.15
5	1.02689	67.77	8.31	1.02898	67.91	3.21
6	1.0302	67.99	8.48	1.03208	68.12	3.25
7	1.0342	68.26	8.61	1.0359	68.37	3.28
8	1.03687	68.43	8.69	1.03845	68.54	3.30
9	1.0382	68.52	8.73	1.03972	68.62	3.31
10	1.01308	66.86	7.58	1.01598	67.05	3.02
11	1.01645	67.09	7.75	1.01912	67.26	3.06
12	1.0205	67.35	7.88	1.02299	67.52	3.09
13	1.0232	67.53	7.97	1.02556	67.69	3.11
14	1.02455	67.62	8.01	1.02685	67.77	3.12
15	1.01888	67.25	7.88	1.02143	67.41	3.01
16	1.02222	67.47	8.06	1.02455	67.62	3.14
17	1.02625	67.73	8.19	1.0284	67.87	3.17
18	1.02894	67.91	8.27	1.03096	68.04	3.19
19	1.03028	68.00	8.32	1.03224	68.13	3.20
20	1.01392	66.92	7.62	1.01676	67.11	3.03
21	1.01728	67.14	7.80	1.0199	67.31	3.07
22	1.02133	67.41	7.93	1.02376	67.57	3.10
23	1.02402	67.59	8.01	1.02634	67.74	3.12
24	1.02537	67.67	8.06	1.02763	67.82	3.13
25	1.0139	66.92	7.62	1.01675	67.11	3.03
26	1.01808	67.19	7.84	1.02066	67.36	3.08
27	1.02142	67.41	8.01	1.02379	67.57	3.13
28	1.02545	67.68	8.14	1.02764	67.82	3.16
29	1.02814	67.86	8.23	1.0302	67.99	3.18
30	1.02948	67.95	8.27	1.03149	68.08	3.19
31	1.01588	67.05	7.73	1.01862	67.23	3.05
32	1.02005	67.32	7.95	1.02252	67.49	3.11
33	1.02339	67.54	8.11	1.02564	67.69	3.16
34	1.02742	67.81	8.25	1.02949	67.95	3.19
35	1.0301	67.99	8.33	1.03205	68.12	3.21
36	1.03144	68.08	8.34	1.03333	68.20	3.22

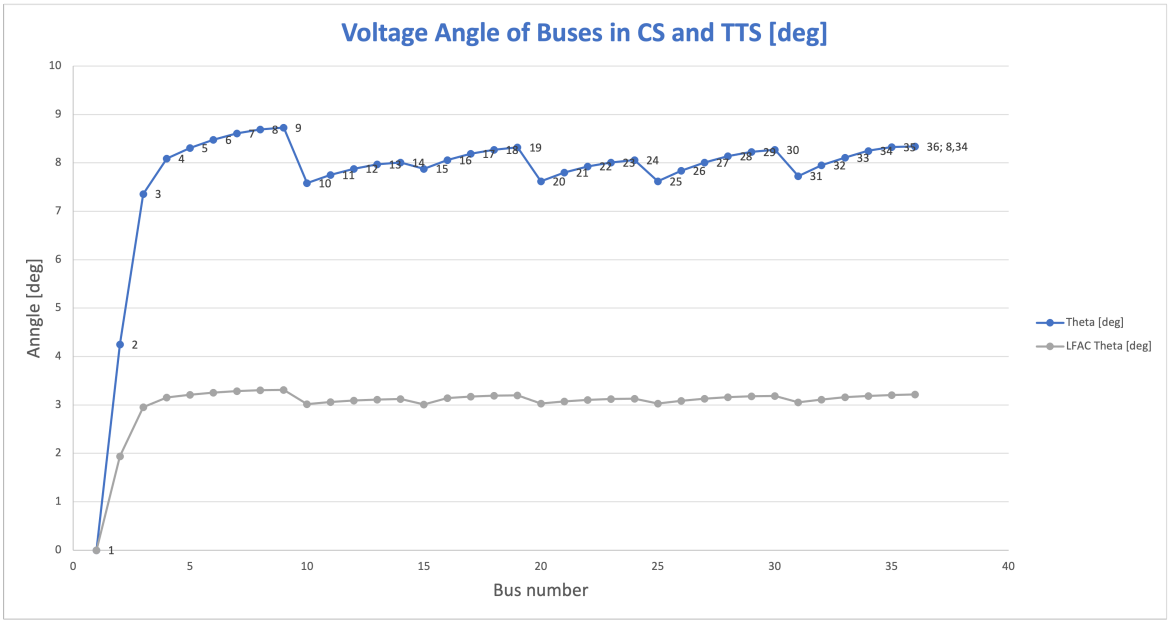

Figure 6.22: *Voltage angle in [deg] of each bus in the case system for both AC and LFAC obtained through the DSA.*

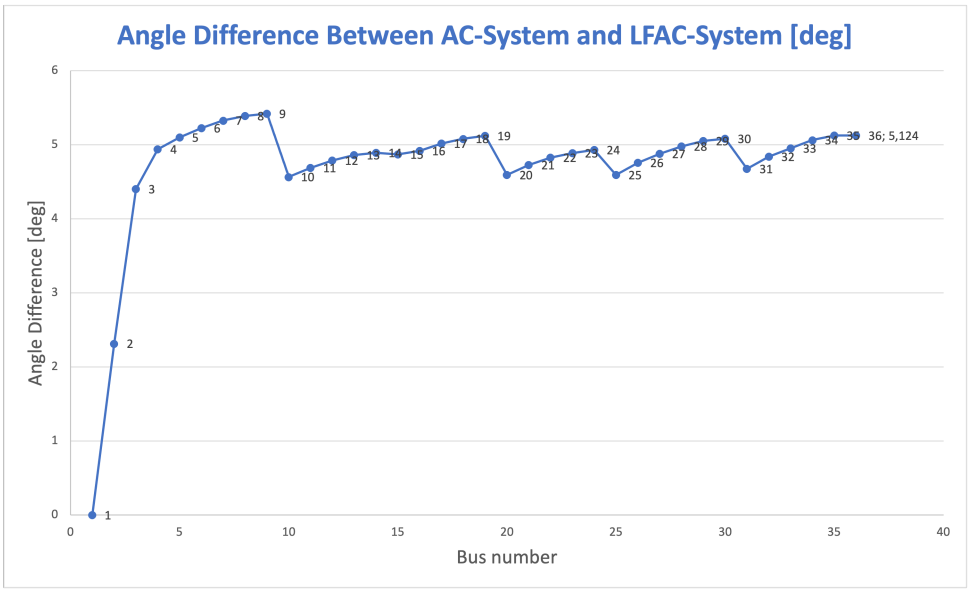

Figure 6.23: *Voltage angle difference between AC- and LFAC-system for all buses in degrees, obtained through the DSA.*

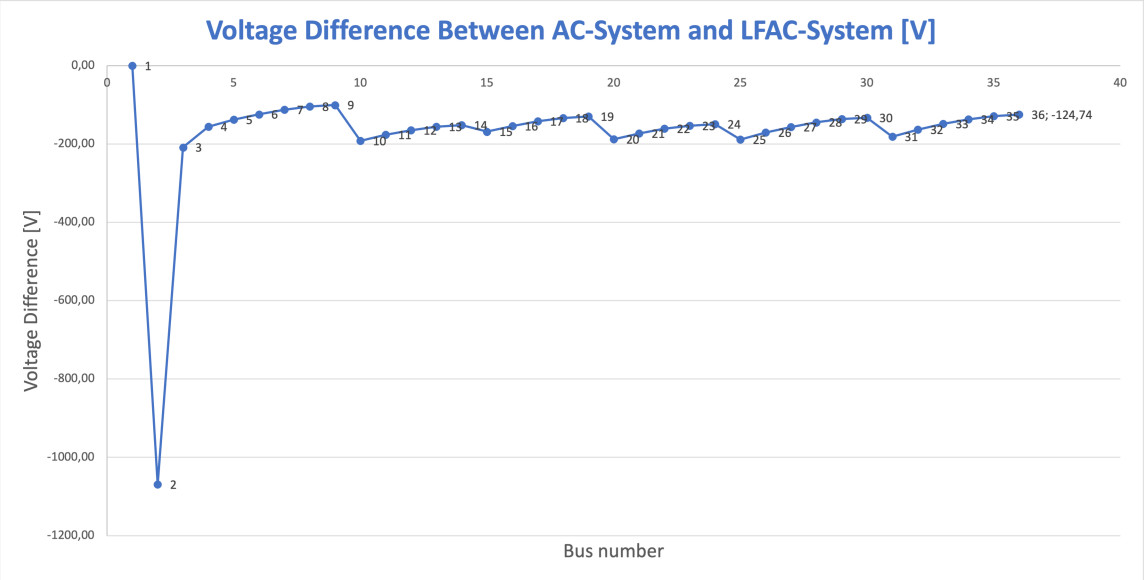

Figure 6.24: *Voltage magnitude difference between AC- and LFAC-system for all buses in [V] obtained through the DSA.*

be seen that the voltage deviation is largest at Bus 2, which is the middle of the TTS. The reason for this will be further discussed in the subsequent discussion section.

In order to improve the visualization of voltage in the radial topology, Figure 6.25 illustrates the voltage profile of string 1, comprising Bus 3 to Bus 9. The plot clearly demonstrates the consistent patterns of voltage variation within the string, independent of the system-configuration (AC or LFAC). Additionally, it reaffirms the observation that the LFAC string exhibits higher voltages throughout the entire string, as anticipated. In general, the voltages of the conventional AC-configuration is approximately 100-200 V lower than the voltages of the LFAC-string, as can be seen in Figure 6.24 as well.

6.3.4 Reliability: RELRAD w/ Radial Topology

As stated in the introduction of this main section, the primary focus of the RELRAD analysis was to calculate the ENS for different system typologies, specifically radial and single-sided ring. Furthermore, the outcomes of the RELRAD analysis are presented similarly to the interpretation of the RELRAD analysis in Section 5.2. As mentioned earlier in this main section, the switching time is disregarded in the radial analysis for the sake of simplicity. This decision is based on the consideration that line outages and

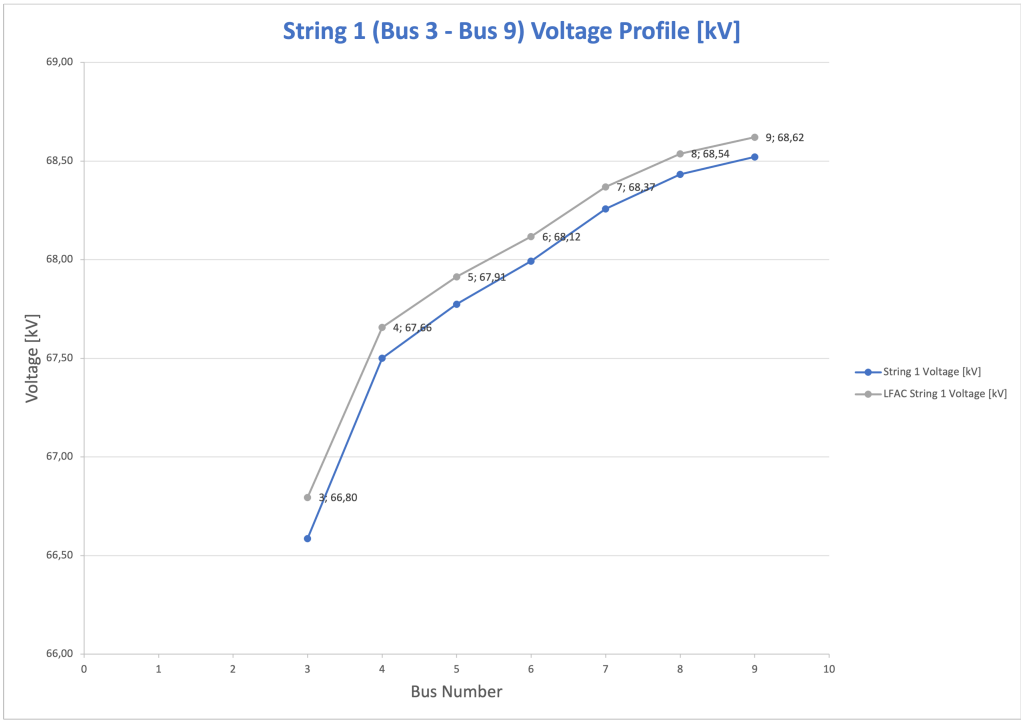

Figure 6.25: *Voltage profile in [kV] for string 1 (Bus 3 - Bus 9) presented for AC and LFAC system obtained in through DSA.*

switching events result in different load curtailments. Furthermore, it is assumed that the impact of switching time on the final results is minimal, as demonstrated by the analysis of the single-sided ring topology.

The average load utilized in this analysis, as calculated from the DSA, was 0.8274 p.u and can be seen in Appendix C.7.1. Based on the assumed operating hours of the OWPP at 5300 hours and the mentioned energy production assumptions regarding the power output from the WTs, an average annual energy production of 2192.6 GWh was considered as the average energy load.

Results from the RELRAD methodology when analysing the two topologies, can be seen in Table 6.10 and 6.11. The interpretation and significance of the system parameters, which include the resulting failure rate, repair time, and unavailability, will be discussed in the subsequent section. The Figures provided in this section are based on the results in the given tables. The load curtailment was determined by combining the average load values with the DSA results for the fault scenarios.

Figure 6.26 visualize the contribution from each component to the system ENS for the

Table 6.10: *Results from reliability analysis of the radial topology through the RELRAD methodology.*

Failing component	λ [$\frac{\text{failures}}{\text{year}}$]	r [$\frac{\text{hours}}{\text{failure}}$]	U [$\frac{\text{hours}}{\text{year}}$]	$P_{\text{delivered}}$ - DSA [p.u.]	L_c [MW]	ENS [MWh]
A	0.03750	1440	54.000	0.8029	12.3	661.5
B	0.03750	1440	54.000	0.7781	24.7	1331.1
C	0.03750	1440	54.000	0.7532	37.1	2003.4
D	0.03750	1440	54.000	0.7281	49.7	2681.1
E	0.03750	1440	54.000	0.7029	62.3	3361.5
F	0.05250	1440	75.600	0.6776	74.9	5662.4
G	0.03750	1440	54.000	0.8028	12.3	664.2
H	0.03750	1440	54.000	0.778	24.7	1333.8
I	0.03750	1440	54.000	0.753	37.2	2008.8
J	0.03750	1440	54.000	0.7279	49.8	2686.5
K	0.03750	1440	54.000	0.7027	62.4	3366.9
L	0.03750	1440	54.000	0.6774	75.0	4050.0
M	0.03750	1440	54.000	0.8027	12.4	666.9
N	0.03750	1440	54.000	0.7777	24.9	1341.9
O	0.03750	1440	54.000	0.7526	37.4	2019.6
P	0.03750	1440	54.000	0.7274	50.0	2700.0
Q	0.04500	1440	64.800	0.7022	62.6	4056.5
R	0.03750	1440	54.000	0.8028	12.3	664.2
S	0.03750	1440	54.000	0.778	24.7	1333.8
T	0.03750	1440	54.000	0.753	37.2	2008.8
U	0.03750	1440	54.000	0.7279	49.8	2686.5
V	0.09000	1440	129.600	0.7027	62.4	8080.6
W	0.03750	1440	54.000	0.8026	12.4	669.6
X	0.03750	1440	54.000	0.7777	24.9	1341.9
Y	0.03750	1440	54.000	0.7526	37.4	2019.6
Z	0.03750	1440	54.000	0.7274	50.0	2700.0
AA	0.03750	1440	54.000	0.7021	62.7	3383.1
AB	0.03750	1440	54.000	0.8031	12.2	656.1
AC	0.03750	1440	54.000	0.7785	24.5	1320.3
AD	0.03750	1440	54.000	0.7538	36.8	1987.2
AE	0.03750	1440	54.000	0.7288	49.3	2662.2
AF	0.03750	1440	54.000	0.7036	61.9	3342.6
AG	0.10500	1440	151.200	0.6784	74.5	11264.4
Offshore Transformer	0.02000	4320	86.400	0	413.7	35743.7
TTS Cable	0.08149	480	39.114	0	413.7	16181.6
Onshore Transformer	0.02000	1440	28.800	0	413.7	11914.6
Total	1.50149	1426	2141.514	-	-	150556.8
Total [GWh]	-	-	-	-	-	**150.56**

Table 6.11: *Results from reliability analysis of the single-sided ring topology through the RELRAD methodology.*

Failing component	λ [$\frac{\text{failures}}{\text{year}}$]	r [$\frac{\text{hours}}{\text{failure}}$]	U [$\frac{\text{hours}}{\text{year}}$]	$P_{\text{delivered}}$ - DSA [p.u.]	L_c [MW]	ENS [MWh]
A	0.03750	0.5	0.019	0.6776	74.9	1.4
B	0.03750	0.5	0.019	0.6776	74.9	1.4
C	0.03750	0.5	0.019	0.6776	74.9	1.4
D	0.03750	0.5	0.019	0.6776	74.9	1.4
E	0.03750	0.5	0.019	0.6776	74.9	1.4
F	0.05250	0.5	0.026	0.6776	74.9	2.0
G	0.03750	0.5	0.019	0.6774	75.0	1.4
H	0.03750	0.5	0.019	0.6774	75.0	1.4
I	0.03750	0.5	0.019	0.6774	75.0	1.4
J	0.03750	0.5	0.019	0.6774	75.0	1.4
K	0.03750	0.5	0.019	0.6774	75.0	1.4
L	0.03750	0.5	0.019	0.6774	75.0	1.4
M	0.03750	0.5	0.019	0.7022	62.6	1.2
N	0.03750	0.5	0.019	0.7022	62.6	1.2
O	0.03750	0.5	0.019	0.7022	62.6	1.2
P	0.03750	0.5	0.019	0.7022	62.6	1.2
Q	0.04500	0.5	0.023	0.7022	62.6	1.4
R	0.03750	0.5	0.019	0.7027	62.4	1.2
S	0.03750	0.5	0.019	0.7027	62.4	1.2
T	0.03750	0.5	0.019	0.7027	62.4	1.2
U	0.03750	0.5	0.019	0.7027	62.4	1.2
V	0.09000	0.5	0.045	0.7027	62.4	2.8
W	0.03750	0.5	0.019	0.7021	62.7	1.2
X	0.03750	0.5	0.019	0.7021	62.7	1.2
Y	0.03750	0.5	0.019	0.7021	62.7	1.2
Z	0.03750	0.5	0.019	0.7021	62.7	1.2
AA	0.03750	0.5	0.019	0.7021	62.7	1.2
AB	0.03750	0.5	0.019	0.6784	74.5	1.4
AC	0.03750	0.5	0.019	0.6784	74.5	1.4
AD	0.03750	0.5	0.019	0.6784	74.5	1.4
AE	0.03750	0.5	0.019	0.6784	74.5	1.4
AF	0.03750	0.5	0.019	0.6784	74.5	1.4
AG	0.10500	0.5	0.053	0.6784	74.5	3.9
Offshore Transformer	0.03000	4320	129.600	0	413.7	53615.5
TTS Cable	0.08149	480	39.114	0	413.7	16181.6
Onshore Transformer	0.02000	1440	28.800	0	413.7	11914.6
Total [MWh]	1.51149	131.1	198.204	-	-	**81759.5**
Total [GWh]	-	-	-	-	-	**81.76**

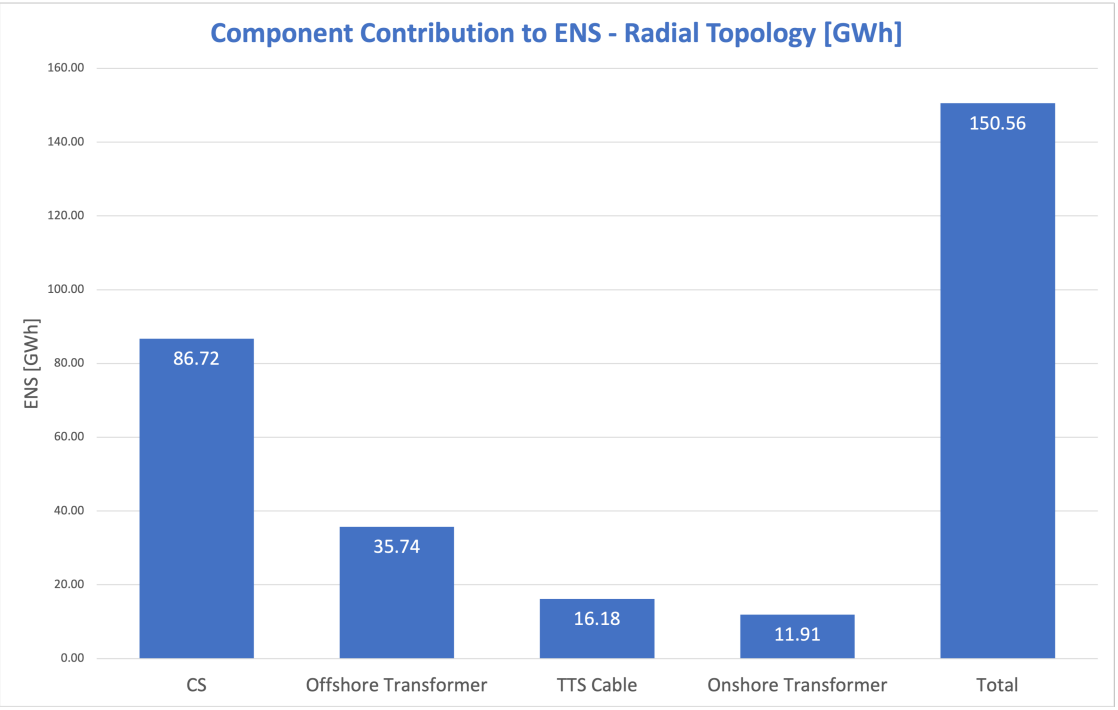

Figure 6.26: *Component contribution to total ENS in [GWh] of the RELRAD-analysis conducted with a radial CS topology.*

system with a radial CS topology. A cumulative ENS of 150.56 GWh is observed. It can also be seen that the CS accounts for the largest contribution to the ENS, accounting to 86.72 GWh. The information is illustrated in a percentage format in Figure 6.27. The contribution from the CS to the system ENS shows to equal 57% of the total ENS. In contrast, the onshore transformer is found to have the smallest contribution to the ENS, accounting for only 8% of the total system ENS.

6.3.5 Reliability: RELRAD w/ Single-Sided Ring Topology

Figure 6.28 depcits the component contribution to the accumulated system ENS in the same way as Figure 6.26. Due to the redundancy lines in the single-sided ring topology, the contribution from the CS is as low as 0.5 GWh. This equals 0% in the pie chart in Figure 6.29. In other words, the CS transitions from being the primary contributor to ENS in the radial topology to becoming the smallest contributor in the single-sided ring topology. These findings will be explored further in the subsequent section.

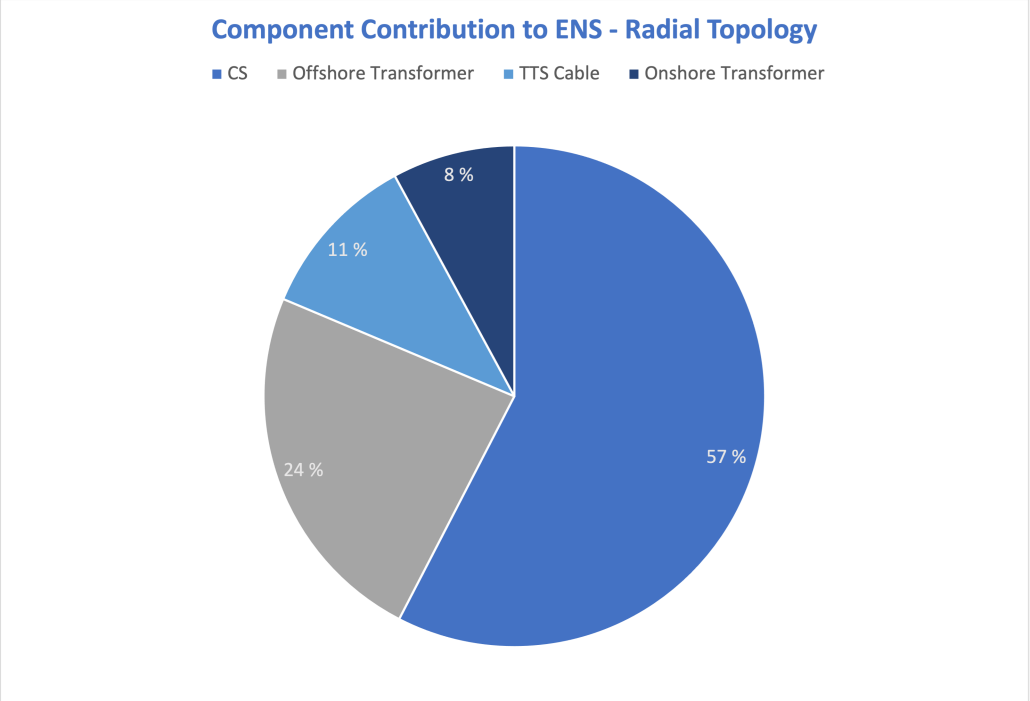

Figure 6.27: *Component contribution to total ENS in [%] of the RELRAD-analysis conducted with a radial CS topology.*

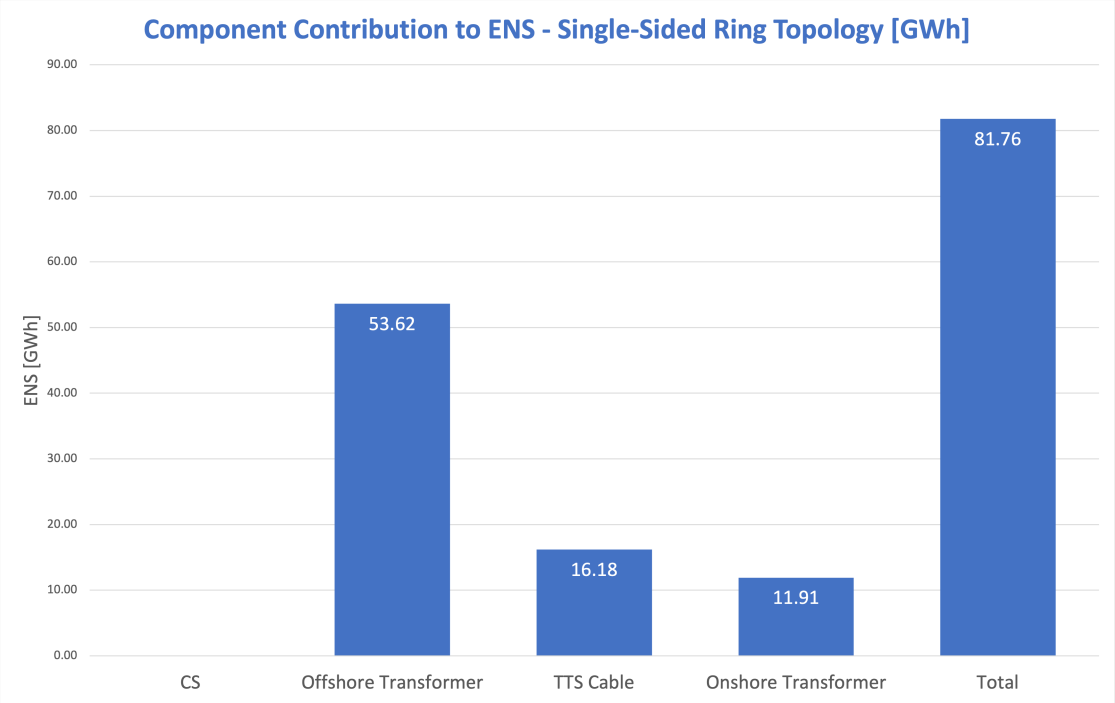

Figure 6.28: *Component contribution to total ENS in [GWh] of the RELRAD-analysis conducted with a single-sided ring CS topology.*

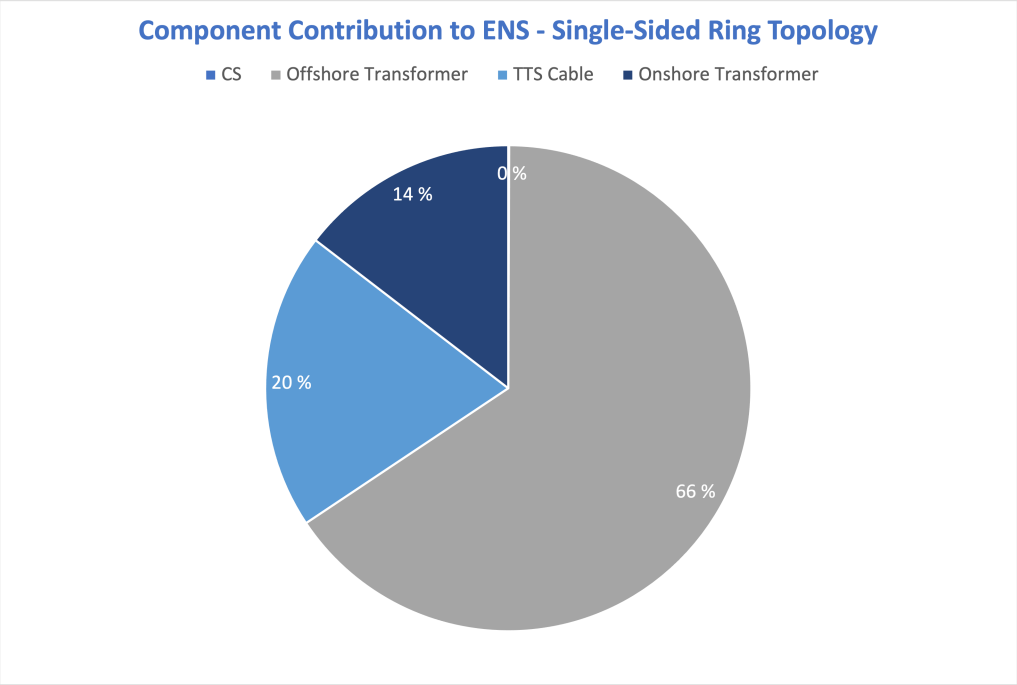

Figure 6.29: *Component contribution to total ENS in [%] of the RELRAD-analysis conducted with a single-sided ring CS topology.*

6.4 Discussion: Reflection of Results and Interesting Findings

The discussion will be structured to highlight the most significant findings from the case study results, starting with the CS. This will be based on the CS results presented in Section 6.3.1 and will be supplemented by relevant observations from Section 6.3.3. Similarly, the most interesting findings from the results based on the TTS analyses presented in Section 6.3.2, along with the relevant findings from Section 6.3.3 regarding the TTS performance efficiency, will be discussed. Eventually, the most significant reliability results for both CS topologies presented in the previous section will be discussed.

6.4.1 Performance Efficiency: Collection System

In terms of the X/R ratio, the OWPP CS cables have a value of less than 1 for the sections of the CS where 500 mm^2 cables are present. It can be argued that even the X/R ratio of the 800 mm^2 cables in the CS is relatively low compared to the TTS and HV power systems in general. As discussed in Section 4.6, several authors have highlighted concerns regarding the X/R ratio in distribution systems and OWPP CSs. However, the analytical

evidence has not been presented to support these claims. The inability of the NR-based methodology used in this Master's work to simulate the CS reinforces the concerns raised by those authors regarding convergence issues associated with such NR-based methods. While additional rigorous testing and analysis would be necessary to establish a stronger and more conclusive evidence for the performance comparison between the two methods, this study has the potential to offer empirical evidence that supports the legitimacy of this concern.

The X/R ratio in LFAC systems is even lower than in the conventional AC configuration. This suggests that the DSA or FBS algorithm is particularly relevant compared to the NR method, not only for radial AC distribution systems in general but also for LFAC distribution systems and OWPP CSs specifically. In addition to the covergence issues, the X/R ratio has, as mentioned in Section 4.6, an influence on the voltage variations within the system. One could observe in Figure 6.22, that the voltage within the LFAC-configuration of the system had a higher voltage profile throughout the whole system.

An observation that could be done in Figure C.28 and C.35 in Appendices C.5 and C.6, is that the share of reactive power delivered to the OSS (and the PCC) is higher for the LFAC-configuration of the system as a result of having lower inductive reactive losses in the cables in the LFAC-configuration. However, it is noteworthy that the LFAC-configured CS delivers only slightly higher active power to the OSS compared to the AC-configured CS. In fact, the LFAC configuration delivers lower active power to the stiff grid compared to the AC configuration. This observation suggests that assuming only the inductive reactance in the cables and neglecting the capacitive effects was a reasonable assumption within the CS. However, according to the author, this assumption led to illogical results within the TTS. In Section 4.5, it was mentioned that there is an observation indicating higher capacitive effects within longer transmission cables with high voltage.

The DSA tool presented in [4] provides the capability to incorporate SVCs into the system. Although this was originally intended by the authors, it became time-consuming and was not given priority. However, as indicated in Section 6.3.3, the bus with the highest voltage deviation from the reference value at 1 p.u was 1.03972 p.u at Bus 9 (in the LFAC-configuration of the full system - can be seen in Table 6.9), resulting in an

approximate 4% deviation from the nominal voltage. The primary objective of this work is not to assess compliance with grid codes or similar regulations. However, this aspect will be addressed in Section 7.1.

In general, the power losses of the CS calculated using the combinatorial methodology were lower compared to the results obtained from the DSA. The exact reason for this is unknown. However, it is reasonable to assume that the DSA, with its more comprehensive information processing and consideration of factors like voltage magnitude and angle changes, is likely to be more accurate compared to the relatively simple combinatorial methodology.

Based on the previous foundational work discussed in Chapter 3, the total active and reactive power losses are found to be within the expected limits. In the LFAC-configuration, the DSA results show only 0.48% reactive power losses, while in the AC-configuration, it is 1.39%, resulting in a total reactive power loss of 2.11 GWh higher in the AC-configuration, as shown in Figure 6.15 and 6.18. The active losses remain unchanged according to both methodologies used, which aligns with expectations.

The voltage profiles of the system shows a logical pattern. As shown in Figure 6.21, the voltage gradually increases towards the end nodes of the system. The voltage on the inner buses within each string is approximately equal, with slight variations depending on the cable length between the inner node and the OSS. Notably, the longest cable in the system is between the OSS (Bus 3) and Bus 4, which explains why Bus 4 has the highest observed voltage among these nodes.

Another notable observation from the voltage profile is the significant influence of the total cable length between the outer WT in the string and the OSS on the voltage level at the outer WT. This factor is equally important, if not more so, compared to the number of WTs in the string. A clear example can be seen by comparing the string with Bus 15-19 (consisting of five WTs) and the string with Bus 25-30 (comprising six WTs). Although the first string has fewer WTs, it has a higher cable length between the OSS and the first WT in the string. The first mentioned string has a cable length of 6 km, while the second mentioned has a significantly shorter cable length of 2.5 km. Consequently, due to the variation in the total cable length between the OSS and the outer WT, the

voltage magnitude at the outer WT differs between the two strings. Specifically, in the string with only five WTs and a cable distance to the OSS that is 3.5 km longer, the voltage magnitude at the outer WT is higher compared to the string with six WTs and a shorter cable distance to the OSS.

6.4.2 Performance Efficiency: Transmission to Shore

In the case of the AC-configuration of the system, the net injections of active power were identical when comparing the two utilized methodologies for both Bus 1 representing the OSS and Bus 2 representing the stiff grid and PCC. For the LFAC-configuration, the net injections of active power were almost identical. However, notable differences were observed in the net reactive power injections. One possible explanation for the significant differences in reactive power is that Bus 2 is assumed to be the slack bus, where the net reactive power injections are not initially specified in the NR-based methodology. In contrast, the DSA methodology requires specified net injections for all buses initially. In the AC-configuration, the voltage levels, both in terms of magnitude and angle, were found to be quite similar. However, larger differences in voltage magnitude were observed in the LFAC-configuration. This difference in voltage magnitude aligns with the observed variations in reactive power, indicating a connection between voltage levels and reactive power in power system analysis.

As mentioned earlier, not considering the shunt capacitance of the TTS cables introduces uncertainties in the analyses. This will be discussed further in the next section, which partly focuses on future work within this topic.

An interesting finding of the full system analyses through the DSA is the contribution from the TTS to active and reactive losses. As mentioned in Section 6.3.3, the TTS is the largest contributor to reactive losses in both system configurations. This matches earlier statements about this in Section 4.5, due to the higher reactance value compared to MV-cables.

The cycloconverter is responsible for both active and reactive power losses, which explains the higher active power losses observed in the DSA of the LFAC-configuration of the full

system. Despite these reactive losses caused by the cycloconverter, the overall reactive losses in the LFAC-configuration were significantly lower than those in the AC-system, as mentioned in Section 6.3.3.

The largest difference in voltage magnitude between the two system configurations (AC and LFAC) was observed at Bus 2, as shown in Figure 6.23. This can be attributed to similar reasons mentioned in the literature review in Section 3. Despite the presence of long cable distances in the CS, the reactance values are generally low, as mentioned earlier, even for conventional AC cables (due to generally low X/R ratio in MV AC-cables). The significant voltage deviation at Bus 2 can be attributed to the relatively high reactance value in the HV-cables of the TTS. This characteristic emphasizes the increasing relevance of LFAC technology for longer-distance TTS. As the distance increases, the voltage deviation further amplifies due to the influence of higher total reactance values in the HV-cables. However, as mentioned earlier, the significance of capacitance is not considered in this exact analysis, which potentially makes it even more important in reality and other more comprehensive analyses.

Comparing the power losses calculated for the DSA (1.94% active losses and 13.94% reactive losses) of the full system with the DSA of the CS separately and the TTS separately, which sums up to 1.97% active losses and 14.06% reactive losses, a small deviation for both active and reactive losses is observed. The deviation in losses observed between the DSA of the CS and TTS can be attributed to inaccuracies in the input values of the TTS DSA, which were based on the output values from the CS DSA. Another possible explanation is the absence of information in the separate analyses that is considered in the comprehensive analysis of the full system.

6.4.3 Reliability: RELRAD Methodology

The reliability findings are greatly influenced by the assumptions made about the failure potential of the components. As an illustration, the circuit breakers were assumed to be faultless and therefore incapable of failing. The consequences of this assumption on the results are uncertain. In this study, another assumption was made regarding the neglect of switching time in the event of faults within the radial CS topology. However, this

assumption was deemed reasonable due to the minimal impact of low switching times (compared tot the repair time) on the overall ENS during the analysis of the single-sided ring topology CS configuration. Moreover, it is important to highlight that the reliability data used in this study may not represent the most recent reliability data. However, it relied on relevant data previously utilized in similar studies, which provide some insight into the results, especially when comparing different system configurations in terms of CS topologies.

The change in CS topology had a substantial effect on the RELRAD results, resulting in significant differences. Notably, the contribution of the CS to the overall ENS varied significantly. In the radial topology, the CS accounted for 57% of the ENS, while in the single-sided ring topology, its contribution dropped to 0% due to the presence of redundancy lines. It should be noted that the analysis did not consider simultaneous faults, which necessitated a zero ENS contribution, given the presence of these redundancy lines.

A cost analysis has not been the primary focus of this report, but it is worth noting that a single-sided ring topology is likely to be more expensive to implement compared to a radial topology. Additionally, when comparing the two system configurations in terms of AC and LFAC, cost considerations become crucial in determining the most suitable technology. Realistically, costs would play a significant role in the decision-making process when selecting the most appropriate technology.

7 Conclusions and Further Work

This Master's work involved conducting a case study to assess the performance efficiency of an Offshore Wind Power Plant (OWPP) situated at Utsira Nord. The study encompassed the evaluation of various system configurations, including AC and LFAC technologies, as well as different CS topologies, specifically radial and single-sided ring topologies. Three different methods were employed in the analysis of performance efficiency, with DSA being the most extensively utilized. The utilization of distinct methodologies laid the groundwork for a potential comparison between them. Additionally, a reliability analysis of the OWPP case study was carried out using the RELRAD methodology. To the best of the knowledge of the author of this thesis, both the application of DSA and the utilization of the RELRAD methodology in the context of offshore wind had not been previously undertaken.

A majority of the main objectives that have been accomplished by the conclusion of this Master's thesis work were not originally included in the initial plan. However, as the idea arose to investigate the methodology for conducting a performance efficiency analysis and a reliability analysis of an OWPP, the decision was made to incorporate these objectives into the research. Thus, the study expanded to encompass these crucial aspects and address the raised questions. Since the interpretation of these analyses had not been conducted previously, the initial expectations for obtaining relevant outputs were not overly high. However, the primary objective was to gain a better understanding of the practical implementation of such analyses and explore the potential possibilities they offer. Nonetheless, the obtained results were significant and added further depth to the work, providing helpful insights and encouraging the formulation of novel research questions for future investigations.

At the initiation of this work, a significant investment of time and effort was devoted to developing a Python script from scratch. This script incorporated diverse combinatorial methods, adopting a component-wise approach to analysis. The main objective behind this effort was to create a standardized tool for analyzing the performance efficiency of OWPPs. Among the different methodologies explored in this study, the utilization of the combinatorial methodology for evaluating the performance efficiency of the CS emerged

as the sole enduring contribution, directly benefiting the overall objectives of this work. Throughout this research, the author arrived at the conclusion that developing such a tool would require the same level of comprehensiveness as algorithms like the DSA. Despite the mentioned methodology being the sole direct contribution towards fulfilling the objectives of this study, it encompassed additional achievements. These include addressing crucial questions that drove the formulation of the research objectives, as well as gaining insights into adapting and applying existing methodologies to different domains. The encountered difficulties in acquiring relevant knowledge within the research field of offshore wind, necessary for achieving the objectives of the study, also motivated a desire to provide others with accessible fundamentals. This would facilitate a better understanding for individuals to interpret and apply them to their own research within the field.

Further reflections and in-depth discussions could have been carried out regarding the performance efficiency and reliability findings of the analyses. However, given the substantial effort invested in executing the analyses and exploring the possibilities offered by different methodologies, a more comprehensive discussion of the results would have necessitated additional time - a constrained resource. As previously indicated, the questions raised and the pursuit of achieving the defined objectives of this work serve as the primary contributions within this thesis, giving rise to new ideas.

7.1 Further Work

The successful utilization of the DSA in the performance efficiency analysis of the examined OWPP case suggests its suitability for adapting to the analysis of OWPPs in general. Considering the empirically proven challenges associated with the use of NR in analyses of the CS of OWPPs, the DSA and the BFS algorithm, in general, demonstrate their compatibility with such analyses. Consequently, these methodologies have the potential to become increasingly crucial in the field of performance efficiency analysis for future applications within the offshore wind research domain. The DSA has certain attributes that make it compatible with reliability analyses, including the development of methods that analyze system behavior in addition to existing methods within the analysis. This

potential extension of the DSA methodology could ultimately lead to a more comprehensive and adaptable framework for conducting performance efficiency and reliability analyses across different OWPPs.

In order to further enhance the study of performance efficiency in OWPPs using the DSA, potential extensions could involve exploring the existing capability of integrating SVCs or other forms of reactive compensation. By incorporating these components into the analysis, it would be possible to evaluate OWPP compliance with grid codes, thereby achieving the objective of assessing OWPP performance in accordance with, say, grid regulations.

For the future continuation or expansion of this work, the importance of capacitance within the TTS should be acknowledged. This aspect could be incorporated into the DSA by placing greater emphasis on the role of charging currents and exploring the potential implications of grid regulations, say, in relation to other relevant components within the research domain, such as SVCs. By considering these factors, a more comprehensive understanding of the system dynamics can be achieved.

The literature review conducted during the specialisation project phase provided an important foundation for the Master's project research, which aimed to analyze the performance efficiency, reliability, and cost aspects of OWPPs. While cost perspectives were initially considered in the literature review, no cost analyses were conducted in this Master's work. Nonetheless, the integration of performance efficiency, reliability, and cost considerations remains a valuable framework for evaluating the technological configurations of OWPPs. By incorporating these three aspects together, a comprehensive evaluation of OWPPs can be achieved, enabling a thorough understanding of their performance, reliability, and cost-effectiveness.

References

[1] C. Ng and L. Ran, "Introduction to offshore wind energy," in Offshore wind farms : technologies, design and operation, 1st ed., C. Ng and L. Ran, Eds. Woodhead Publishing, 2016, ch. 1, pp. 1–8.

[2] G. Ellis and G. Ferraro, "The social acceptance of wind energy: Where we stand and the path ahead," 2017. [Online]. Available: https://pure.qub.ac.uk/en/publications/the-social-acceptance-of-wind-energy-where-we-stand-and-the-path--2

[3] E. A. Jakobsen, "Grid Architectures for Offshore Wind," Specialisation Project Report, Department of Electric Energy, Norwegian University of Science and Technology (NTNU), Trondheim, Norway, 12 2022.

[4] O. Bjarte Fosso, "PyDSAL - Python distribution system analysis library," in 2020 IEEE International Conference on Power Systems Technology, POWERCON 2020. Institute of Electrical and Electronics Engineers Inc., 9 2020.

[5] O. B. Fosso, "PyDSAL · GitHub." [Online]. Available: https://github.com/obfosso/PyDSAL/blob/master/README.md

[6] J. Ogle, "Grid Architecture," 6 2022. [Online]. Available: https://gridarchitecture.pnnl.gov/

[7] "Grid Architecture." [Online]. Available: https://www.pnnl.gov/grid-architecture

[8] O. Dahmani, S. Bourguet, M. Machmoum, P. Guerin, P. Rhein, and L. Josse, "Optimization and Reliability Evaluation of an Offshore Wind Farm Architecture," IEEE Transactions on Sustainable Energy, vol. 8, no. 2, pp. 542–550, 4 2017.

[9] Y. Liu, Y. Fu, L. l. Huang, Z. x. Ren, and F. Jia, "Optimization of offshore grid planning considering onshore network expansions," Renewable Energy, vol. 181, pp. 91–104, 1 2022.

[10] O. Anaya-Lara, "Offshore wind farm arrays," in Offshore wind farms : technologies, design and operation, 1st ed., C. Ng and L. Ran, Eds. Woodhead Publishing, 2016, ch. 12, pp. 389–417.

[11] AkerSolutions, "Offshore Wind — Aker Solutions." [Online]. Available: https://www.akersolutions.com/what-we-do/renewable-energy-solutions/offshore-wind-solutions/

[12] M. Toulotte, "Nexans - Floating wind farms rely on dynamic power cables," 9 2020. [Online]. Available: https://www.nexans.com/en/nexans_blog/nexans_blog_posts/floating-wind-farms-rely-on-dynamic-power-cables.html

[13] Narakorn Srinil, "Cabling to connect offshore wind turbines to onshore facilities," in Offshore wind farms : technologies, design and operation, 1st ed., C. Ng and L. Ran, Eds. Woodhead Publishing, 2016, ch. 13, pp. 418–440.

[14] G. Davies, "Deeper waters, stronger winds," Ørsted, Tech. Rep., 2022. [Online]. Available: https://orstedcdn.azureedge.net/-/media/www/docs/corp/com/about-us/whitepaper/orsted-floating-offshore-wind-oct-2022-web.ashx?rev=f040419236b14d77935f8f3b4d184085&hash=C627E8B1BD613B8E7F2C2E091F808931

[15] P. Tavner, "Introduction to off-shore wind," in Offshore Wind Power : Reliability, Availability and Maintenance., 2nd ed., ser. Energy Engineering Ser. London, UK: Institution of Engineering & Technology, 2021, ch. 1, pp. 1–28.

[16] A. Ferguson, P. de Villiers, B. Fitzgerald, and J. Matthiesen, "Benefits in moving the intra-array voltage from 33 kV to 66 kV AC for large offshore wind farms," in EWEA 2012 Conference Proceedings, Copenhagen, Denmark, 2012, pp. 16–19.

[17] L.-H. Tsai, "Network reconfiguration to enhance reliability of electric distribution systems," Electric Power Systems Research, vol. 27, no. 2, pp. 135–140, 3 1993.

[18] P. Lakshmanan, J. Liang, and N. Jenkins, "Assessment of collection systems for HVDC connected offshore wind farms," Electric Power Systems Research, vol. 129, pp. 75–82, 8 2015.

[19] J. Dakic, M. Cheah-Mane, O. Gomis-Bellmunt, and E. Prieto-Araujo, "HVAC Transmission System for Offshore Wind Power Plants including Mid-Cable Reactive Power

Compensation: Optimal Design and Comparison to VSC-HVDC Transmission," IEEE Transactions on Power Delivery, vol. 36, no. 5, pp. 2814–2824, 10 2021.

[20] ——, "Low frequency AC transmission systems for offshore wind power plants: Design, optimization and comparison to high voltage AC and high voltage DC," International Journal of Electrical Power and Energy Systems, vol. 133, 12 2021.

[21] P. Lakshmanan, R. Sun, and J. Liang, "Electrical collection systems for offshore wind farms: A review," CSEE Journal of Power and Energy Systems, vol. 7, no. 5, pp. 1078–1092, 9 2021.

[22] A. Anaya-Lara, "Control Challenges and Possibilities for Offshore Wind Farms," SINTEF, Trondheim, Norway, Tech. Rep., 2 2013. [Online]. Available: https://ntnuopen.ntnu.no/ntnu-xmlui/handle/11250/2482888

[23] A. Afanoukoe and K. Kanareva, "Nexans is awarded a multimillion-euro contract for Ørsted's Borssele 1 and 2 wind farms off the Netherlands coast," Paris, Tech. Rep., 11 2018. [Online]. Available: https://tinyurl.com/NexansOrstedBorssele

[24] M.-A. Faedy and I. Scian, "WindSTAR-World's first large 33 and 66 kV offshore wind turbine transformer," ABB, Tech. Rep., 2018. [Online]. Available: https://library.e.abb.com/public/c6c8608a3b1e4b7a95c2d27c9820deb4/54-59%20m7060_EN_72dpi.pdf?x-sign=nZldRCA9XTmZAK+8X0d6/IKXfHMuT3dTrWbuE8DQiwN361J4ngfhOjc4VORFjAl+

[25] P. Tavner, "Off-shore wind farm layouts and grid connection," in Offshore Wind Power : Reliability, Availability and Maintenance., 2nd ed., ser. Energy Engineering Ser. London, UK: Institution of Engineering & Technology, 2021, ch. 8, pp. 157–177.

[26] A. P. Neumann, M. J. Mulroy, and C. Ebden, "The Use of 66kV technology for Offshore Wind Demonstration sites," in 3rd Renewable Power Generation Conference. Naples, Italy: IEEE, 9 2014, pp. 1–6.

[27] S. Gasnier, V. Debusschere, S. Poullain, and B. Francois, "Technical and economic assessment tool for offshore wind generation connection scheme: Application to comparing 33 kV and 66 kV AC collector grids authors," in 2016 18th European

Conference on Power Electronics and Applications. Karlsruhe, Germany: IEEE, 10 2016, pp. 1–8.

[28] J. Ruddy, R. Meere, and T. O'Donnell, "Low Frequency AC transmission for offshore wind power: A review," Renewable and Sustainable Energy Reviews, vol. 56, pp. 75–86, 4 2016.

[29] ——, "A comparison of VSC-HVDC with low frequency AC for offshore wind farm design and interconnection," in 12th Deep Sea Offshore Wind R&D Conference, vol. 80. Trondheim, Norway: Elsevier Ltd, 2 2015, pp. 185–192.

[30] L. Hytten, "Power Frequency Optimization for offshore wind farms," in 12th Deep Sea Offshore Wind R&D Conference. Trondheim, Norway: SINTEF, 2 2015. [Online]. Available: https://www.sintef.no/globalassets/project/eera-deepwind-2015/presentations/a/a2_hytten_dnvgl.pdf

[31] W. Flesland Blytt and E. A. Jakobsen, "State of the Art Possible Improvements to Increase Offshore Winds Competitiveness in the Market," Tech. Rep., 2022.

[32] J. Michline Rupa and S. Ganesh, "Power Flow Analysis for Radial Distribution System Using Backward/Forward Sweep Method," World Academy of Science, Engineering and Technology International Journal of Electrical and Computer Engineering, vol. 8, no. 10, pp. 1628–1632, 2014.

[33] R. Srikakulapu and U. Vinatha, "Electrical collector topologies for offshore wind power plants: A survey," in 2015 IEEE 10th International Conference on Industrial and Information Systems, ICIIS 2015 - Conference Proceedings. Institute of Electrical and Electronics Engineers Inc., 2 2016, pp. 338–343.

[34] K. Das and N. A. Cutululis, "Advanced integrated supervisory and wind turbine control for optimal operation of large Wind Power Plants," Total Control, Tech. Rep., 2019.

[35] G. Diaz, J. Gomez-Aleixandre, and J. Coto, "Direct Backward/Forward Sweep Algorithm for Solving Load Power Flows in AC Droop-Regulated Microgrids," IEEE Transactions on Smart Grid, vol. 7, no. 5, pp. 2208–2217, 9 2016.

[36] H. J. Bahirat, B. A. Mork, and H. K. Hoidalen, "Comparison of wind farm topologies for offshore applications," in IEEE Power and Energy Society General Meeting. San Diego, CA, USA: IEEE, 7 2012, pp. 1–8.

[37] E. Muljadi, C. P. Butterfield, A. Ellis, J. Mechenbier, J. Hochheimer, R. Young, N. Miller, R. Delmerico, R. Zavadil, and J. C. Smith, "Equivalencing the collector system of a large wind power plant," in 2006 IEEE Power Engineering Society General Meeting, PES. IEEE Computer Society, 2006.

[38] R. Meere, J. Ruddy, and T. O'Donnell, "Variable frequency operation for future offshore wind farm design: A comparison with conventional wind turbines," in Energy Procedia, vol. 53, no. C. Elsevier Ltd, 2014, pp. 280–289.

[39] H. Waje-Andreassen, "Low Frequency AC Transmission Investigating the Dynamics of an Export Cable for Offshore Wind Power Applications," Master's Thesis, Department of Electric Power Engineering, Norwegian University of Science and Technology (NTNU), Trondheim, Norway, 2016.

[40] M. Khatir, S. A. Zidi, S. Hadjeri, and M. K. Fellah, "Comparison of HVDC Line Models in PSB/Simulink Based on Steady-State and Transients Considerations," Acta Electrotechnica et Informatica, vol. 8, no. 2, pp. 50–55, 2008.

[41] A. Jerkø, "Reactive Power and Voltage Control of Offshore Wind Farms," Master's Thesis, Department of Electric Power Engineering, Norwegian University of Science and Technology (NTNU), Trondheim, Norway, pp. 1–106, 6 2014.

[42] L. R. de Araujo, D. R. R. Penido, N. A. do Amaral Filho, and T. A. P. Beneteli, "Sensitivity analysis of convergence characteristics in power flow methods for distribution systems," International Journal of Electrical Power and Energy Systems, vol. 97, pp. 211–219, 4 2018.

[43] H. Zhao, Q. Wu, J. Wang, Z. Liu, M. Shahidehpour, and Y. Xue, "Combined Active and Reactive Power Control of Wind Farms Based on Model Predictive Control," IEEE Transactions on Energy Conversion, vol. 32, no. 3, pp. 1177–1187, 9 2017.

[44] R. Billinton and R. N. Allen, "Approximate System Reliability Evaluation," in

Reliability Evaluation of Engineering Systems, 2nd ed. New York, USA: Springer Science+Business Media New York, 1992, ch. 11, pp. 340–352.

[45] K. Sand and G. Kjølle, "RELRAD - An analytical Approach for Distribution System Reliability Assessment," IEEE Transactions on Power Delivery, vol. 7, no. 2, pp. 809–814, 1992.

[46] R. Billinton and R. N. Allan, "Distribution systems - basic techniques and radial networks," in Reliability Evaluation of Power Systems, 2nd ed. New York, USA: Plenum Press - New York and London, 1996, ch. 7, pp. 224–227.

[47] T. Pereira and R. Castro, "Comparison of internal grid topologies of offshore wind farms regarding reliability and economic performance metrics analysis," IET Renewable Power Generation, vol. 13, no. 5, pp. 750–761, 4 2019.

[48] S. Chatterjee and S. Mandal, "A novel comparison of gauss-seidel and newton-raphson methods for load flow analysis," in International Coference on Power and Embedded Drive Control. Chennai, India: IEEE, 3 2017.

[49] H. Bøhler and J.-T. Horn, "Vind AI," 2023. [Online]. Available: https://app.vind.ai/design/park/uBUY0CcpofiL1XsFQ-saM/2NPfrvCXatGPUS1BImRrmpYl09o/2NPfrxG8M4ko7urCCN5zTbO4ppL/2494affa-2e83-4953-896a-e63389268ab4

[50] ABB, "XLPE Submarine Cable Systems Attachment to XLPE Land Cable Systems-User´s Guide Rev 5 2 XLPE Submarine Cable Systems — ABB," Tech. Rep. [Online]. Available: www.abb.com/cables

[51] J. Larsson, "Transmission Systems for Grid Connection of Offshore Wind Farms - HVAC vs HVDC Breaking Point," Ph.D. dissertation, Uppsala Universitet, Uppsala, 5 2021. [Online]. Available: http://www.teknat.uu.se/student

[52] Prysmian Group, "66 kV Submarine Cable Systems FOR OFFSHORE WIND," Prysmian Group, Milan, Italy, Tech. Rep.

[53] F. Ying, L. Huang, J. Yan, Y. Liu, Q. Wang, and Y. Miao, "Power System Reliability Assessment with Offshore Wind Farms," in 2021 IEEE 2nd China International Youth Conference on Electrical Engineering, CIYCEE 2021. Institute of Electrical and Electronics Engineers Inc., 2021.

[54] NVE, "Vestavind F (inkl. Utsira Nord)," Trondheim, Norway, 4 2023. [Online]. Available: https://veiledere.nve.no/havvind/identifisering-av-utredningsomrader-for-havvind/nye-omrader-for-havvind/vestavind-f-inkl-utsira-nord/

Appendices

A Previous work

A.1 Python script calculations on LFAC from [31]

```
import numpy as np
import matplotlib.pyplot as plt

C = 0.13 * (10**(-6))  # Capacitance [microF]
E = 300  # Voltage [kV]
f = 16.67  # frequency [f]
I = 1  # Current [kA]
l = range(0, 100, 1) # List for lengths
                     #   up to 100 [km]
xi = 50  # Transmission distance from
         # cite to onshore connection point [km]

Ic = np.zeros(len(l))  # Capacitive current
                       # in cable
Qc = np.zeros(len(l))  # Reactive power
                       # produced in cable [MVAr]
Pr = np.zeros(len(l))  # Active power
                       # delivered to shore [MW]
S = E * I  # Apparent power in [MVA]

plt.figure()  # Creating a figure for the plots
Pr1 = None
Pr2 = None
for i in range(2):
```

```
    if i == 1:  # First, plot for f = 16.67 Hz
                # Second, plot for f = 50 Hz
                # to compare
        f = 50
    for n in range(len(l)):  # Going through all
                             # elements in the
                             # length list to
                             # find Pr for all
                             # lengths to plot
        Ic[n] = 2 * np.pi * f * l[n] * C * E
        Qc[n] = (Ic[n] * E) / (10 ** 0)
        Pr[n] = np.sqrt((S ** 2) - ((Qc[n]) ** 2))
        if Pr[n] < 100:  # within limits -
                         # CHANGE NUMBER
            Pr[n] = 0
    if i == 0:  # f= 16.67 Hz
        Pr1 = Pr
        plt.plot(l, Pr1)
        plt.scatter(xi, Pr1[xi], color='black')
        loss1 = S - Pr1[xi]  # delivered active
                             # power to shore,
                             # 16.67 Hz
    else:  # f = 50 Hz
        Pr2 = Pr
        plt.plot(l, Pr2)
        plt.scatter(xi, Pr2[xi], color='black')
        loss2 = S - Pr2[xi]  # Delivered active
                             # power to shore,
                             # f = 50 Hz
plt.suptitle('Utsira Nord transfer capabilities'
             , fontsize=15)
plt.title('Delivered active power given reactive
```

```
            power production in cable')
plt.ylabel('Pr [MW]')
plt.xlabel('Length [km]')
plt.legend(['Frequency: 16.67 [Hz]',
            'Delivered power at given distance',
                        'Frequency: 50 [Hz]'])
plt.axvline(x=xi, color='y', linestyle='--')
plt.show()

print(loss1, loss2)
```

B Methodologies

B.1 Distibution System Analysis

```
    def outage(self):
        """
        Checking all lines and removing the outer part of branch if faulted
        :return:
        """

        branches = [[]]
        n = 0
        for line in LineList:
            if line.fbus == line.tbus - 1:
                branches[n].append(BusList[line.fbus - 1])
            elif line.fbus == 3:  # for TTS + CS - must change manunally
                                  # to 1 for only CS
                branches[n].append(BusList[line.tbus-2])
                n += 1
```

```
            branches.append([])
    branches[n].append(BusList[-1])



    """
    Now, create list with all lines in each branch:
    """

    stringLines = []
    c = 0  # counting parameter
    for string in branches:
        stringLines.append([])
        for bus in string:
            for line in LineList:
                if line.tbus == bus.busnum and not line.redLine:
                    stringLines[c].append(line)
        c += 1

    """
    Now, all the strings are one list in the list "branches" like:
    [main string, string 2, ... , string n]
    where string 1 = [8, 9, ... , 12] etc.
    And, all lines are sorted in a similar way: stringLines =
    [string1lines, string2lines, ..., strinNNlines]
    where
    string1lines = [line 1, line 2, ... , line 6] etc.

    Next, check if any lines has an outage and if so - diconnnect
    all buses on the "outside" of this line.
    """
    count = 0
    for line in LineList:  # line-number with fault
```

```
        if line.ibstat == 0 and not line.redLine:
            fl = count  # faulted line
        count +=1

    faultedBuses = []
    faultedLines = []
    stringNum = 0
    beenthere = False
    # Here, finding all buses that will be disconnected due to
    # faulted line
    for string in stringLines:
        lineNumInList = 0
        for line in string:
            if not line.redLine:  # if normal line / not redundancy
                                  # line
                if not line.ibstat:  # if faulted line
                    for bus in branches[stringNum][lineNumInList:]:
                        if stringNum == 0 and not beenthere:  # if first
                                                              # string, to get correct index
                            beenthere = True
                            continue
                        faultedBuses.append(bus)  # all
                        # buses that will be disconnected due to the
                        # outage
                    for fLine in stringLines[stringNum][lineNumInList:]:
                    # all lines disconnected
                        faultedLines.append(fLine)
                    break
            lineNumInList += 1
        stringNum += 1

    # Disconnecting buses and lines
```

```
        for fltbus in faultedBuses:
            BusList.remove(fltbus)
        for fltline in faultedLines:
            LineList.remove(fltline)

        # renumber bus number
        lfb = faultedBuses[-1].busnum - len(faultedLines) # last faulted
                        # line
        lfl = fl
        lob = faultedBuses[0].busnum - 1  # last operating bus
        numFaultedBuses = len(faultedBuses)
        for bus in BusList[lob:]:
            bus.busnum -= numFaultedBuses
            bus.busname
        for bus in BusList:
            bus.busCount -= numFaultedBuses
            bus.busname = 'Bus' + str(bus.busnum)
        for line in LineList[lfl:]:
            if line.fbus != 3:  # Change manually if only CS
                line.fbus -= numFaultedBuses
                line.tbus -= numFaultedBuses
            else:
                line.tbus -= numFaultedBuses

        a = 0



    #
    # First checking for outage, if outage - run self.outage()
    #
    def checkOutage(self):
```

```
        for line in LineList:
            if line.ibstat:
                continue
            elif not line.ibstat and not line.redLine:
                self.outage()
                break
```

B.2 Combinatorial Methodology

```
class CS_cables:
    def __init__(self):
        self.f = 50  # frequency [Hz]
        self.v = 1  # CS voltage [p.u]
        self.i = i_cs  # output current from each WT [A]
        self.r_wt2wt = r_wt2wt_cs  # resistance in WT-to-WT cable CS
                                    # [ohm]
        self.x_wt2wt = x_wt2wt_cs  # reactance in WT-to-WT cable CS
                                    # [ohm]
        self.r_wt2tr = r_wt2tr_cs  # resistance in WT-to-Transformer
                                    # cable [ohm]
        self.x_wt2tr = x_wt2tr_cs  # reactance in WT-to-Transformer
                                    # cable [ohm]
        self.z_wt2wt = complex(self.r_wt2wt, self.x_wt2wt)  # impedance
                       # of CS
                       # cables [ohm]
        self.z_wt2tr = complex(self.r_wt2tr, self.x_wt2tr)  # impedance
                       # of CS
                       # cables [ohm]
        self.c = c_cs  # capacitance of CS cable for dielectric losses
                        # calculation [F]
```

```
        self.tanDelta = tanDelta_cs  # insulation loss factor for
                                     # calculating the dielectric losses
                                     # in the CS cables
        self.l_wt2wt = l_wt2wt  # length between each WT [m]
        self.l_wt2tr = l_wt2tr  # length between inner WT to the offshore
                                # [m]
                                # transformer [m]
        self.n_wt = n_wt  # number of WTs in each string
        self.n_strings = n_strings  # number of parallel radials/strings
                                    # in the CS
        self.C = self.c * ((self.n_wt - 1) * self.l_wt2wt + self.l_wt2tr)

    # Methods ---------------------------------------

    # Total impedance of cable between WT and WT
    def Z_wt2wt(self):
        return self.l_wt2wt * self.z_wt2wt

    # Total resistance of cable between WT and WT
    def R_wt2wt(self):
        Z_wt2wt = self.Z_wt2wt()
        return Z_wt2wt.real

    # Total reactance of cable between WT and WT
    def X_wt2wt(self):
        Z_wt2wt = self.Z_wt2wt()
        return Z_wt2wt.imag

    # Total impedance of cable between WTs and offshore transformer
    def Z_wt2tr(self):
        return self.l_wt2tr * self.z_wt2tr
```

```
    # Total resistance of cable between WTs and offshore transformer
    def R_wt2tr(self):
        Z_wt2tr = self.Z_wt2tr()
        return Z_wt2tr.real

    # Total reactance of cable between WTs and offshore transformer
    def X_wt2tr(self):
        Z_wt2tr = self.Z_wt2tr()
        return Z_wt2tr.imag

    # Total impedance in CS
    def Z_S(self):
        Z_m = self.Z_wt2wt()
        msum = 0
        for m in range(self.n_wt):
            msum += m**2
        Z_S = msum * Z_m / self.n_wt ** 2
        return Z_S

    # Active power losses in CS
    def PcableLoss_cs(self):
        n = self.n_wt  # number of WTs
        i = self.i  # output current from each WT
        R_wt2wt = self.R_wt2wt()  # total resistance in cables between
                                  # each WT
        R_wt2tr = self.R_wt2tr()  # total resistance in cable between
                                  # last WT
                                  # in string and offshore transformer
        I_s = n * i  # current in cable between last WT and offshore
                     # transformer
        frac = (n * (n + 1) * (2*n + 1)) / 6  # fraction in expression
        pLoss = (frac * i**2 * R_wt2wt)  # active cable losses in CS
```

```
                                        # except cable loss between
                                        # last WT and off transformer
        pLoss_wt2tr = (I_s * R_wt2tr)  # active cable losses between last
                                       # WT and offshore transformer
        pLoss_cs = pLoss + pLoss_wt2tr # total active cable losses in CS
        return pLoss_cs

    # Reactive power losses in CS
    def QcableLoss_cs(self):
        n = self.n_wt  # number of WTs
        i = self.i  # output current from each WT
        X_wt2wt = self.X_wt2wt()  # total reactance in cables between
                                  # each WT
        X_wt2tr = self.X_wt2tr()  # total reactance in cable between
                                  # last WT
                                  # in string and offshore transformer
        I_s = n * i  # current in cable between last WT and offshore
                     # transformer
        frac = (n * (n + 1) * (2*n + 1)) / 6  # fraction in expression
        qLoss = frac * i**2 * X_wt2wt  # reactive cable losses in CS
                                       # except cable loss between last
                                       # WT and off transformer
        qLoss_wt2tr = (I_s * X_wt2tr) # reactive cable losses between
                                      # last WT and offshore transformer
        qLoss_cs = (qLoss + qLoss_wt2tr)  # total reactive cable losses
                                          # in CS
        return qLoss_cs

    def dielectricLosses(self):
        return 2 * np.pi * self.f * self.C * self.v**2 * np.tan(self.tanDelta)
```

C Case and Results

C.1 Input data

C.1.1 DSA - Python Input File - *componentData.py*

```
"""
Master's Thesis - Grid Architectures for Offshore Wind
Spring 2023
author: ********
This file includes relevant component data for the
simulation part of my Master's Thesis.


"""

import numpy as np

class CableType:
    def __init__(self, r, h):
        self.LFAC = False
        self.f = 50  # Hz
        self.r = r  # resistance [Ohm/km]
        self.h = h  # inductance [H/km]
        self.x = 0  # reactance [j Ohm/km]
        self.z = 0  # impedance [Ohm]

    def calcz(self):
        self.r = self.r * 10 ** (-3)
        self.h = self.h * 10 ** (-3)
        xl = self.h * 2 * np.pi * self.f
        self.x = xl
```

```
        self.z = complex(self.r, self.x)

    def setLFAC(self):
        self.LFAC = True
        self.f = 50 / 3



class Cable(CableType):
    def __init__(self, r, h, l):
        super().__init__(r, h)
        self.l = l  # length [km]
        self.R = 0  # total resistance [Ohm]
        self.H = 0  # total inductance [H]
        self.X = 0  # total reactance [j Ohm]
        self.Z = 0  # total impedance [Ohm]


    def calcZ(self):
        self.calcz()
        self.R = self.r * self.l
        self.H = self.h * self.l
        XL = self.H * 2 * np.pi * self.f
        self.X = XL
        self.Z = complex(self.R, self.X)

    def parallel(self, numEqLines):
        self.Z = self.Z / numEqLines
        self.R = self.Z.real
        self.X = self.Z.imag
```

```
"""
Cables for Utsira Nord Case
"""
# Z_base
Z_baseCS = 8.712  # [ohm]
Z_baseTTS = 96.8  # [ohm]
Z_basePCC = 352.5  # [ohm]


# Collection System
# Cable type
lowCapCSType = CableType(150 / Z_baseCS, 0.34 / Z_baseCS)
highCapCSType = CableType(90 / Z_baseCS, 0.32 / Z_baseCS)  # r, h
# lowCapC = 0.29  # microF/km
# highCapC = 0.35  # microF/km

# Cable CS
lowCapCable25km = Cable(lowCapCSType.r, lowCapCSType.h, 2.5)
highCapCable25km = Cable(highCapCSType.r, highCapCSType.h, 2.5)
highCapCable3km = Cable(highCapCSType.r, highCapCSType.h, 3)
highCapCable35km = Cable(highCapCSType.r, highCapCSType.h, 3.5)
highCapCable6km = Cable(highCapCSType.r, highCapCSType.h, 6)
highCapCable7km = Cable(highCapCSType.r, highCapCSType.h, 7)
# LFAC Cable CS
LFAClowCapCable25km = Cable(lowCapCSType.r, lowCapCSType.h, 2.5)
LFAClowCapCable25km.setLFAC()
LFAChighCapCable25km = Cable(highCapCSType.r, highCapCSType.h, 2.5)
```

```
LFAChighCapCable25km.setLFAC()
LFAChighCapCable3km = Cable(highCapCSType.r, highCapCSType.h, 3)
LFAChighCapCable3km.setLFAC()
LFAChighCapCable35km = Cable(highCapCSType.r, highCapCSType.h, 3.5)
LFAChighCapCable35km.setLFAC()
LFAChighCapCable6km = Cable(highCapCSType.r, highCapCSType.h, 6)
LFAChighCapCable6km.setLFAC()
LFAChighCapCable7km = Cable(highCapCSType.r, highCapCSType.h, 7)
LFAChighCapCable7km.setLFAC()

# Transmission To Shore
# Cable Type
ttsCableType = CableType(22.4 / Z_baseTTS, 0.35 / Z_baseTTS)
# ttsCableC = 0.19  # microF/km
# Transformers Equivalent impedance
offTransEqImpedance = complex(0.001, 0.05)
onsTransEqImpedance = complex(0.0025, 0.07)

# Cable TTS
ttsCable = Cable(ttsCableType.r, ttsCableType.h, 34)  # 34 km
# LFAC TTS Cable
LFACttsCable = Cable(ttsCableType.r, ttsCableType.h, 34)  # 34 km
LFACttsCable.setLFAC()


"""
Calculating Impedance for All Cables
"""

# CS Cables
lowCapCable25km.calcZ()
highCapCable25km.calcZ()
```

```
highCapCable3km.calcZ()
highCapCable35km.calcZ()
highCapCable6km.calcZ()
highCapCable7km.calcZ()
# LFAC CS Cables
LFAClowCapCable25km.calcZ()
LFAChighCapCable25km.calcZ()
LFAChighCapCable3km.calcZ()
LFAChighCapCable35km.calcZ()
LFAChighCapCable6km.calcZ()
LFAChighCapCable7km.calcZ()

# TTS Cable
ttsCable.calcZ()
ttsCable.parallel(3)
# LFAC TTS Cable
LFACttsCable.calcZ()

"""
Reliability data
"""
lambdaCableCS = 0.008  # fail/(year*km)
lambdaOffTrans = 0.02  # fail/year
lambdaCableTTS = 0.08  # fail/(year*km)
lambdaOnsTrans = 0.02  # fail/year
lambdaCyclo = 0.1  # fail/year

# Example usage
components = ["A", "B", "C", "D"]
lambdas = [0.05, 0.05, 0.05, 0.05]  # Replace A, B, C, D with the
                                    # respective values
repair_rates = [20/8760, 20/8760, 20/8760, 20/8760]  # Replace a, b, c, d
```

```
# lambda_s2 = 4 * l**4 * r**4
```

C.2 DSA - CS - Performance Efficiency Analysis Results

Bus Voltages

	Bus no	Vmag	Theta
Bus 2	2	1.01397	0.74719
Bus 3	3	1.01815	0.96555
Bus 4	4	1.02150	1.13889
Bus 5	5	1.02553	1.26858
Bus 6	6	1.02822	1.35448
Bus 7	7	1.02956	1.39726
Bus 8	8	1.00424	0.22447
Bus 9	9	1.00763	0.40262
Bus 10	10	1.01171	0.53589
Bus 11	11	1.01444	0.62415
Bus 12	12	1.01580	0.66809
Bus 13	13	1.01008	0.53562

Figure C.1: *Results from performance efficiency analysis with DSA and base case site. Voltage magnitude and angle on bus 2 - 12.*

Bus Voltages

	Bus no	Vmag	Theta
Bus 14	14	1.01345	0.71173
Bus 15	15	1.01752	0.84348
Bus 16	16	1.02022	0.93073
Bus 17	17	1.02158	0.97418
Bus 18	18	1.00508	0.26914
Bus 19	19	1.00846	0.44699
Bus 20	20	1.01255	0.58005
Bus 21	21	1.01527	0.66815
Bus 22	22	1.01663	0.71203
Bus 23	23	1.00505	0.26921
Bus 24	24	1.00927	0.49144
Bus 25	25	1.01264	0.66783

Figure C.2: *Results from performance efficiency analysis with DSA and base case site. Voltage magnitude and angle on bus 13 - 23.*

Bus Voltages

	Bus no	Vmag	Theta
Bus 26	26	1.01671	0.79979
Bus 27	27	1.01942	0.88718
Bus 28	28	1.02077	0.93070
Bus 29	29	1.00705	0.37615
Bus 30	30	1.01126	0.59750
Bus 31	31	1.01463	0.77320
Bus 32	32	1.01869	0.90465
Bus 33	33	1.02139	0.99170
Bus 34	34	1.02274	1.03505

Figure C.3: *Results from performance efficiency analysis with DSA and base case site. Voltage magnitude and angle on bus 24 - 34.*

Transmission line flow

	FromBus :	ToBus :	Pfrom :	Qfrom :	Pto :	Qto :
Line 0	1	2	-0.1763	-0.0141	0.1786	-0.0141
Line 1	2	3	-0.1486	-0.0136	0.1491	-0.0136
Line 2	3	4	-0.1191	-0.0112	0.1195	-0.0112
Line 3	4	5	-0.0895	-0.0086	0.0898	-0.0086
Line 4	5	6	-0.0598	-0.0059	0.0600	-0.0059
Line 5	6	7	-0.0300	-0.0030	0.0300	-0.0030
Line 6	1	8	-0.1485	-0.0136	0.1491	-0.0136
Line 7	8	9	-0.1191	-0.0112	0.1195	-0.0112
Line 8	9	10	-0.0895	-0.0086	0.0898	-0.0086
Line 9	10	11	-0.0598	-0.0059	0.0600	-0.0059
Line 10	11	12	-0.0300	-0.0030	0.0300	-0.0030
Line 11	1	13	-0.1477	-0.0127	0.1491	-0.0127

Figure C.4: *Results from performance efficiency analysis with DSA and base case site. Line flows on line 0(1-2) - 10(11-12).*

Transmission line flow

	FromBus :	ToBus :	Pfrom :	Qfrom :	Pto :	Qto :
Line 12	13	14	-0.1191	-0.0112	0.1195	-0.0112
Line 13	14	15	-0.0895	-0.0086	0.0898	-0.0086
Line 14	15	16	-0.0598	-0.0059	0.0600	-0.0059
Line 15	16	17	-0.0300	-0.0030	0.0300	-0.0030
Line 16	1	18	-0.1484	-0.0134	0.1491	-0.0134
Line 17	18	19	-0.1191	-0.0112	0.1195	-0.0112
Line 18	19	20	-0.0895	-0.0086	0.0898	-0.0086
Line 19	20	21	-0.0598	-0.0059	0.0600	-0.0059
Line 20	21	22	-0.0300	-0.0030	0.0300	-0.0030
Line 21	1	23	-0.1777	-0.0157	0.1785	-0.0157
Line 22	23	24	-0.1485	-0.0136	0.1491	-0.0136
Line 23	24	25	-0.1191	-0.0112	0.1195	-0.0112

Figure C.5: *Results from performance efficiency analysis with DSA and base case site. Line flows on line 11(1-13) - 21(1-23).*

Transmission line flow

	FromBus :	ToBus :	Pfrom :	Qfrom :	Pto :	Qto :
Line 24	25	26	-0.0895	-0.0086	0.0898	-0.0086
Line 25	26	27	-0.0598	-0.0059	0.0600	-0.0059
Line 26	27	28	-0.0300	-0.0030	0.0300	-0.0030
Line 27	1	29	-0.1774	-0.0153	0.1785	-0.0153
Line 28	29	30	-0.1485	-0.0136	0.1491	-0.0136
Line 29	30	31	-0.1191	-0.0112	0.1195	-0.0112
Line 30	31	32	-0.0895	-0.0086	0.0898	-0.0086
Line 31	32	33	-0.0598	-0.0059	0.0600	-0.0059

Figure C.6: *Results from performance efficiency analysis with DSA and base case site. Line flows on line 22(23-24) - 32(33-34).*

```
Iter:  1 Pload: -0.9900 Qload: -0.0990 Ploss:  0.0142 Qloss:  0.0146
Iter:  2 Pload: -0.9900 Qload: -0.0990 Ploss:  0.0139 Qloss:  0.0142
Iter:  3 Pload: -0.9900 Qload: -0.0990 Ploss:  0.0139 Qloss:  0.0142
Iter:  4 Pload: -0.9900 Qload: -0.0990 Ploss:  0.0139 Qloss:  0.0142

 ****** Load flow completed ******

time elapsed: 0.00s




 Ploss: 0.013886980351204047    Qloss: 0.014232236597022215
```

Figure C.7: *Output from performance efficiency analysis with DSA and base case site.*

C.3 DSA - LFAC CS - Performance Efficiency Analysis Results

Bus Voltages

	Bus no	Vmag	Theta
Bus 2	2	1.01397	0.74719
Bus 3	3	1.01815	0.96555
Bus 4	4	1.02150	1.13889
Bus 5	5	1.02553	1.26858
Bus 6	6	1.02822	1.35448
Bus 7	7	1.02956	1.39726
Bus 8	8	1.00424	0.22447
Bus 9	9	1.00763	0.40262
Bus 10	10	1.01171	0.53589
Bus 11	11	1.01444	0.62415
Bus 12	12	1.01580	0.66809
Bus 13	13	1.01008	0.53562

Figure C.8: *Results from performance efficiency analysis with DSA LFAC CS. Voltage magnitude and angle on bus 2 - 12.*

Bus Voltages

	Bus no	Vmag	Theta
Bus 14	14	1.01345	0.71173
Bus 15	15	1.01752	0.84348
Bus 16	16	1.02022	0.93073
Bus 17	17	1.02158	0.97418
Bus 18	18	1.00508	0.26914
Bus 19	19	1.00846	0.44699
Bus 20	20	1.01255	0.58005
Bus 21	21	1.01527	0.66815
Bus 22	22	1.01663	0.71203
Bus 23	23	1.00505	0.26921
Bus 24	24	1.00927	0.49144
Bus 25	25	1.01264	0.66783

Figure C.9: *Results from performance efficiency analysis with DSA LFAC CS. Voltage magnitude and angle on bus 13 - 23.*

Bus Voltages

	Bus no	Vmag	Theta
Bus 26	26	1.01671	0.79979
Bus 27	27	1.01942	0.88718
Bus 28	28	1.02077	0.93070
Bus 29	29	1.00705	0.37615
Bus 30	30	1.01126	0.59750
Bus 31	31	1.01463	0.77320
Bus 32	32	1.01869	0.90465
Bus 33	33	1.02139	0.99170
Bus 34	34	1.02274	1.03505

Figure C.10: *Results from performance efficiency analysis with DSA and LFAC CS. Voltage magnitude and angle on bus 24 - 34.*

Transmission line flow

	FromBus :	ToBus :	Pfrom :	Qfrom :	Pto :	Qto :
Line 0	1	2	-0.1763	-0.0141	0.1786	-0.0141
Line 1	2	3	-0.1486	-0.0136	0.1491	-0.0136
Line 2	3	4	-0.1191	-0.0112	0.1195	-0.0112
Line 3	4	5	-0.0895	-0.0086	0.0898	-0.0086
Line 4	5	6	-0.0598	-0.0059	0.0600	-0.0059
Line 5	6	7	-0.0300	-0.0030	0.0300	-0.0030
Line 6	1	8	-0.1485	-0.0136	0.1491	-0.0136
Line 7	8	9	-0.1191	-0.0112	0.1195	-0.0112
Line 8	9	10	-0.0895	-0.0086	0.0898	-0.0086
Line 9	10	11	-0.0598	-0.0059	0.0600	-0.0059
Line 10	11	12	-0.0300	-0.0030	0.0300	-0.0030
Line 11	1	13	-0.1477	-0.0127	0.1491	-0.0127

Figure C.11: *Results from performance efficiency analysis with DSA and LFAC CS. Line flows on line 0(1-2) - 10(11-12).*

Transmission line flow

	FromBus :	ToBus :	Pfrom :	Qfrom :	Pto :	Qto :
Line 12	13	14	-0.1191	-0.0112	0.1195	-0.0112
Line 13	14	15	-0.0895	-0.0086	0.0898	-0.0086
Line 14	15	16	-0.0598	-0.0059	0.0600	-0.0059
Line 15	16	17	-0.0300	-0.0030	0.0300	-0.0030
Line 16	1	18	-0.1484	-0.0134	0.1491	-0.0134
Line 17	18	19	-0.1191	-0.0112	0.1195	-0.0112
Line 18	19	20	-0.0895	-0.0086	0.0898	-0.0086
Line 19	20	21	-0.0598	-0.0059	0.0600	-0.0059
Line 20	21	22	-0.0300	-0.0030	0.0300	-0.0030
Line 21	1	23	-0.1777	-0.0157	0.1785	-0.0157
Line 22	23	24	-0.1485	-0.0136	0.1491	-0.0136
Line 23	24	25	-0.1191	-0.0112	0.1195	-0.0112

Figure C.12: *Results from performance efficiency analysis with DSA LFAC CS. Line flows on line 11(1-13) - 21(1-23).*

Transmission line flow

	FromBus :	ToBus :	Pfrom :	Qfrom :	Pto :	Qto :
Line 24	25	26	-0.0895	-0.0086	0.0898	-0.0086
Line 25	26	27	-0.0598	-0.0059	0.0600	-0.0059
Line 26	27	28	-0.0300	-0.0030	0.0300	-0.0030
Line 27	1	29	-0.1774	-0.0153	0.1785	-0.0153
Line 28	29	30	-0.1485	-0.0136	0.1491	-0.0136
Line 29	30	31	-0.1191	-0.0112	0.1195	-0.0112
Line 30	31	32	-0.0895	-0.0086	0.0898	-0.0086
Line 31	32	33	-0.0598	-0.0059	0.0600	-0.0059
Line 32	33	34	-0.0300	-0.0030	0.0300	-0.0030

Figure C.13: *Results from performance efficiency analysis with DSA and LFAC CS. Line flows on line 22(23-24) - 32(33-34).*

```
Iter:  1 Pload: -0.9900 Qload: -0.0990 Ploss:  0.0142 Qloss:  0.0146
Iter:  2 Pload: -0.9900 Qload: -0.0990 Ploss:  0.0139 Qloss:  0.0142
Iter:  3 Pload: -0.9900 Qload: -0.0990 Ploss:  0.0139 Qloss:  0.0142
Iter:  4 Pload: -0.9900 Qload: -0.0990 Ploss:  0.0139 Qloss:  0.0142

 ****** Load flow completed ******

time elapsed: 0.00s




 Ploss: 0.013886980351204047    Qloss: 0.014232236597022215
```

Figure C.14: *Output from performance efficiency analysis with DSA and LFAC CS.*

```
------------------------------
Collection system active losses:  0.011500218932399999
(0.06149305555555556+0.04659722222222223j)
Collection system reactive losses:  0.011628917704799999
------------------------------
```

Figure C.15: *Output from performance efficiency analysis with combinatorial method on AC-system.*

```
------------------------------
Collection system active losses:  0.011500218932399999
(0.06149305555555556+0.01565972222222222j)
Collection system reactive losses:  0.0038570039243999996
------------------------------
```

Figure C.16: *Output from performance efficiency analysis with combinatorial method on LFAC-system.*

C.4 DSA - TTS - Performance Efficiency Analysis Results

Bus Voltages

	Bus no	Vmag	Theta
Bus 2	2	0.99814	3.91617
Bus 3	3	1.00041	4.63902
Bus 4	4	1.00179	7.42905

Figure C.17: *Result from performance efficiency analysis with DSA for TTS. Voltage magnitude and angle.*

Transmission line flow

	FromBus :	ToBus :	Pfrom :	Qfrom :	Pto :	Qto :
Line 0	1	2	-0.9705	0.0945	0.9729	0.0945
Line 1	2	3	-0.9729	0.0280	0.9753	0.0280
Line 2	3	4	-0.9753	0.0157	0.9763	0.0157

Figure C.18: *Results from performance efficiency analysis with DSA and TTS line flows.*

```
Iter:  1 Pload: -0.9763 Qload: -0.0318 Ploss:  0.0058 Qloss:  0.1263
Iter:  2 Pload: -0.9763 Qload: -0.0318 Ploss:  0.0058 Qloss:  0.1263
Iter:  3 Pload: -0.9763 Qload: -0.0318 Ploss:  0.0058 Qloss:  0.1263
Iter:  4 Pload: -0.9763 Qload: -0.0318 Ploss:  0.0058 Qloss:  0.1263

 ****** Load flow completed ******

time elapsed: 0.00s


 Ploss: 0.005821146498680697    Qloss: 0.12633163204582154
```

Figure C.19: *Output from performance efficiency analysis with DSA for TTS.*

```
------------------------------------------------------------------------------------------------------------------------
Iteration:  1
------------------------------------------------------------------------------------------------------------------------
                            P                         Q                        Theta                    V
------------------------------------------------------------------------------------------------------------------------
Bus1                    0.9765                    0.0185                    0.13                     1
Bus2                    -0.9706                    0.1082                    0.0                     1
[[7.4916938]]
------------------------------------------------------------------------------------------------------------------------
Iteration:  2
------------------------------------------------------------------------------------------------------------------------
                            P                         Q                        Theta                    V
------------------------------------------------------------------------------------------------------------------------
Bus1                    0.9763                    0.0185                    0.13                     1
Bus2                    -0.9705                    0.1082                    0.0                     1
[[7.49170821]]
------------------------------------------------------------------------------------------------------------------------
COVERGED! Total number of iterations:  2
```

Figure C.20: *Output from NR load flow on TTS.*

Bus Voltages

	Bus no	Vmag	Theta
Bus 2	2	1.00621	1.83089
Bus 3	3	1.00900	2.05808
Bus 4	4	1.01110	2.96774

Figure C.21: *Result from performance efficiency analysis with DSA for LFAC TTS. Voltage magnitude and angle.*

Transmission line flow

	FromBus :	ToBus :	Pfrom :	Qfrom :	Pto :	Qto :
Line 0	1	2	-0.9683	-0.0258	0.9730	-0.0258
Line 1	2	3	-0.9730	-0.0570	0.9755	-0.0570
Line 2	3	4	-0.9755	-0.0611	0.9764	-0.0611

Figure C.22: *Results from performance efficiency analysis with DSA and LFAC TTS line flows.*

```
Iter:  1 Pload: -0.9764 Qload: -0.0767 Ploss:  0.0082 Qloss:  0.0517
Iter:  2 Pload: -0.9764 Qload: -0.0767 Ploss:  0.0081 Qloss:  0.0509
Iter:  3 Pload: -0.9764 Qload: -0.0767 Ploss:  0.0081 Qloss:  0.0509
Iter:  4 Pload: -0.9764 Qload: -0.0767 Ploss:  0.0081 Qloss:  0.0509

 ****** Load flow completed ******

time elapsed: 0.00s


 Ploss: 0.008090462809149728    Qloss: 0.050940723751401136
```

Figure C.23: *Output from performance efficiency analysis with DSA for LFAC TTS.*

```
------------------------------------------------------------------------------------------------------------------------
Iteration:  1
------------------------------------------------------------------------------------------------------------------------
                            P                         Q                         Theta                 V
------------------------------------------------------------------------------------------------------------------------
Bus1                    0.9788                   -0.0545                    0.0732                    1
Bus2                    -0.9722                   0.1259                    0.0                     1
[[13.4011386]]
------------------------------------------------------------------------------------------------------------------------
Iteration:  2
------------------------------------------------------------------------------------------------------------------------
                            P                         Q                         Theta                 V
------------------------------------------------------------------------------------------------------------------------
Bus1                    0.9764                   -0.0545                    0.073                     1
Bus2                    -0.9698                   0.1255                    0.0                     1
[[13.40109206]]
------------------------------------------------------------------------------------------------------------------------
COVERGED! Total number of iterations:  2
```

Figure C.24: *Output from NR load flow on LFAC TTS.*

C.5 DSA - CS + TTS - Performance Efficiency Analysis Results

Bus Voltages

	Bus no	Vmag	Theta
Bus 2	2	1.00337	4.24902
Bus 3	3	1.00889	7.35822
Bus 4	4	1.02274	8.09249
Bus 5	5	1.02689	8.30714
Bus 6	6	1.03020	8.47755
Bus 7	7	1.03420	8.60507
Bus 8	8	1.03687	8.68954
Bus 9	9	1.03820	8.73161
Bus 10	10	1.01308	7.57877
Bus 11	11	1.01645	7.75384
Bus 12	12	1.02050	7.88482
Bus 13	13	1.02320	7.97156

Figure C.25: *Result from performance efficiency analysis with DSA for CS and TTS. Voltage magnitude and angle on bus 2 - 13.*

Bus Voltages

	Bus no	Vmag	Theta
Bus 14	14	1.02455	8.01476
Bus 15	15	1.01888	7.88455
Bus 16	16	1.02222	8.05764
Bus 17	17	1.02625	8.18715
Bus 18	18	1.02894	8.27292
Bus 19	19	1.03028	8.31564
Bus 20	20	1.01392	7.62267
Bus 21	21	1.01728	7.79745
Bus 22	22	1.02133	7.92821
Bus 23	23	1.02402	8.01482
Bus 24	24	1.02537	8.05795
Bus 25	25	1.01390	7.62273

Figure C.26: *Result from performance efficiency analysis with DSA for CS and TTS. Voltage magnitude and angle on bus 14 - 25.*

Bus Voltages

	Bus no	Vmag	Theta
Bus 26	26	1.01808	7.84113
Bus 27	27	1.02142	8.01449
Bus 28	28	1.02545	8.14420
Bus 29	29	1.02814	8.23011
Bus 30	30	1.02948	8.27290
Bus 31	31	1.01588	7.72782
Bus 32	32	1.02005	7.94536
Bus 33	33	1.02339	8.11806
Bus 34	34	1.02742	8.24727
Bus 35	35	1.03010	8.33286
Bus 36	36	1.03144	8.37548

Figure C.27: *Result from performance efficiency analysis with DSA for CS and TTS. Voltage magnitude and angle on bus 26 - 36.*

Transmission line flow

	FromBus :	ToBus :	Pfrom :	Qfrom :	Pto :	Qto :
Line 0	1	2	-0.9706	0.0404	0.9742	0.0404
Line 1	2	3	-0.9742	-0.0318	0.9763	-0.0318
Line 2	3	4	-0.1764	-0.0141	0.1786	-0.0141
Line 3	4	5	-0.1486	-0.0136	0.1491	-0.0136
Line 4	5	6	-0.1191	-0.0112	0.1195	-0.0112
Line 5	6	7	-0.0895	-0.0086	0.0898	-0.0086
Line 6	7	8	-0.0598	-0.0059	0.0600	-0.0059
Line 7	8	9	-0.0300	-0.0030	0.0300	-0.0030
Line 8	3	10	-0.1486	-0.0136	0.1491	-0.0136
Line 9	10	11	-0.1191	-0.0112	0.1195	-0.0112
Line 10	11	12	-0.0895	-0.0086	0.0898	-0.0086
Line 11	12	13	-0.0598	-0.0059	0.0600	-0.0059

Figure C.28: *Result from performance efficiency analysis with DSA for CS and TTS. Line flows on line 0(1-2) - 11(12-13).*

Transmission line flow

	FromBus :	ToBus :	Pfrom :	Qfrom :	Pto :	Qto :
Line 12	13	14	-0.0300	-0.0030	0.0300	-0.0030
Line 13	3	15	-0.1478	-0.0127	0.1491	-0.0127
Line 14	15	16	-0.1191	-0.0112	0.1195	-0.0112
Line 15	16	17	-0.0895	-0.0086	0.0898	-0.0086
Line 16	17	18	-0.0598	-0.0059	0.0600	-0.0059
Line 17	18	19	-0.0300	-0.0030	0.0300	-0.0030
Line 18	3	20	-0.1484	-0.0135	0.1491	-0.0135
Line 19	20	21	-0.1191	-0.0112	0.1195	-0.0112
Line 20	21	22	-0.0895	-0.0086	0.0898	-0.0086
Line 21	22	23	-0.0598	-0.0059	0.0600	-0.0059
Line 22	23	24	-0.0300	-0.0030	0.0300	-0.0030
Line 23	3	25	-0.1778	-0.0157	0.1786	-0.0157

Figure C.29: *Result from performance efficiency analysis with DSA for CS and TTS. Line flows on line 12(13-14) - 23(3-25).*

Transmission line flow

	FromBus :	ToBus :	Pfrom :	Qfrom :	Pto :	Qto :
Line 24	25	26	-0.1486	-0.0136	0.1491	-0.0136
Line 25	26	27	-0.1191	-0.0112	0.1195	-0.0112
Line 26	27	28	-0.0895	-0.0086	0.0898	-0.0086
Line 27	28	29	-0.0598	-0.0059	0.0600	-0.0059
Line 28	29	30	-0.0300	-0.0030	0.0300	-0.0030
Line 29	3	31	-0.1774	-0.0154	0.1786	-0.0154
Line 30	31	32	-0.1486	-0.0136	0.1491	-0.0136
Line 31	32	33	-0.1191	-0.0112	0.1195	-0.0112
Line 32	33	34	-0.0895	-0.0086	0.0898	-0.0086
Line 33	34	35	-0.0598	-0.0059	0.0600	-0.0059
Line 34	35	36	-0.0300	-0.0030	0.0300	-0.0030

Figure C.30: *Result from performance efficiency analysis with DSA for CS and TTS. Line flows on line 24(25-26) - 34(35-36).*

```
Iter:  1 Pload: -0.9900 Qload: -0.0990 Ploss:  0.0201 Qloss:  0.1412
Iter:  2 Pload: -0.9900 Qload: -0.0990 Ploss:  0.0194 Qloss:  0.1394
Iter:  3 Pload: -0.9900 Qload: -0.0990 Ploss:  0.0194 Qloss:  0.1394
Iter:  4 Pload: -0.9900 Qload: -0.0990 Ploss:  0.0194 Qloss:  0.1394

 ****** Load flow completed ******

time elapsed: 0.00s




 Ploss: 0.019429255179582557    Qloss: 0.13937566585175618
```

Figure C.31: *Output from performance efficiency analysis with DSA for CS and TTS.*

C.6 DSA - CS + TTS (LFAC) - Performance Efficiency Analysis Results

Bus Voltages

	Bus no	Vmag	Theta
Bus 2	2	1.00823	1.93712
Bus 3	3	1.01205	2.95635
Bus 4	4	1.02510	3.15185
Bus 5	5	1.02898	3.20906
Bus 6	6	1.03208	3.25450
Bus 7	7	1.03590	3.28302
Bus 8	8	1.03845	3.30191
Bus 9	9	1.03972	3.31133
Bus 10	10	1.01598	3.01504
Bus 11	11	1.01912	3.06164
Bus 12	12	1.02299	3.09089
Bus 13	13	1.02556	3.11026

Figure C.32: *Result from performance efficiency analysis with DSA of LFAC CS and TTS. Voltage magnitude and angle on bus 2 - 13.*

Bus Voltages

	Bus no	Vmag	Theta
Bus 14	14	1.02685	3.11991
Bus 15	15	1.02143	3.09645
Bus 16	16	1.02455	3.14256
Bus 17	17	1.02840	3.17150
Bus 18	18	1.03096	3.19067
Bus 19	19	1.03224	3.20022
Bus 20	20	1.01676	3.02672
Bus 21	21	1.01990	3.07325
Bus 22	22	1.02376	3.10245
Bus 23	23	1.02634	3.12180
Bus 24	24	1.02763	3.13144
Bus 25	25	1.01675	3.02674

Figure C.33: *Result from performance efficiency analysis with DSA for LFAC CS and TTS. Voltage magnitude and angle on bus 14 - 25.*

Bus Voltages

	Bus no	Vmag	Theta
Bus 26	26	1.02066	3.08489
Bus 27	27	1.02379	3.13107
Bus 28	28	1.02764	3.16005
Bus 29	29	1.03020	3.17925
Bus 30	30	1.03149	3.18882
Bus 31	31	1.01862	3.05472
Bus 32	32	1.02252	3.11266
Bus 33	33	1.02564	3.15867
Bus 34	34	1.02949	3.18755
Bus 35	35	1.03205	3.20668
Bus 36	36	1.03333	3.21621

Figure C.34: *Result from performance efficiency analysis with DSA for LFAC CS and TTS. Voltage magnitude and angle on bus 26 - 36.*

Transmission line flow

	FromBus :	ToBus :	Pfrom :	Qfrom :	Pto :	Qto :
Line 0	1	2	-0.9683	-0.0433	0.9742	-0.0433
Line 1	2	3	-0.9742	-0.0767	0.9764	-0.0767
Line 2	3	4	-0.1764	-0.0167	0.1786	-0.0167
Line 3	4	5	-0.1486	-0.0145	0.1491	-0.0145
Line 4	5	6	-0.1191	-0.0117	0.1195	-0.0117
Line 5	6	7	-0.0895	-0.0089	0.0898	-0.0089
Line 6	7	8	-0.0598	-0.0060	0.0600	-0.0060
Line 7	8	9	-0.0300	-0.0030	0.0300	-0.0030
Line 8	3	10	-0.1486	-0.0145	0.1491	-0.0145
Line 9	10	11	-0.1191	-0.0117	0.1195	-0.0117
Line 10	11	12	-0.0895	-0.0089	0.0898	-0.0089
Line 11	12	13	-0.0598	-0.0060	0.0600	-0.0060

Figure C.35: *Result from performance efficiency analysis with DSA for LFAC CS and TTS. Line flows on line 0(1-2) - 11(12-13).*

Transmission line flow

	FromBus :	ToBus :	Pfrom :	Qfrom :	Pto :	Qto :
Line 12	13	14	-0.0300	-0.0030	0.0300	-0.0030
Line 13	3	15	-0.1478	-0.0142	0.1491	-0.0142
Line 14	15	16	-0.1191	-0.0117	0.1195	-0.0117
Line 15	16	17	-0.0895	-0.0089	0.0898	-0.0089
Line 16	17	18	-0.0598	-0.0060	0.0600	-0.0060
Line 17	18	19	-0.0300	-0.0030	0.0300	-0.0030
Line 18	3	20	-0.1484	-0.0145	0.1491	-0.0145
Line 19	20	21	-0.1191	-0.0117	0.1195	-0.0117
Line 20	21	22	-0.0895	-0.0089	0.0898	-0.0089
Line 21	22	23	-0.0598	-0.0060	0.0600	-0.0060
Line 22	23	24	-0.0300	-0.0030	0.0300	-0.0030
Line 23	3	25	-0.1778	-0.0172	0.1786	-0.0172

Figure C.36: *Result from performance efficiency analysis with DSA for LFAC CS and TTS. Line flows on line 12(13-14) - 23(3-25).*

Transmission line flow

	FromBus :	ToBus :	Pfrom :	Qfrom :	Pto :	Qto :
Line 24	25	26	-0.1486	-0.0145	0.1491	-0.0145
Line 25	26	27	-0.1191	-0.0117	0.1195	-0.0117
Line 26	27	28	-0.0895	-0.0089	0.0898	-0.0089
Line 27	28	29	-0.0598	-0.0060	0.0600	-0.0060
Line 28	29	30	-0.0300	-0.0030	0.0300	-0.0030
Line 29	3	31	-0.1775	-0.0171	0.1786	-0.0171
Line 30	31	32	-0.1486	-0.0145	0.1491	-0.0145
Line 31	32	33	-0.1191	-0.0117	0.1195	-0.0117
Line 32	33	34	-0.0895	-0.0089	0.0898	-0.0089
Line 33	34	35	-0.0598	-0.0060	0.0600	-0.0060
Line 34	35	36	-0.0300	-0.0030	0.0300	-0.0030

Figure C.37: *Result from performance efficiency analysis with DSA for LFAC CS and TTS. Line flows on line 24(25-26) - 34(35-36).*

```
Iter:  1 Pload: -0.9900 Qload: -0.0990 Ploss:  0.0225 Qloss:  0.0568
Iter:  2 Pload: -0.9900 Qload: -0.0990 Ploss:  0.0217 Qloss:  0.0557
Iter:  3 Pload: -0.9900 Qload: -0.0990 Ploss:  0.0217 Qloss:  0.0557
Iter:  4 Pload: -0.9900 Qload: -0.0990 Ploss:  0.0217 Qloss:  0.0557

 ****** Load flow completed ******

time elapsed: 0.00s




 Ploss: 0.02169636682017372    Qloss: 0.055650530279261846
```

Figure C.38: *Output from performance efficiency analysis with DSA and LFAC CS and TTS.*

C.7 DSA - Reliability Analysis Results

C.7.1 DSA Results to Determine Active Power Output With 85% Electrical Efficiency

Transmission line flow

	FromBus :	ToBus :	Pfrom :	Qfrom :	Pto :	Qto :
Line 0	1	2	-0.8274	0.0170	0.8300	0.0170
Line 1	2	3	-0.8300	-0.0353	0.8316	-0.0353
Line 2	3	4	-0.1504	-0.0125	0.1520	-0.0125
Line 3	4	5	-0.1265	-0.0118	0.1269	-0.0118
Line 4	5	6	-0.1014	-0.0097	0.1016	-0.0097
Line 5	6	7	-0.0761	-0.0074	0.0764	-0.0074
Line 6	7	8	-0.0509	-0.0050	0.0510	-0.0050
Line 7	8	9	-0.0255	-0.0025	0.0255	-0.0025
Line 8	3	10	-0.1264	-0.0117	0.1269	-0.0117
Line 9	10	11	-0.1014	-0.0096	0.1016	-0.0096
Line 10	11	12	-0.0761	-0.0074	0.0764	-0.0074
Line 11	12	13	-0.0509	-0.0050	0.0510	-0.0050

Figure C.39: *DSA results to obtain active power delivered to main grid for usage in reliability analysis.*

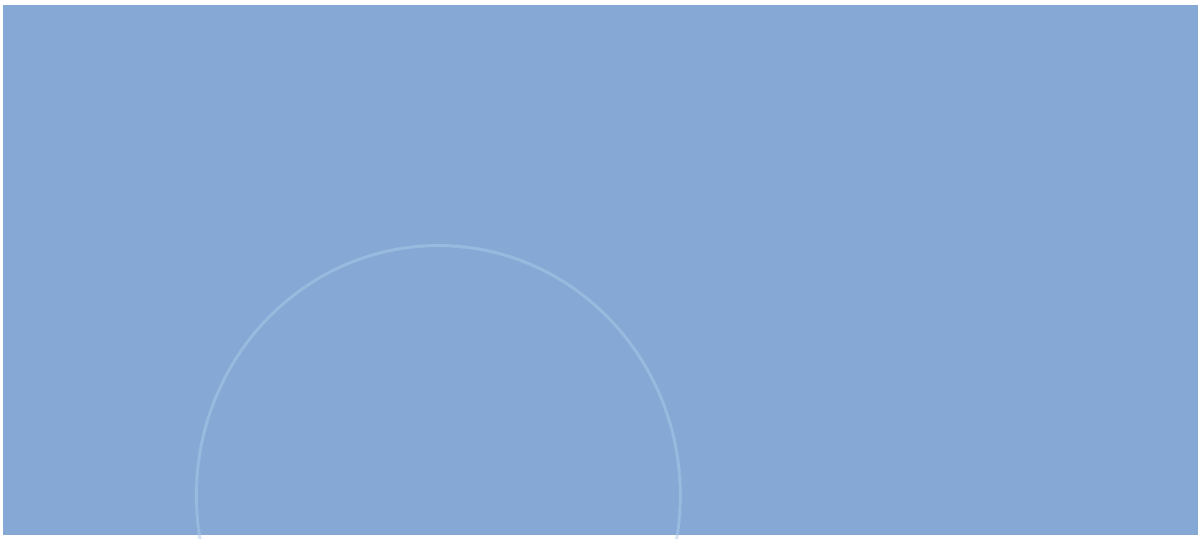

NTNU
Norwegian University of
Science and Technology

ZEPHYR